Distribution Category:
Biology and Medicine
(UC-48)

ANL-83-100
Part I

ANL--83-100-Pt.1

DE85 009364

ARGONNE NATIONAL LABORATORY
9700 South Cass Avenue
Argonne, Illinois 60439

ENVIRONMENTAL RESEARCH DIVISION*
ANNUAL REPORT

Fundamental Molecular Physics and Chemistry
January - December 1983

P. F. Gustafson, Acting Division Director

Mitio Inokuti, Program Manager

March 1985

Preceding Report
ANL-82-65 Part I, October 1981 - December 1982

*The Radiological and Environmental Research (REE) Division became part of the Environmental Research (ER) Division on the latter's formation in May 1983.

FOREWORD

We are pleased to present the thirteenth Annual Report of our group. Our work deals with the physical and chemical properties of molecules related to their interactions with external agents such as photons, electrons, and other charged particles. Within this broad field of research, we select certain topics of study with the intention of filling some of the needs of agencies that support us: Office of Health and Environmental Research and Office of Energy Research (U.S. Department of Energy), Office of Naval Research (U.S. Department of Defense), and National Bureau of Standards (U.S. Department of Commerce).

A portion of our work is devoted to fundamental aspects of radiation physics, e.g., the determination of cross sections for the interactions of electrons and photons with molecules. The cross-section data are indispensable to the microscopic analysis of the physical stage of radiation action on any matter, including the biological cell and its constituents. Another part of our work involves use of resonance-enhanced multiphoton ionization to investigate high-resolution spectroscopy and dynamics of excited molecular states. This is a new research direction in our group with importance in the areas of advanced measurement science, highly selective and chemically specific analytical techniques, and also for the examination of excited states in radiation physics and chemistry.

The articles in this volume are loosely arranged according to subject matter. Articles 1-3 treat photoionization of radicals or excited states. Articles 4-9 concern molecular spectroscopy by resonant multiphoton ionization, probed by the detection of either ions or electrons. Articles 10-13 report on studies conducted with the synchrotron radiation facility at the National Bureau of Standards. Articles 14 and 15 describe theoretical studies on molecular photoabsorption. Articles 16 and 17 present a method of analysis of photoabsorption spectra of open-shell atoms. Articles 18-22 deal with the electron energy-loss spectra of a number of molecules. Articles 23-32 concern cross sections, stopping powers, and other data, as well as their applications to radiation physics and chemistry.

In testimony of our close contacts outside the Laboratory, many of the co-authors of the articles presented here are our collaborators from other

institutions both in the United States and abroad. I deeply thank them all for their interest in working with us and sincerely hope that they maintain contact with us for years to come.

In conclusion we may note some examples of our interactions with other institutions. First, we hosted the Workshop on Electronic and Ionic Collision Cross Sections Needed in the Modeling of Radiation Interactions with Matter, held at Argonne on 6-8 December 1983. J. L. Dehmer served on the Editorial Board of The Journal of Chemical Physics, as well as on the National Academy of Science - National Research Council Committee on Atomic and Molecular Science. P. M. Dehmer was Secretary-Treasurer and a member of the Executive Committee of the Division of Electron and Atomic Physics of the American Physical Society, as well as a member of the Program Committee of the same Division. Finally, I continued to work as Correspondent to Comments on Atomic and Molecular Physics and as Vice-Chairman of the Committee on Stopping Power, International Commission on Radiation Units and Measurements.

Mitio Inokuti
Program Manager

TABLE OF CONTENTS

Foreword

1. Photoionization of the OH Radical 1
   P. M. Dehmer

2. Photoionization of Vibrationally Excited N_2 5
   P. M. Dehmer, P. J. Miller, and W. A. Chupka

3. Photoionization of Excited Molecular States. H_2 C $^1\Pi_u$ 10
   S. T. Pratt, P. M. Dehmer, and J. L. Dehmer

4. Resonant Multiphoton Ionization of Molecular Oxygen 13
   S. T. Pratt, P. M. Dehmer, and J. L. Dehmer

5. State Selection by Resonant Multiphoton Ionization: N_2^+ A $^2\Pi_u$, v^+ 15
   S. T. Pratt, P. M. Dehmer, and J. L. Dehmer

6. Two-Color Multiphoton Ionization of N_2 and CO 18
   S. T. Pratt, P. M. Dehmer, and J. L. Dehmer

7. Photoelectron Studies of Resonant Multiphoton Ionization of Molecular Nitrogen 20
   S. T. Pratt, P. M. Dehmer, and J. L. Dehmer

8. Multiphoton Ionization and Dissociation of Xe_2 26
   S. T. Pratt, P. M. Dehmer, and J. L. Dehmer

9. Photoelectron Angular Distributions from Resonant Multiphoton Ionization of Atomic Carbon 29
   S. T. Pratt, P. M. Dehmer, and J. L. Dehmer

10. Angle-Resolved Photoelectron Study of the Valence Levels of BF_3 in the Range $17 \leq h\nu \leq 28$ eV 35
    J. L. Dehmer, A. C. Parr, S. H. Southworth, and D. M. P. Holland

11. Photoelectron Branching Ratios and Asymmetry Parameters for the Two Outermost Molecular Orbitals of Hydrogen Cyanide 36
    D. M. P. Holland, A. C. Parr, and J. L. Dehmer

12. Photoelectron Branching Ratios and Asymmetry Parameters of the Two Outermost Molecular Orbitals of Methyl Cyanide 37
    D. M. P. Holland, A. C. Parr, and J. L. Dehmer

13. Fluorescence Excitation Studies of Molecular Photoionization in External Electric Fields 38
    E. D. Poliakoff, J. L. Dehmer, A. C. Parr, and G. E. Leroi

14. Shape Resonances in Molecular Fields 39
    J. L. Dehmer

15. Complete Dipole Oscillator Strength Distribution and Its Moments for N_2 — 40
W. M. Kosman and Scott Wallace

16. Eigenchannel Quantum Defect Theory of Open-Shell Atoms: Autoionization Resonances and Eigenphase Shifts of Chlorine — 41
Z.-W. Wang and K. T. Lu

17. Eigenchannel Quantum Defect Theory of Open-Shell Atoms: Calculation of $3p^4(^3P)ns$ Rydberg Spectra of the Chlorine Atom — 42
Z.-W. Wang and K. T. Lu

18. Electron Impact Spectroscopy of Methane, Silane, and Germane — 43
M. A. Dillon, R.-G. Wang, and David Spence

19. Electron Energy Loss Spectroscopy of Molecular Fluorine — 53
R.-G. Wang, Z.-W. Wang, M. A. Dillon, and David Spence

20. Electronic Structure of Cl_2 from 5 to 15 eV by Electron Energy Loss Spectroscopy — 61
David Spence, R. H. Huebner, H. Tanaka, M. A. Dillon, and R.-G. Wang

21. Excitation of Rydberg States of $HgCl_2$ and $HgBr_2$ by Electron Impact — 67
David Spence, R.-G. Wang, and M. A. Dillon

22. Observation of a Rapid Change in the Shape of the $6\sigma \rightarrow np\pi$ Window Resonances in N_2O — 73
David DeMille, David Spence, and M. A. Dillon

23. Report of the Workshop on Electronic and Ionic Collision Cross Sections Needed in the Modeling of Radiation Interactions with Matter — 76
Mitio Inokuti

24. What Formulas Are Good for Representing Dipole and Generalized Oscillator-Strength Spectra? — 78
Mitio Inokuti and M. A. Dillon

25. Total Ionization Cross Sections for Electron Impact — 96
F. J. de Heer and Mitio Inokuti

26. Electron Production in Proton Collisions: Total Cross Sections — 97
M. E. Rudd, Y.-K. Kim, D. H. Madison, and J. W. Gallagher

27. How Do We Decide Whether the First Born Approximation Applies to Inelastic Collisions of Charged Particles with an Atom or Molecule? — 98
Mitio Inokuti and S. T. Manson

28. Stopping Powers of Electrons and Positrons — 100
Mitio Inokuti

29. Inner-Shell Corrections to the Bethe Stopping-Power Formula Evaluated from a Realistic Atomic Model 101
Mitio Inokuti and S. T. Manson

30. A Theoretical Study of Excited-State Formation Due to Sub-Excitation Electrons in Rare Gas - Nitrogen Mixtures 103
C. A. Naleway, Mitio Inokuti, and M. C. Sauer, Jr.

31. Mechanisms for the Sputtering of Condensed-Gas Solids by Charged Particles 104
R. E. Johnson and Mitio Inokuti

32. The Optical Properties and Complex Dielectric Function of Metallic Aluminum from 0.04 to 10^4 eV 106
D. Y. Smith, E. Shiles, and M. Inokuti

Publications 107

1. PHOTOIONIZATION OF THE OH RADICAL*

P. M. Dehmer

The hydroxyl radical (OH) is one of the most thoroughly studied free radicals because of its importance in atmospheric chemistry,[1,2] combustion processes,[3,4] and the interstellar medium.[5,6] Detailed experimental[7] and theoretical studies[8-11] have been performed on the ground electronic state ($X\ ^2\Pi_i$) and on the four lowest bound excited electronic states ($A\ ^2\Sigma^+$, $B\ ^2\Sigma^+$, $D\ ^2\Sigma^-$, and $C\ ^2\Sigma^+$). However, because it is difficult to distinguish the spectrum of OH from the spectra of the various radical precursors, the absorption spectrum in the wavelength region below 1200 Å has not been well characterized. In the present work, the spectrum of OH has been determined in the wavelength region from 750 to 950 Å using the technique of photoionization mass spectrometry. This technique allows complete separation of the spectrum of OH from that of the other components of the discharge and permits the unambiguous determination of the spectrum of OH.

The OH was produced using the standard method of reacting H atoms generated in a microwave discharge with NO_2. The NO_2 was titrated into the flow of H atoms (which were produced in a large excess of He buffer gas) at a point approximately 2 cm from the exit aperture of the molecular beam source. The pyrex discharge tube was coated with teflon or with phosphoric acid to prevent recombination of the radicals.

Figure 1 shows the relative photoionization cross section of OH determined at a wavelength resolution of 0.23 Å, and Figure 2 shows the region from 900 to 920 Å taken at a resolution of 0.12 Å (a portion of the spectrum near 915 Å was determined at a resolution of 0.07 Å and is shown as the inset to this figure).

The photoionization spectrum consists of a large number of preionized bands superimposed on a direct ionization continuum background. In the wavelength region above 815 Å, the bands exhibit sharp structure. This is particularly the case in the region from 900 to 920 Å (Figure 2), in which are

---

*Summary of a paper published in Chem. Phys. Lett. 110, 79 (1984).

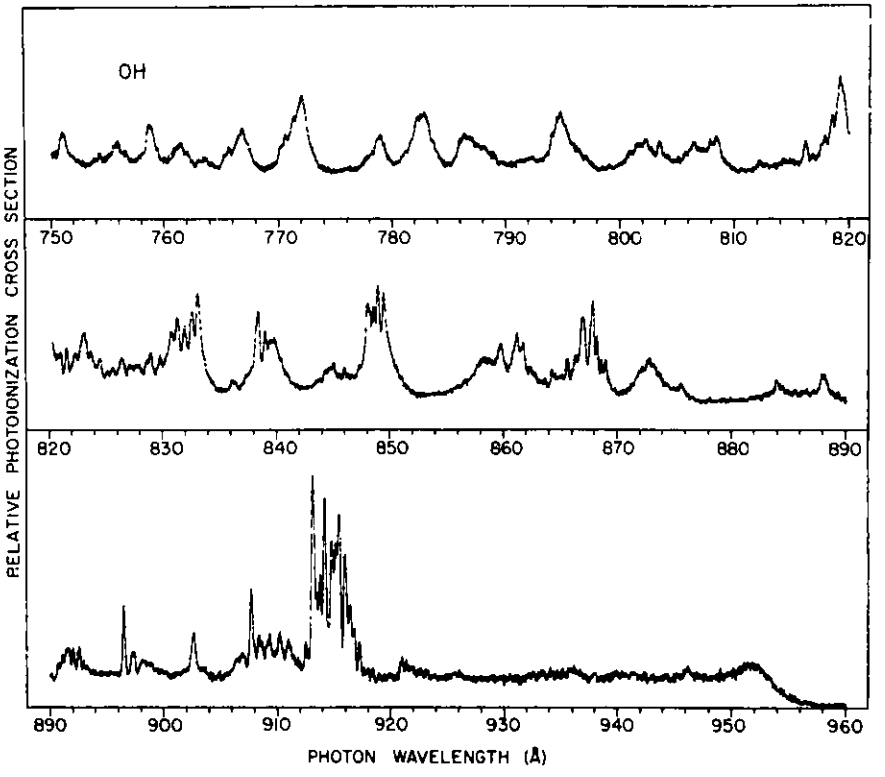

Fig. 1. Relative photoionization cross section for OH determined at a resolution of 0.23 Å.

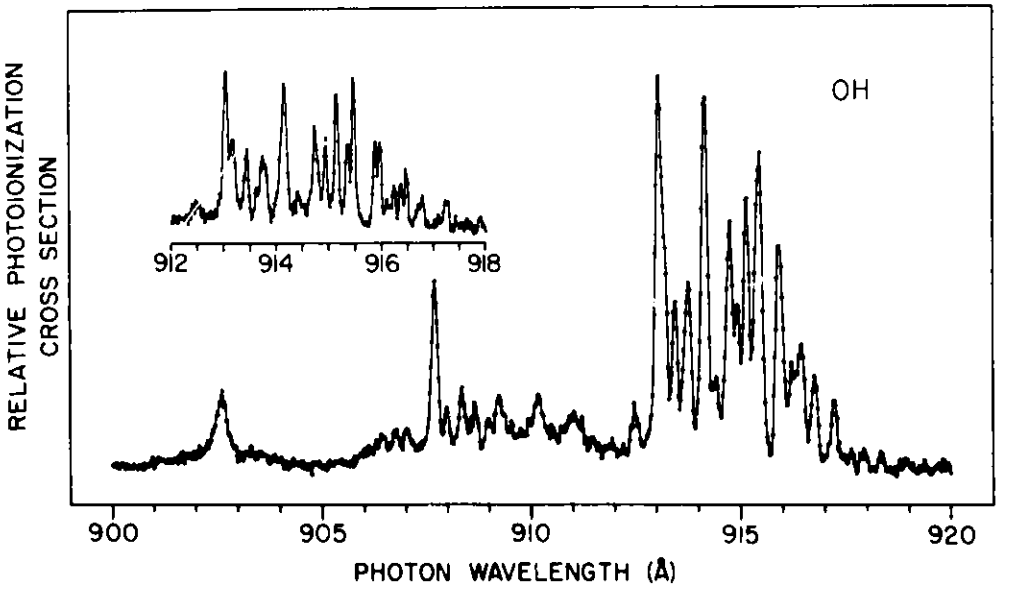

Fig. 2. Relative photoionization cross section for OH in the region from 900 to 920 Å determined at a resolution of 0.12 Å. The inset shows the region near 915 Å determined at a resolution of 0.07 Å.

observed narrow lines with widths equal to the highest instrumental resolution of 0.07 Å. In the wavelength region below 815 Å, the bands are noticeably broader and do not show increased structure at higher instrumental resolution.

These bands shown are members of Rydberg series converging to the a $^1\Delta$, A $^3\Pi_i$ and b $^1\Sigma^+$ excited states of OH^+, which have ionization potentials of 15.17 eV (817.3 Å), 16.48 eV (752.3 Å), and 16.61 eV (746.4 Å), respectively.[12] The configuration of the OH X $^2\Pi_i$ ground state is $(2s\sigma)^2(2p\sigma)^2(2p\pi)^3$. Rydberg series converging to the OH^+ X $^3\Sigma^-$ ground state and the OH^+ a $^1\Delta$ and b $^1\Sigma^+$ excited states result from excitation of an electron in the $(2p\pi)$ molecular orbital, while series converging to the OH^+ A $^3\Pi_i$ excited state result from excitation of an electron in the $(2p\sigma)$ orbital.[13]

If one assumes that the prominent band centered at approximately 915 Å is a member of a Rydberg series converging to the $v^+ = 0$ level of the a $^1\Delta$ state of the ion at 15.17 eV, then the effective principal quantum number (n^*) for this state is 2.90. The resulting small quantum defect (0.10) suggests that the Rydberg state is a member of an nd series. It follows from this conclusion that the 915 Å band is not a single state, but rather consists of transitions to a number of terms resulting from the configurations $(2p\sigma)^2(2p\pi)^2 3d\sigma$, $3d\pi$, and/or $3d\delta$.[13] From a consideration of both angular momentum coupling rules and dipole selection rules,[13] we expect $3d\sigma\ ^2\Delta$, $3d\pi\ ^2\Pi$, and $3d\delta\ ^2\Sigma$ states in the photoabsorption and photoionization spectra. Higher members of this nd series are predicted to appear at 868.58 Å (4d, $n^* = 3.90$), 849.05 Å (5d, $n^* = 4.90$), 838.94 Å (6d, $n^* = 5.90$), and 833.01 Å (7d, $n^* = 6.90$). This is in good agreement with the prominent features observed in the spectrum at 867.2 Å, 848.7 Å, 839.0 Å, and 831.8 Å. If these assignments are correct, weaker features converging to a $^1\Delta$, $v^+ = 1$ also should be observed in the spectrum, since the Franck-Condon calculations predict that the intensity of the a $^1\Delta$, $v^+ = 1$ ionizing transition is about 20% of the intensity of the corresponding $v^+ = 0$ transition. The energy difference between the $v^+ = 0$ and 1 levels of the a $^1\Delta$ state of the ion is 0.367 eV.[12,14] Assuming that the vibrational spacing in the Rydberg states is the same as that in the ionic convergence limit and that the $v' = 0$ Rydberg bands correspond to the observed features listed above, the predicted positions of the $v' = 1$ Rydberg bands are 890.87 Å (3d, $n^* = 2.90$), 845.50 Å (4d, $n^* = 3.90$), 827.90 Å (5d, $n^* = 4.90$), 818.67 (6d, $n^* = 5.90$), and 811.81 (7d, $n^* = 6.90$). For the first two states

(3d and 4d), there is good correlation between the predicted positions and the observation of weak features in the photoionization spectrum; however, for the remaining states (5d - 7d), the predicted positions of the v' = 1 bands are in regions of dense structure, making even tentative assignments impossible.

References

1. M. J. McEwan and L. F. Phillips, Chemistry of the Atmosphere (Edward Arnold Publishers, London, 1975).
2. J. Heicklen, Atmospheric Chemistry (Academic Press, New York, 1976).
3. A. G. Gaydon, Spectroscopy and Combustion Theory (Chapman and Hall, London, 1948).
4. G. J. Minkoff and C. F. H. Tipper, Chemistry of Combustion Reactions (Butterworths, London, 1962).
5. A. Dalgarno and J. H. Black, Rep. Prog. Phys. 39, 573 (1976).
6. W. D. Watson, Rev. Mod. Phys. 48, 513 (1976).
7. K. P. Huber and G. Herzberg, Molecular Spectra and Molecular Structure IV. Constants of Diatomic Molecules (Van Nostrand Reinhold, New York, 1979).
8. I. Easson and M. H. L. Pryce, Can. J. Phys. 51, 518 (1972).
9. H. Lefebvre-Brion, J. Mol. Struct. 19, 103 (1973).
10. S. R. Langhoff, E. F. van Dishoeck, R. Wetmore, and A. Dalgarno, J. Chem. Phys. 77, 1379 (1982).
11. E. F. van Dishoeck, S. R. Langhoff, and A. Dalgarno, J. Chem. Phys. 78, 4552 (1983).
12. H. van Lonkhuyzen and C. A. deLange, Mol. Phys. 51, 551 (1984).
13. G. Herzberg, Molecular Spectra and Molecular Structure I. Spectra of Diatomic Molecules (Van Nostrand Company, Princeton, 1950).
14. D. M. Hirst and M. F. Guest, Mol. Phys. 49, 1461 (1983).

2. PHOTOIONIZATION OF VIBRATIONALLY EXCITED N_2*

P. M. Dehmer, P. J. Miller,† and W. A. Chupka‡

Introduction

The high-resolution relative photoionization cross section for N_2 is reported in the wavelength region between the N_2^+ X $^2\Sigma_g^+$, v' = 0 and 1 ionization limits. Cross sections from both the X $^1\Sigma_g^+$, v" = 0 and 1 vibrational levels were determined in this region, and preionized members of the $np\pi_u$ $^1\Pi_u$ Worley-Jenkins Rydberg series converging to N_2^+ X $^2\Sigma_g^+$, v' = 1 are observed in both spectra (see Figures 1 and 2). In the spectrum excited from v" = 1, the Worley-Jenkins series appears prominently as a result of good Franck-Condon overlap between the N_2 X $^1\Sigma_g^+$, v" = 1 and the N_2^+ X $^2\Sigma_g^+$, v^+ = 1 levels; the intensities of the series members decrease approximately as $1/n^{*3}$, in accord with simple theoretical predictions. However, in the spectrum excited from v" = 0, the Worley-Jenkins series converging to N_2^+ X $^2\Sigma_g^+$, v^+ = 1 is weak as a result of a poor Franck-Condon overlap with the ground vibrational level. The intensities of the series members show large deviations from the simple theory as a result of channel interactions with Rydberg states converging to N_2^+ A $^2\Pi_u$. These perturbing Rydberg states have low photoabsorption oscillator strengths for excitation from v" = 1 (in contrast to excitation from v" = 0) and hence have only a small effect on the cross section from the excited vibrational level. Just as in the case of photoionization of H_2, the results demonstrate that channel interaction can redistribute the oscillator strength of a perturbing Rydberg state of low principal quantum number over a number of members of an interacting Rydberg series and that the spectral range affected by the perturber can be much greater than the width of the perturbing level.

---

*Summary of a paper published in J. Chem. Phys. 80, 1030 (1984).

†Participant in the Summer 1983 Student Research Participation Program coordinated by the Division of Educational Programs, ANL. Present address: Department of Chemistry, Yale University, New Haven, Connecticut 06511.

‡Present address: Department of Chemistry, Yale University, New Haven, Connecticut 06511.

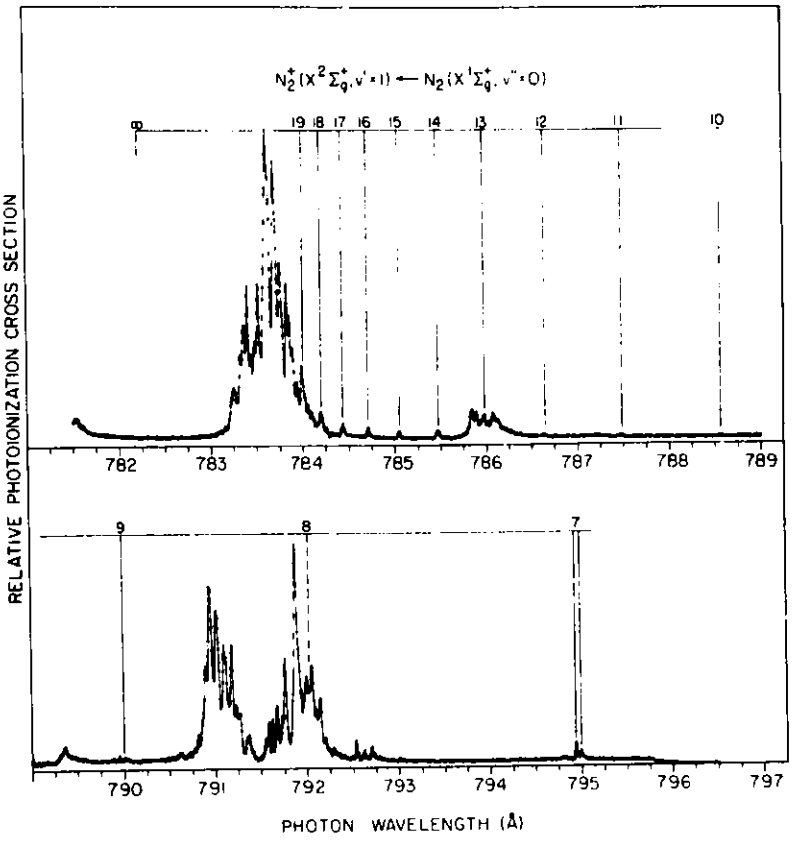

Fig. 1. Relative photoionization cross section for N_2 X $^1\Sigma_g^+$, v" = 0 taken at a temperature of 78 K and at a wavelength resolution of 0.017 Å in the region between the N_2^+ X $^2\Sigma_g^+$, $v^+ = 0$ and 1 ionization thresholds. The running index m is equal to n - 1.

Results

Dipole-allowed Rydberg series converging to the N_2^+ X $^2\Sigma_g^+$ ground state result from excitation of an electron in the ($\sigma_g 2p$) molecular orbital to $np\sigma_u$ and $np\pi_u$ series of states. Evidence of the series converging to N_2^+ X $^2\Sigma_g^+$, $v^+ = 0$ was first reported Worley and Jenkins,[1] and individual series members subsequently were tabulated by Worley.[2] Tanaka and Takamine[3] later observed the much weaker series converging to $v^+ = 1$ of the ion, which is the series observed in the present work, and Ogawa and Tanaka[4] extended both of these series to higher principal quantum number. As in the case of H_2, the lower members of the Carroll-Yoshino and Worley-Jenkins series correspond to $np\sigma_u$ $^1\Sigma_u^+$ and $np\pi_u$ $^1\Pi_u$ states. These low-lying states have been the subject of considerable study and reinterpretation over the years, since homogeneous perturbations between the valence and lowest Rydberg states are severe. As n increases there is a gradual transition from Hund's case (b) to Hund's case (d) as a result of ℓ-uncoupling, and at high n the appearance of the spectrum is determined largely by the effects of ℓ-uncoupling and to a much lesser extent by the effects of homogeneous perturbations.

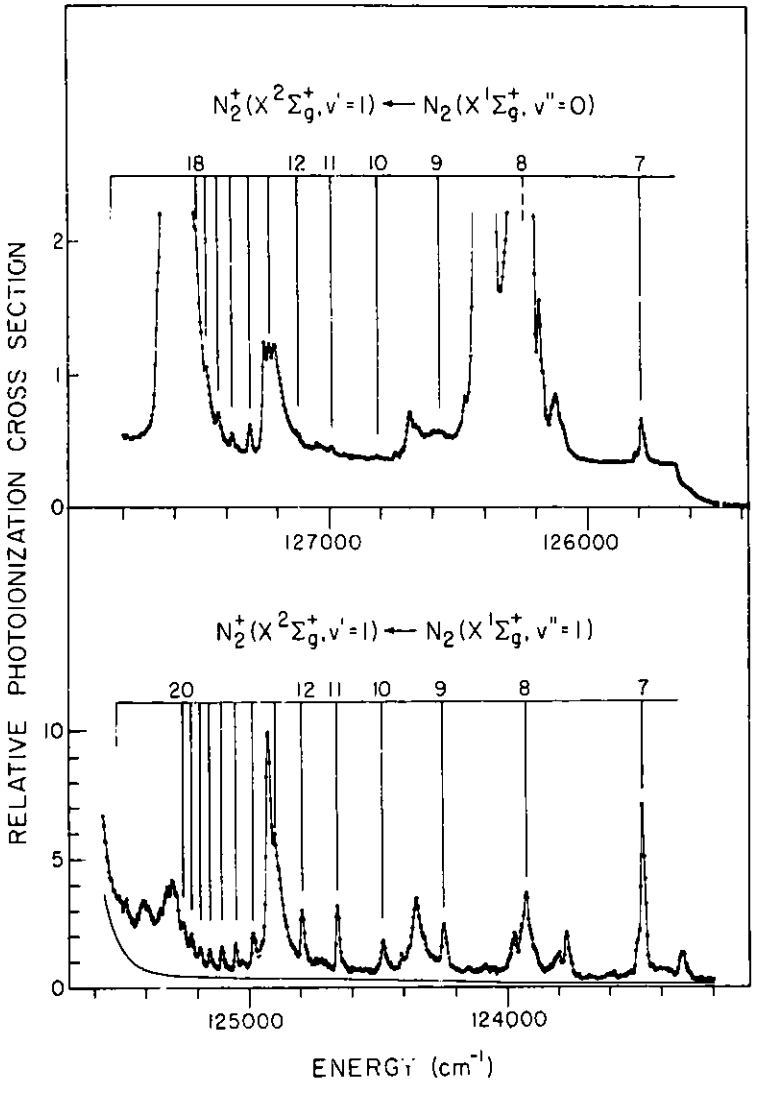

Fig. 2. Relative photoionization cross sections for excitation from N_2 X $^1\Sigma_g^+$, v" = 0 (upper trace) and v" = 1 (lower trace) to the region containing the preionizing members of the Worley-Jenkins Rydberg series converging to N_2^+, v^+ = 1 taken at a wavelength resolution of 0.10 Å. In each spectrum, the ordinate has a maximum value of 10.0 on the most intense preionizing peak in the region. The solid baseline shown in the lower trace gives the magnitude of the N_2^+ ion signal resulting from ionization of N_2 in the v" = 0 ground vibrational level. This ion signal, which appears energetically below the threshold for ionization from v" = 0, results from ionization by scattered light and from collisional ionization of high Rydberg states. The running index m is equal to n - 1.

The data of Figure 1 show that in addition to members of the Worley-Jenkins Rydberg series converging to N_2^+ X $^2\Sigma_g^+$, v^+ = 1, several prominent interlopers appear in the energy region between the v^+ = 0 and v^+ = 1

thresholds. The features at approximately 783.31 and 785.93 Å have been assigned as the m = 4 members of series I and II converging to the $\Omega = 1/2$ and $\Omega = 3/2$ levels of the N_2^+ A $^2\Pi_u$ state, respectively;[4] however, these features do not account for all of the structure in the two bands. Series I, known as Worley's third series, is postulated to have the electron configuration $(\pi_u 2p)^3(\sigma_g 2p)^2\ ns\sigma_g\ ^1\Pi_u$ (n = 3, 4,...). The upper levels of transitions to the first two members of the series (R-branch bandheads at 946.132 and 818.536 Å) are known to be $^1\Pi_u$ in character from a rotational analysis of the bands. Transitions to higher series members exhibit diffuse rotational structure and have not been analyzed. It is believed that the peaks at 783.265 and 783.361 Å correspond to the R and Q branch heads, respectively, of the transition to the third member of the series.

The relative intensities for the preionized members of the N_2^+ X $^2\Sigma_g^+$, $v^+ = 1 \leftarrow N_2$ X $^1\Sigma_g^+$, v" = 0, 1 Worley-Jenkins Rydberg series are given in Table 1. Even with substantial error limits assigned to these values, there are

Table 1. Photoionization intensities of members of the N_2^+ X $^2\Sigma_g^+$, $v^+ = 1 \leftarrow N_2$ X $^1\Sigma_g^+$, v" = 0, 1 Worley-Jenkins Rydberg series.

m = n - 1	v" = 0[a]	v" = 1[b]	$1/n^{*3}$ [c]
7	1.00	1.00	1.000
8	---	0.61	0.680
9	---	0.25	0.483
10	---	0.20	0.357
11	0.08	0.33	0.267
12	0.10	0.25	0.209
13	---	---	0.166
14	0.45	0.14	0.133
15	0.27	0.10	0.109
16	0.33	0.10	0.090
17	0.52	0.08	0.075
18	0.88	0.06	0.064
19	2.07	0.06	0.054
20	---	0.04	0.047

[a]Uncertainties in the determination of the peak areas are estimated to be ±15% for m = 11, 12; and ±10% for m = 14 - 19.
[b]Uncertainties in the determination of the peak areas are estimated to be ±10% for m = 8 - 12; ±15% for m = 14 - 17; ±20% for m = 18, 19; and ±30% for m = 20.
[c]Calculated from the values of n^* for the R bandheads as given in Ref. 4.

striking differences between the relative intensities in the two Rydberg series.

The data of Table 1 show that for excitation from v" = 1, the Rydberg intensities decrease approximately as $1/n^{*3}$; however, this is not true for excitation from v" = 0. In the latter case, Giusti-Suzor and Lefebvre-Brion[5,6] attribute the increase in intensity for m > 15 to the interaction of the $5s\sigma_g\ ^1\Pi_u$ state with the higher members of the $np\pi_u\ ^1\Pi_u$ Worley-Jenkins series. The results of their calculations show that if only vibrational interaction with the continuum is included, the calculated cross section shows narrow peaks of constant height whose widths decrease with increasing principal quantum number as expected. When the interaction between the two electronic channels is included, the widths of the peaks are much larger and their intensities decrease as the separation from the $5s\sigma_g$ resonance decreases, in qualitative agreement with experiment. It is significant that the Worley-Jenkins series members appear in the calculated ionization cross section even when vibrational coupling with the continuum is neglected. Giusti-Suzor and Lefebvre-Brion term this an indirect electronic autoionization, and point out that vibrational preionization often will be contaminated with electronic preionization in molecules other than H_2.

References

1. R. E. Worley and F. A. Jenkins, Phys. Rev. 54, 305 (1938).
2. R. E. Worley, Phys. Rev. 64, 207 (1943).
3. Y. Tanaka and T. Takamine, Sci. Pap. Inst. Phys. Chem. Res. (Tokyo) 39, 427 (1942).
4. M. Ogawa and Y. Tanaka, Can. J. Phys. 40, 1593 (1962).
5. A. Giusti-Suzor and H. Lefebvre-Brion, Chem. Phys. Lett. 76, 132 (1980).
6. H. Lefebvre-Brion and A. Giusti-Suzor, in Electron-Atom and Electron-Molecule Collisions, edited by J. Hinze (Plenum, New York, 1983), p. 215.

3. PHOTOIONIZATION OF EXCITED MOLECULAR STATES. H_2 C $^1\Pi_u$*

S. T. Pratt, P. M. Dehmer, and J. L. Dehmer

Resonantly enhanced multiphoton ionization (REMPI) affords the researcher the opportunity to select a specific ionization pathway in order to produce a particular ionic state for further study or to investigate detailed aspects of excited state photoionization dynamics. Here we demonstrate both of these possibilities in the context of the most fundamental and theoretically tractable molecule, H_2.

The production of vibrationally state-selected molecular ions using multiphoton ionization techniques can be achieved by first preparing an intermediate Rydberg state that has a potential energy curve similar to that of the final ionic state, and then ionizing the Rydberg state with a single additional photon. Under these circumstances, the Franck-Condon factors governing the final ionization step strongly favor the preservation of the vibrational level of the Rydberg state. Thus, REMPI often may serve as an attractive alternative to more complex coincidence techniques presently used to study the properties and reactions of vibrationally state-selected ions. Here we demonstrate the final vibrational state selectivity of REMPI for the photoionization of the $2p\pi_u$ C $^1\Pi_u$ Rydberg state of H_2, which was prepared by a resonant three-photon transition from the ground electronic state.

The observed vibrational intensity distributions also reflect the dynamics of the excited-state photoionization process. In particular, a comparison of the observed vibrational intensities with the corresponding Franck-Condon factors will display the more subtle dynamical effects of the photoionization process. This scheme is currently under very active investigation.[1-10] The present example contributes to this by combining a single-photon ionization step with accurately known potential energy curves. In fact, we observe substantial departures from the simple Franck-Condon factors, which should provide a point of departure for future theoretical work on excited-state photoionization dynamics of molecules.

---

*Summary of a paper published in Chem. Phys. Lett. 105, 28 (1984).

The photoelectron spectra obtained at the wavelengths of the three-photon Q(1) transitions of the C $^1\Pi_u$, v' = 0 - 4, + X $^1\Sigma_g^+$, v" = 0 bands are shown in Figure 1. The most striking aspect of the photoelectron spectra is the dominance of the photoelectron peak corresponding to the $v^+(X\ ^2\Sigma_g^+) = v'(C\ ^1\Pi_u)$ transitions. In addition, the weaker peaks with the greatest intensity are those adjacent to the $v^+ = v'$ peak. This agrees with expectations based on Franck-Condon factor calculations performed using the numerical potential of Kołos and Rychlewski[11] for the C $^1\Pi_u$ neutral state and that of Wind[12] with the adiabatic corrections of Bishop and Wetmore[13] for the X $^2\Sigma_g^+$ ionic state. However, while the qualitative agreement with the calculations is very good, the quantitative agreement is poor. For example, in the spectrum excited via the C $^1\Pi_u$, v' = 4 level, the v^+ = 3, 5, and 6 peaks are too large by factors of 3, 2, and 23, respectively, and the intensity of the v^+ = 4 peak accounts for only 43% of the total, rather than the predicted 90%.

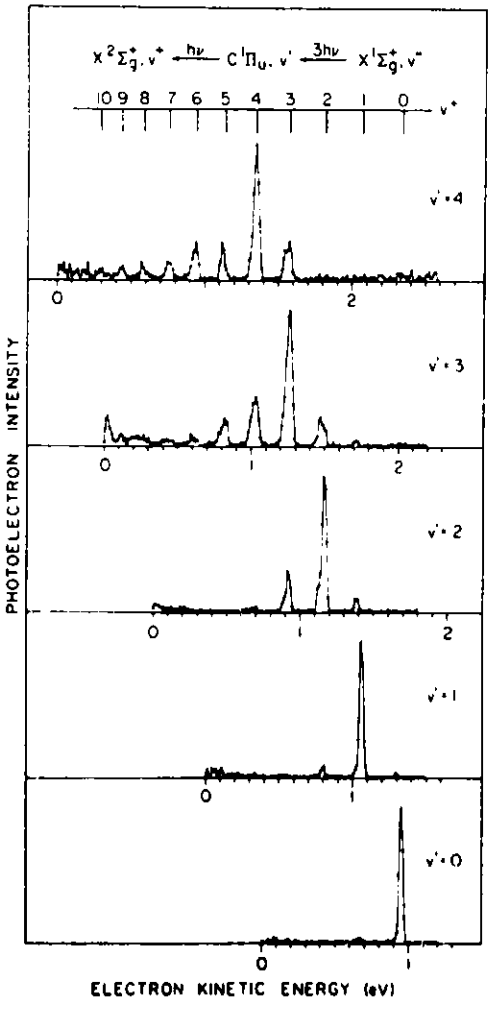

Fig. 1. Photoelectron spectra of H_2 determined at the wavelengths of the resonant three-photon C $^1\Pi_u$, v' = 0 - 4 + X $^1\Sigma_g^+$, v" = 0, Q(1) transitions.

The most likely causes of such deviations are: (1) a kinetic-energy dependence of the electronic transition matrix element, which must be taken into consideration even within the Franck-Condon approximation; (2) an R dependence of the same electronic transition matrix element, which, by definition, constitutes a breakdown of the Franck-Condon approximation; (3) a v^+ dependence of the photoelectron angular distribution; and (4) other effects such as perturbations or overlapping lines at the three-photon level and accidental resonances with autoionizing states at the four-photon level. Of these possibilities, accidental resonances and perturbations are not important in the present case. Hence, the data in Figure 1 represent a well-defined case for theoretical investigation of the excited-state dynamics outlined in (1)-(3) above.

References

1. J. C. Miller and R. N. Compton, J. Chem. Phys. 75, 22 (1981).
2. M. G. White, M. Seaver, W. A. Chupka, and S. D. Colson, Phys. Rev. Letters 49, 28 (1982).
3. J. Kimman, P. Kruit, and M. J. van der Wiel, Chem. Phys. Letters 88, 576 (1982).
4. J. H. Glownia, S. J. Riley, S. D. Colson, J. C. Miller, and R. N. Compton, J. Chem. Phys. 77, 68 (1982).
5. Y. Achiba, K. Sato, K. Shobatake, and K. Kimura, J. Chem. Phys. 78, 5474 (1983).
6. S. R. Long, J. T. Meek, and J. P. Reilly, J. Chem. Phys. 79, 3206 (1983).
7. S. L. Anderson, G. B. Kubiak, and R. N. Zare, Chem. Phys. Letters 105, 22 (1984).
8. S. T. Pratt, E. D. Poliakoff, P. M. Dehmer, and J. L. Dehmer, J. Chem. Phys. 78, 65 (1983).
9. S. T. Pratt, P. M. Dehmer, and J. L. Dehmer, J. Chem. Phys. 79, 3234 (1983).
10. S. T. Pratt, P. M. Dehmer, and J. L. Dehmer, J. Chem. Phys. 78, 4315 (1983).
11. W. Kołos and J. Rychlewski, J. Mol. Spectry. 62, 109 (1976).
12. H. Wind, J. Chem. Phys. 42, 2371 (1965).
13. D. M. Bishop and R. W. Wetmore, Mol. Phys. 26 145 (1973).

4. RESONANT MULTIPHOTON IONIZATION OF MOLECULAR OXYGEN

S. T. Pratt, P. M. Dehmer, and J. L. Dehmer

Resonantly enhanced multiphoton ionization (REMPI) of molecules has been used to obtain detailed spectroscopic information on the neutral intermediate states.[1] In particular, because the electric dipole selection rules are different than for the single-photon case, two-photon resonant, n-photon ionization has been used to observe new electronic states in several molecules.[1] Recently, we have studied molecular oxygen using two-photon resonant, three-photon ionization. From the two-photon selection rules it is known that two-photon transitions from the O_2 $^3\Sigma_g^-$ state must access electronic states of the g symmetry. Using a time-of-flight mass spectrometer, the O_2^+ ion signal was monitored as the wavelength of the frequency-doubled dye laser was scanned near 2880 Å. Figure 1 shows a small portion of the spectrum, in which the two-photon energy corresponds to ~ 8.610 eV. Although the structure shown in Figure 1 is diffuse, the band displays sharp structure at wavelengths

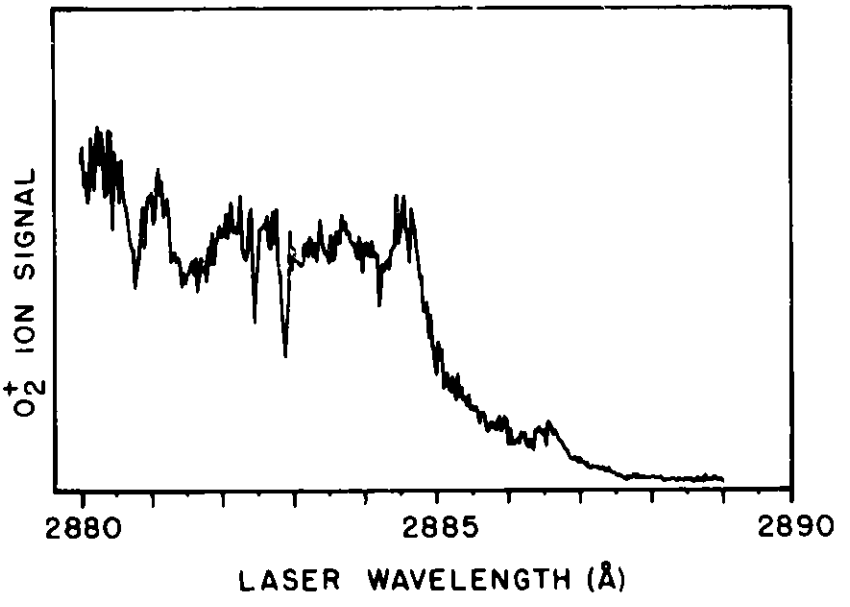

Fig. 1. Relative multiphoton ionization cross section for the production of O_2^+. The wavelength is that of the frequency-doubled dye laser and has not been accurately calibrated.

shorter than shown here. This is consistent with other unpublished results.[2] Comparison with the results from electron energy-loss (EELS) measurements (such as those of York and Comer,[3] for example) suggests that the observed structure is due to the single-photon forbidden C $^3\Pi_g$, v' = 2 ← X $^3\Sigma_g^-$, v" = 0 transition. However, it should be mentioned that another band has been observed at nearly the same energy using EELS at low incident energy and high scattering angle, which has only tentatively been assigned as a spin forbidden transition to the d $^1\Pi_g$ state.

These preliminary results suggest a number of possible studies on oxygen using REMPI. In particular, use of these two-photon transitions as the first step of double resonance studies may allow the examination of highly excited states of molecular oxygen with unprecedented detail.

References

1. P. M. Johnson and C. E. Otis, Ann. Rev. Phys. Chem. 32, 139 (1981).
2. S. Arepalli, B. Marinelli, R. Ogorzalek, P. Houston, and J. Wiesenfeld, Cornell University, unpublished results.
3. T. A. York and J. Comer, J. Phys. B 16, 3627 (1983).

5. STATE SELECTION BY RESONANT MULTIPHOTON IONIZATION: N_2^+ A $^2\Pi_u$, v^+ *

S. T. Pratt, P. M. Dehmer, and J. L. Dehmer

In this work we demonstrate the production of electronically excited, vibrationally state-selected molecular ions by resonant multiphoton ionization via a Rydberg state with an electronically excited ion core. Specifically, it is shown that the dominant ionization pathway for three-photon resonant, four-photon ionization of N_2 via the o_3 $^1\Pi_u$, $v' = 1, 2$ levels leads to the production of N_2^+ A $^2\Pi_u$, $v^+ = 1, 2$, respectively. The o_3 $^1\Pi_u$ state of N_2 has the electron configuration $...(1\pi_u)^3(3\sigma_g)^2\ 3s\sigma_g$ and is the lowest member of Worley's third series,[1] which converges to N_2^+ A $^2\Pi_{1/2\ u}$. The ionizing transition strongly favors the removal of the outer $3s\sigma_g$ electron, leading to the direct production of N_2^+ A $^2\Pi_u$. This is the first experimental evidence in a molecular system showing the degree to which the electronic excitation of the ion core is retained following photoionization of a Rydberg state. Ganz et al.[2,3] recently observed similar effects in the photoionization of Ne $^3D_3$, that is, in all of the transitions that they observed the spin-orbit state of the ion core was preserved (also see Stebbings et al.[4]).

In addition to preserving the electronic state of the ion core, the A $^2\Pi_u \leftarrow o_3$ $^1\Pi_u$ ionizing transition also preserves the vibrational level of the o_3 $^1\Pi_u$ Rydberg state. This is in accord with calculations for the A $^2\Pi_u$, $v^+ \leftarrow o$ $^1\Pi_u$, v' ionizing transition, which give Franck-Condon factors greater than 0.99 for the $v' = v^+$ transition for $v' = 1$ and 2. Although it has been shown that multiphoton ionization through certain Rydberg states of NH_3 and NO leads predominantly to electronic ground state, v^+-selected ions,[5,6] one cannot in general rely on the Franck-Condon principle to predict vibrational branching ratios following resonant multiphoton ionization, as has been demonstrated recently in the case of H_2 C $^1\Pi_u$.[7]

Photoelectron spectra were recorded at the wavelengths corresponding to the three photon transitions to the R-branch bandhead of the o_3 $^1\Pi_u$, $v' = 2 \leftarrow$ X $^1\Sigma_g^+$, $v'' = 0$ band and to three positions, including the R-branch bandhead,

---

*Summary of a paper published in J. Chem. Phys. 80, 1706 (1984).

within the $o_3\ ^1\Pi_u$, v' = 1 ← X $^1\Sigma_g^+$, v" = 0 band. The photoelectron spectra obtained via the $o_3\ ^1\Pi_u$, v' = 1 and 2 bands are shown in Figure 1. Of the three spectra obtained via the v' = 1 band, that shown in Figure 1 displays the greatest fraction (~ 20%) of photoelectrons with $v^+ \neq v'$. At other wavelengths, N_2^+ A $^2\Pi_u$, v^+ = 1 could be produced with > 90% purity. It is clear that the dominant ionization process corresponds to excitation of the Rydberg electron, with preservation of the electronic and vibrational state of the ion core. In addition, a large fraction of those ions produced by core-switching transitions undergo a change only in vibrational state, while retaining the A $^2\Pi_u$ ion core.

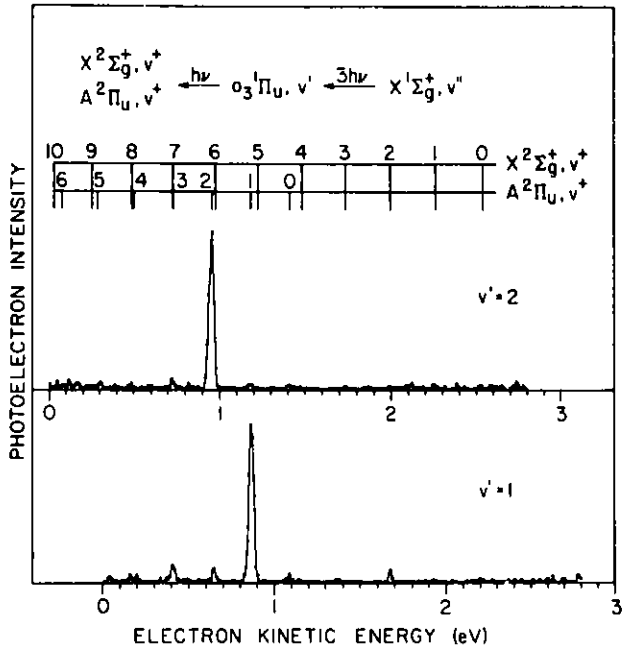

Fig. 1. Photoelectron spectra obtained following three-photon resonant, four-photon ionization of N_2 via the $o_3\ ^1\Pi_u$, v' = 1, 2 levels. The energy levels of N_2^+ were obtained from Reference 1.

An extensive analysis of the vibronic structure in the region of the N_2 spectrum containing the $o_3\ ^1\Pi_u$, v' = 1, 2 ← X $^1\Sigma_g^+$, v" = 0 bands has been reported recently by Stahel et al.[8] This region is extremely complicated because of the mixing of three different $^1\Pi_u$ states, and because of the presence of three $^1\Sigma_u^+$ states that are also strongly mixed. In the analysis of Stahel et al., the $o_3\ ^1\Pi_u$ v' = 1, 2 vibronic levels are found to contain 8.4% and 10.0% b $^1\Pi_u$ character, respectively, and somewhat less c $^1\Pi_u$ character. In addition, a rotational analysis by Yoshino et al.[9] of the single-photon absorption data for the $o_3\ ^1\Pi_u$ ← X $^1\Sigma_g^+$ transition indicates much stronger mixing at the R-branch bandhead of the v' = 1 band because of a perturbation by the b $^1\Pi_u$ v' = 12 level. One would expect these perturbations to strongly affect the vibrational branching ratios following multiphoton ionization. In

particular, photoionization of high vibrational levels of the b $^1\Pi_u$ state, which is a valence state, would be expected to populate a wide distribution of N_2^+ vibrational levels in both the X $^2\Sigma_g^+$ and A $^2\Pi_u$ states. It is clear from Figure 1 that this is not the case. Calculations by Michels[10] indicate that two different electron configurations are important in describing the b $^1\Pi_u$ state of N_2. Both of these configurations, $...(2\sigma_u)^2(1\pi_u)^3(3\sigma_g)^1(1\pi_g)^2$ and $...(2\sigma_u)^1(1\pi_u)^4(3\sigma_g)^2(1\pi_g)^1$, differ from the X $^2\Sigma_g^+$ and A $^2\Pi_u$ states of N_2^+ by two orbitals. For this reason, the photoionization cross section for the b $^1\Pi_u$ state may be relatively small, leading to a dominance of the o_3 $^1\Pi_u$ character in the photoionization of the intermediate state.

References

1. A. Lofthus and P. H. Krupenie, J. Phys. Chem. Ref. Data 6, 113 (1977).
2. J. Ganz, B. Lewandowski, A. Siegel, W. Bussert, H. Waibel, M. W. Ruf, and H. Hotop, J. Phys. B 15, L485 (1982).
3. A. Siegel, J. Ganz, W. Bussert, and H. Hotop, J. Phys. B 16, 2945 (1983).
4. R. F. Stebbings, F. B. Dunning, and R. D. Rundel, in Atomic Physics Vol. 4, edited by G. zu Putlitz, E. W. Weber, and A. Winnacker (Plenum, New York, 1975), p. 713, and references therein.
5. J. H. Glownia, S. J. Riley, S. D. Colson, J. C. Miller, and R. N. Compton, J. Chem. Phys. 77, 68 (1982).
6. Y. Achiba, K. Sato, K. Shobatake, and K. Kimura, J. Chem. Phys. 78, 5474 (1983).
7. S. T. Pratt, P. M. Dehmer, and J. L. Dehmer, Chem. Phys. Lett. 105, 28 (1984).
8. D. Stahel, M. Leoni, and K. Dressler, J. Chem. Phys. 79, 2541 (1983).
9. K. Yoshino, Y. Tanaka, P. K. Carroll, and P. Mitchell, J. Mol. Spectrosc. 54, 87 (1975).
10. H. H. Michels, Adv. Chem. Phys. 45, 225 (1981).

6. TWO-COLOR MULTIPHOTON IONIZATION OF N_2 AND CO

S. T. Pratt, P. M. Dehmer, and J. L. Dehmer

Optical-optical double resonance techniques using fluorescence detection have been used for a number of years as a means of reducing spectral congestion and greatly simplifying spectroscopic analysis.[1] In one version of these two-laser experiments, the first laser frequency is fixed to pump a particular rovibronic transition of interest, while the second laser is used to probe transitions from the upper level of the pump transition to higher excited states. More recently this technique has been coupled with ionization detection, which provides increased sensitivity in many instances and allows the study of levels that do not fluoresce. In the past year we have used this technique to study N_2 and CO.

The apparatus has been described in detail in a previous publication.[2] In the experiments discussed here, the Nd:YAG laser is used to pump a commercial dye laser as well as a homemade dye laser of the modified Littman design described by Mahon and Tomkins.[3] Both dye lasers can be frequency-doubled. The experiments are performed in two parts, with the time-of-flight mass spectrometer used to monitor the ion signal. In the first part, the single-laser, resonant multiphoton ionization spectrum is recorded via the pump transition. In the examples discussed here, ionization occurs via a two-photon resonant, four photon process. The laser is then tuned to the pump transition of interest and the power is reduced to produce a small background of ionization. At this point the probe laser is made collinear and copropagating with the pump beam by combining them on an appropriate dichroic mirror. In the experiments discussed here, the two pulses are overlapped temporally as well. The probe laser wavelength is then scanned and the two-color ionization spectrum is recorded.

We have performed these experiments on CO by pumping the A $^1\Pi$, $v' = 3 \xleftarrow{2h\nu_1} X\ ^1\Sigma^+$, $v'' = 0$ transition and probing the C $^1\Pi_u$, $v' = 0 \xleftarrow{h\nu_2} A\ ^1\Pi$, $v'' = 3$ transition, and on N_2 by pumping the a $^1\Pi_g$, $v' = 1 \xleftarrow{2h\nu_1} X\ ^1\Sigma_g^+$, $v'' = 0$ transition and probing transitions from the a $^1\Pi_g$, $v' = 1$ level to the c' $^1\Sigma_u^+$, $v' = 1,2$, c $^1\Pi_u$, $v' = 1,2$, o $^1\Pi_u$, $v' = 0$, and b $^1\Pi_u$, $v' = 6$ states.

Ionization occurs by the absorption of a single photon of either $h\nu_1$ or $h\nu_2$. Figure 1 shows a two-color spectrum of N_2 in which the pump laser is tuned to the a $^1\Pi_g$, v' = 1, J' = 4 $\xleftarrow{2h\nu_1}$ X $^1\Sigma_g^+$, v" = 0, J" = 2 transition (the S(2) line) and the probe laser is scanned in the region of the b $^1\Pi_u$, v' = 6 band. The P, Q, and R branches from the a $^1\Pi_g$, v" = 1, J" = 4 level are clearly revealed, and the assignment is trivial. The R(15) line arises as the a $^1\Pi_g$, v' = 1 $\xleftarrow{2h\nu_1}$ X $^1\Sigma_g^+$, v" = 0 S(2) transition overlaps the S(13) transition of the same band, producing some N_2^* in the a $^1\Pi_g$, v = 1, J = 15 level from which the R(15) signal in Figure 1 is observed.

While these studies are of interest in their own right, it is our goal to use these two-color transitions as the base for studying autoionizing levels by bringing in a third laser to promote transitions from the upper level of the probe transition into the ionization continuum. Such studies are currently underway.

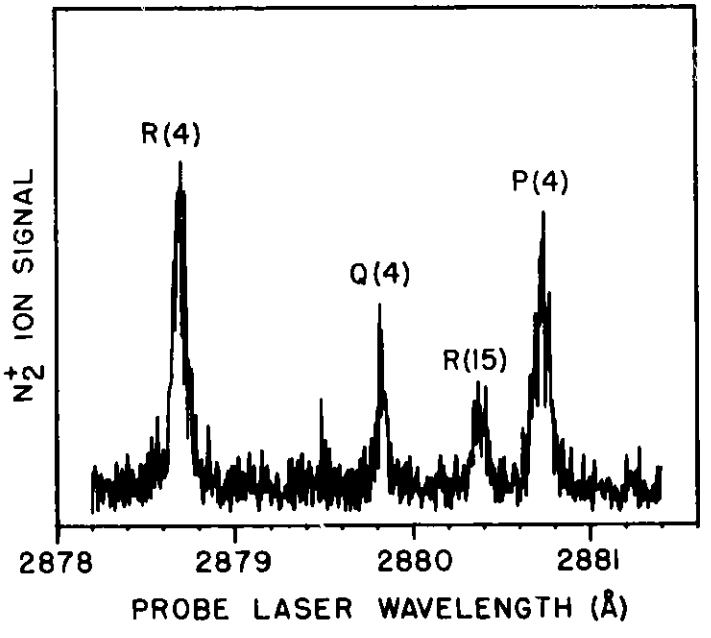

Fig. 1. Two-color ionization spectrum of N_2. The pump laser is tuned to the S(2) line of the a $^1\Pi_g$, v' = 1 ←---- X $^1\Sigma_g^+$, v" = 0 transition and the probe laser is scanned across the b $^1\Pi_u$, v' = 6 ←---- a $^1\Pi_g$, v" = 1 band. The R(15) line in the probe spectrum occurs as the S(13) line of the pump transition is overlapped with the S(2) line.

References

1. R. W. Field, Disc. Farad. Soc. 71, 111 (1981).
2. S. T. Pratt, E. D. Poliakoff, P. M. Dehmer, and J. L. Dehmer, J. Chem. Phys. 78, 65 (1983).
3. R. Mahon and F. S. Tomkins, IEEE J. Quantum Elec. 18, 913 (1982).

7. PHOTOELECTRON STUDIES OF RESONANT MULTIPHOTON IONIZATION OF MOLECULAR NITROGEN*

S. T. Pratt, P. M. Dehmer, and J. L. Dehmer

Introduction

In the present paper we present a study of (3 + 1) resonantly enhanced multiphoton ionization (REMPI) of N_2 via the b $^1\Pi_u$, v' = 0 - 5, c $^1\Pi_u$, v' = 0, 1, and c' $^1\Sigma_u^+$, v' = 0, 1 levels. The potential energy curves relevant to this study are shown in Figure 1. Nominally, the b $^1\Pi_u$ state is a valence state, and the c $^1\Pi_u$ and c' $^1\Sigma_u^+$ states are the $3p\pi_u$ and $4p\sigma_u$ Rydberg states, respectively, both of which have the N_2^+ X $^2\Sigma_g^+$ ion core.[1] However, in this spectral region the c $^1\Pi_u$ and b $^1\Pi_u$ states are strongly mixed by a homogeneous perturbation, as are the c' $^1\Sigma_u^+$ and b' $^1\Sigma_u^+$ states (the latter also nominally a valence state). Recently these perturbations have been extensively analyzed at the vibronic level by Stahel et al.[2] This analysis is quite useful in understanding the photoelectron branching ratios from several of these strongly perturbed levels. However, in some instances the situation is complicated further by strong local perturbations and predissociations that affect the rotational structure of these bands, as well as the photoelectron branching ratios, and these cases require going beyond the vibronic approximation.

REMPI Spectra

As an example of the REMPI spectra, Figure 2 shows the spectrum of the (3 + 1) ionization of N_2 via the b $^1\Pi_u$, v' = 5 level. The top frame shows the REMPI spectrum obtained using a commercial Molectron dye laser with a bandwidth of 0.3 cm^{-1}; the bottom frame shows the REMPI spectrum of the same band obtained using our modified Littman dye laser with a bandwidth of ~ 0.05 cm^{-1}. The rotational structure is much better resolved in the latter spectrum, making the 2:1 intensity alternations in the rotational structure due to the nuclear spin statistics quite apparent. Figure 3 shows the (3 + 1) ionization spectrum via the c' $^1\Sigma_u^+$, v' = 0 level. This "three-headed" band

*Summary of a paper published in J. Chem. Phys. 81, 3444 (1984).

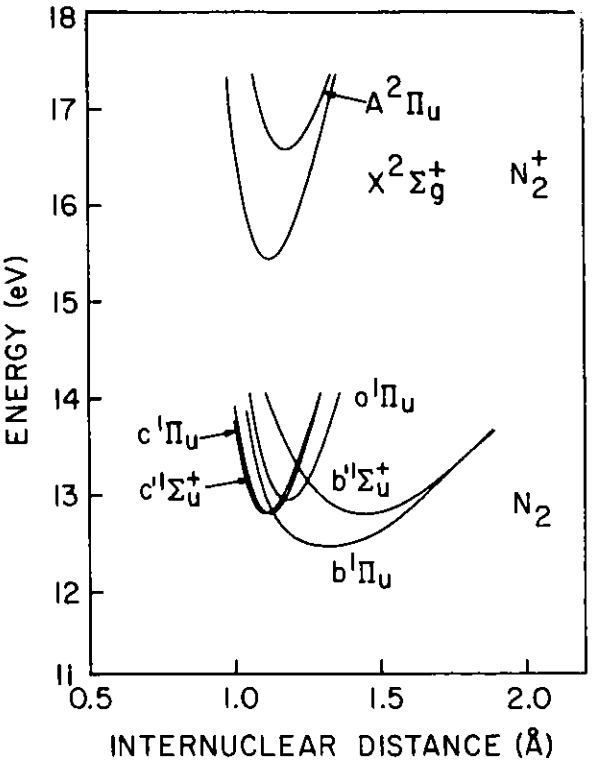

Fig. 1. Relevant potential energy curves of N_2 and N_2^+.

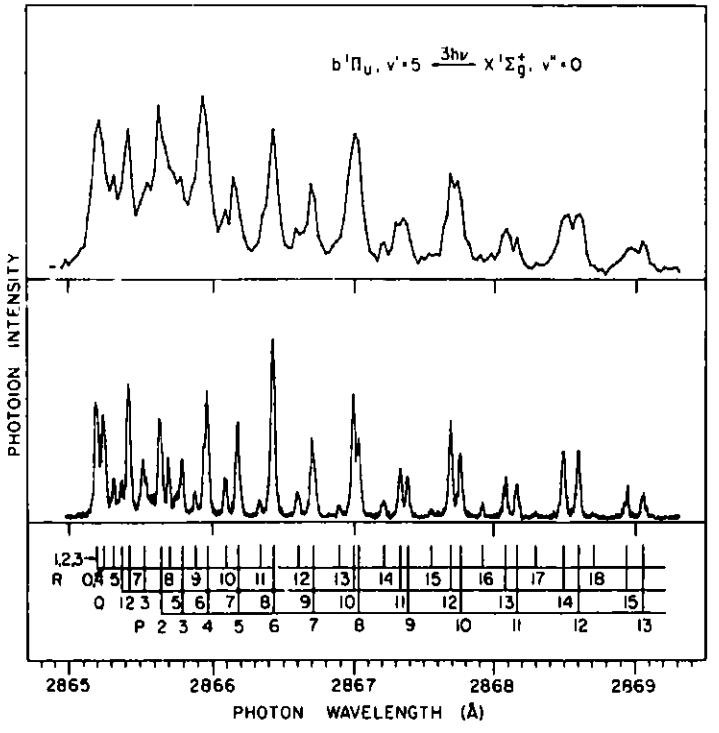

Fig. 2. The (3 + 1) ionization spectrum of N_2 via the $b\ ^1\Pi_u$, $v' = 5$ level. The top frame shows the low-resolution spectrum obtained using the commercial dye laser, and the bottom frame shows the high-resolution spectrum obtained using the modified Littman dye laser.

has been observed previously both in absorption and in emission. The intensity minimum in the R-branch between R(9) and R(10) is due to a strong perturbation by the b' $^1\Sigma_u^+$, v = 1 level, as is the disruption in the intensity alternation at the P(12) line of the P-branch, which is due to a blending of the P(11) and P(12) lines.

Photoelectron Spectra

The photoelectron spectra obtained at the R-branch bandheads of the b $^1\Pi_u$, v' = 0 - 5 ← X $^1\Sigma_g^+$, v" = 0 three-photon transitions are shown in Fig. 4 and the corresponding spectra for the c $^1\Pi_u$, v' = 0, 1 ← X $^1\Sigma_g^+$, v" = 0, and c' $^1\Sigma_u^+$, v' = 0, 1 ← X $^1\Sigma_g^+$ transitions are shown in Figures 5a and 5b, respectively.

According to the analysis of Stahel et al.,[2] the b $^1\Pi_u$, v' = 0 - 2 vibronic levels contain very little c $^1\Pi_u$ character, and are therefore relatively unperturbed, although the b $^1\Pi_u$, v' = 2 level shows indication of predissociation in the region of the bandhead. Thus, the photoelectron spectra obtained via all three levels should reflect relatively pure b $^1\Pi_u$ character. As is expected, photoionization from these levels populates a broad distribution of vibrational levels, in qualitative (but not quantitative) agreement with the corresponding Franck-Condon factors.

Unlike the b $^1\Pi_u$, v' = 0 - 2 photoelectron spectra, which exhibit a number of intense peaks, the b $^1\Pi_u$, v' = 3 - 5 photoelectron spectra each display a single intense $v^+ = 0$ peak, with very little intensity in any of the other peaks. This is somewhat surprising since the Franck-Condon factors predict a number of other moderately intense peaks. The single intense $v^+ = 0$ peak suggests that photoionization from these levels may be dominated by a v' = 0 Rydberg state component in the wavefunction of the intermediate state, since photoionization from a Rydberg level is expected to preserve the vibrational quantum number of the intermediate state. This is illustrated in the photoelectron spectrum obtained following photoionization of the c $^1\Pi_u$, v' = 0 Rydberg level (see Figure 5a). The analysis of Stahel et al.[2] shows that the b $^1\Pi_u$, v' = 3 - 5 wavefunctions contain 5.8%, 16.0%, and 22.1% c $^1\Pi_u$, v' = 0 character, respectively, and this admixture almost certainly accounts for the intense $v^+ = 0$ peak observed in the b $^1\Pi_u$, v' = 3 - 5 photoelectron spectra.

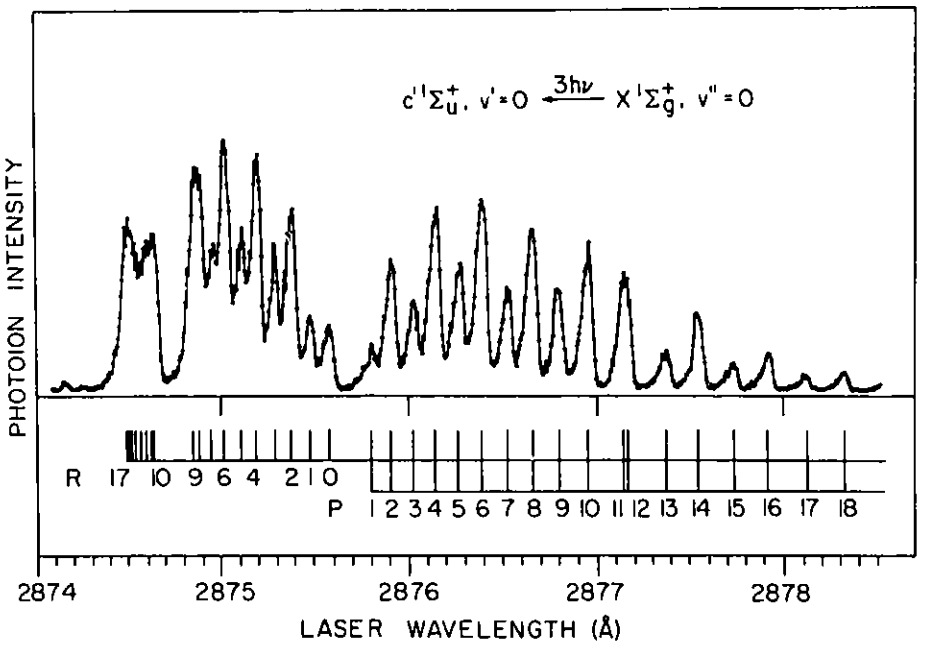

Fig. 3. High-resolution (3 + 1) ionization spectrum of N_2 via the c' $^1\Sigma_u^+$, v' = 0 level.

While the c $^1\Pi_u$, v' = 0 photoelectron spectrum shown in Figure 5a can be understood by assuming that photoionization from a Rydberg level preserves the vibrational quantum number and the electronic state of the ion core, the c $^1\Pi_u$, v' = 1 photoelectron spectrum cannot be viewed in this way. Although the latter spectrum does display a prominent N_2^+ X $^2\Sigma_g^+$, v^+ = 1 peak, the A $^2\Pi_u$, v^+ = 0 peak is equally intense. Production of the A $^2\Pi_u$ electronic state from the c $^1\Pi_u$ state requires a two-electron transition. The appearance of the strong A $^2\Pi_u$, v^+ = 0 peak can be rationalized by the existence of 7% o $^1\Pi_u$, v' = 0 state character in the c $^1\Pi_u$, v' = 1 wavefunction. Similarly, the appearance of the A $^2\Pi_u$, v^+ = 1 peak in the photoelectron spectrum may be due to the existence of 2% o $^1\Pi_u$, v'=1 character in the c $^1\Pi_u$, v' = 1 wavefunction. However, the large relative intensity of the A $^2\Pi_u$ peaks with respect to the X $^2\Sigma_g^+$ peaks is more difficult to understand, unless the A $^2\Pi_u$ ← o $^1\Pi_u$ electronic matrix element is very much larger than the X $^2\Sigma_g^+$ ← c $^1\Pi_u$ matrix element.

The photoelectron spectra obtained at the R-branch bandheads of the c' $^1\Sigma_u^+$, v' = 0, 1 ← X $^1\Sigma_g^+$, v" = 0 three-photon transitions shown in Figure 5b are more difficult to explain. While the X $^2\Sigma_g^+$, v^+ = 0 peak is the most intense in the v' = 0 photoelectron spectrum, in agreement with Franck-Condon factors, the A $^2\Pi_u$, v^+ = 0, 1 photoelectron peaks are much larger than expected for

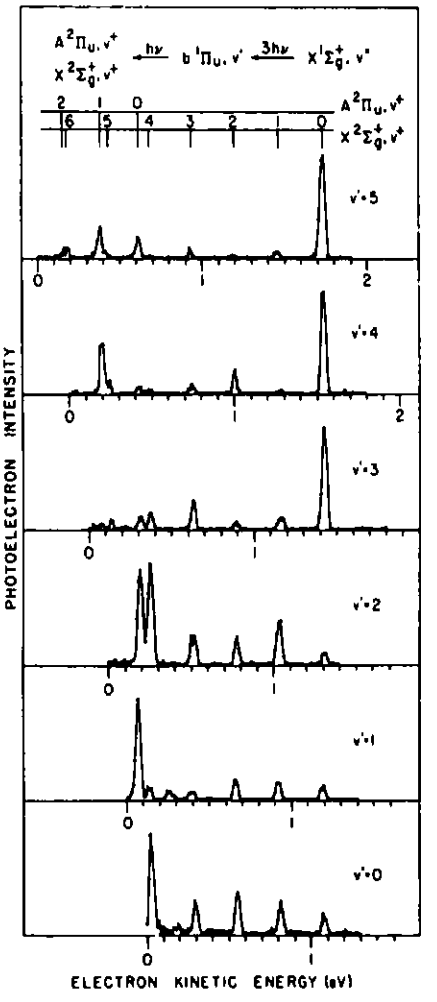

Fig. 4. Photoelectron spectra of N_2 following (3 + 1) ionization of N_2 via the b $^1\Pi_u$, v' = 0 - 5 levels. The impurity peaks at 0.26 eV and 0.50 eV in the v' = 1 spectrum are due to (2 + 1) ionization of O_2.

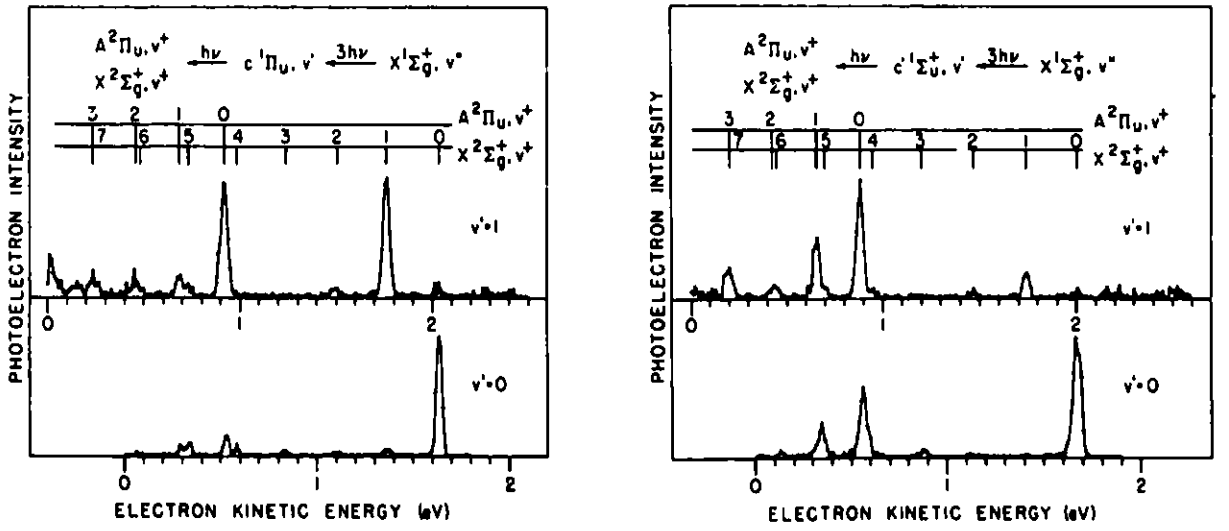

(a) (b)

Fig. 5. Photoelectron spectra of N_2 following (3 + 1) ionization of N_2 via the (a) c $^1\Pi_u$, v' = 0, 1 levels and (b) the c' $^1\Sigma_u^+$, v' = 0, 1 levels.

photoionization from a Rydberg state converging to the X $^2\Sigma_g^+$ state of N_2^+. This indicates that the c' $^1\Sigma_u^+$, v' = 0 Rydberg state ion core does not act like a spectator in the ionizing transition as it did in the o $^1\Pi_u$ studies reported previously.[3] The c' $^1\Sigma_u^+$, v' = 1 photoelectron spectrum in Figure 5b is even more intriguing, as the X $^2\Sigma_g^+$, v^+ = 1 peak is completely overshadowed by the intense A $^2\Pi_u$, v^+ = 0, 1 peaks.

References

1. A. Lofthus and P. H. Krupenie, J. Phys. Chem. Ref. Data 6, 113 (1977).
2. D. Stahel, M. Leoni, and K. Dressler, J. Chem. Phys. 79, 2541 (1983).
3. S. T. Pratt, P. M. Dehmer, and J. L. Dehmer, J. Chem. Phys. 80, 1706 (1984).

8. MULTIPHOTON IONIZATION AND DISSOCIATION OF Xe_2

S. T. Pratt, P. M. Dehmer, and J. L. Dehmer

Recently, Gornik et al.[1] observed two-photon excitation to dissociative states of Xe_2 in the region of the Xe $6s[3/2]_1^\circ$ and Xe $6s[3/2]_2^\circ$ levels in a high-pressure (50-500 Torr) cell. The dominant decay mechanism for these states of the g symmetry is dissociation into either a $6s[3/2]_1^\circ$ or $6s[3/2]_2^\circ$ Xe atom plus a ground state Xe atom followed by recombination of the excited atom and fluorescence.

In the present work, we have examined the dissociative states of the g symmetry in the region of the $6s[3/2]_1^\circ$ level using two-photon resonant, three-photon ionization of Xe_2 formed in a supersonic molecular beam, and monitoring either the photoion or photoelectron signal. Using a time-of-flight mass spectrometer, we recorded the photoion spectrum by monitoring either the Xe^+ or Xe_2^+ ion signal as the wavelength of the frequency-doubled dye laser was scanned. The laser was then tuned to the wavelength of interest and the photoelectron spectrum was recorded. Photoion spectra were recorded using both a 35-μm jet and an effusive jet.

Photoion spectra obtained by monitoring the Xe_2^+ ion signal were very weak and showed no structure. This is not surprising, as the two-photon intermediate levels are known to be purely dissociative.[1] Thus, at the laser powers of the present studies, dissociation is a much faster process than absorption of the third photon necessary for ionization. However, photoion spectra obtained by monitoring the Xe^+ ion signal were relatively strong and displayed broad structure. No such structure was observed with an effusive jet at the equivalent chamber pressure, indicating that the Xe^+ ion signal observed in the supersonic jet spectra is due to two-photon dissociation of Xe_2 into Xe $6s[3/2]_1^\circ$ + Xe $^1S_0$, followed by a single-photon ionization of the excited Xe atom.

This mechanism was verified by measuring the photoelectron spectrum at 2910 Å, which is in the middle of a broad feature. Figure 1 shows two photoelectron spectra, both obtained with the 35-μm jet. The lower spectrum was obtained under conditions designed to maximize the Xe_2 contribution to the beam (0.64 Atm. stagnation pressure), and at relatively lower power (0.25 mJ),

while the upper spectrum was obtained under conditions designed to maximize three-photon nonresonant ionization of atomic Xe (0.14 Atm. stagnation pressure, 1.9 mJ). By analyzing the energetics[2] of the reactions

$$Xe_2 \xrightarrow{2h\nu} Xe\ {}^1S_0 + Xe\ 6s[3/2]_1^0 \xrightarrow{h\nu} Xe\ {}^1S_0 + Xe^+\ {}^2P_{3/2} + e^-(0.567\ eV) \quad (1)$$

$$Xe \xrightarrow{3h\nu} Xe^+\ {}^2P_{3/2} + e^-(0.652\ eV), \quad (2)$$

it is possible to assign the lower energy peak to mechanism 1 and the higher energy peak (which is very weak in the lower spectrum) to mechanism 2.

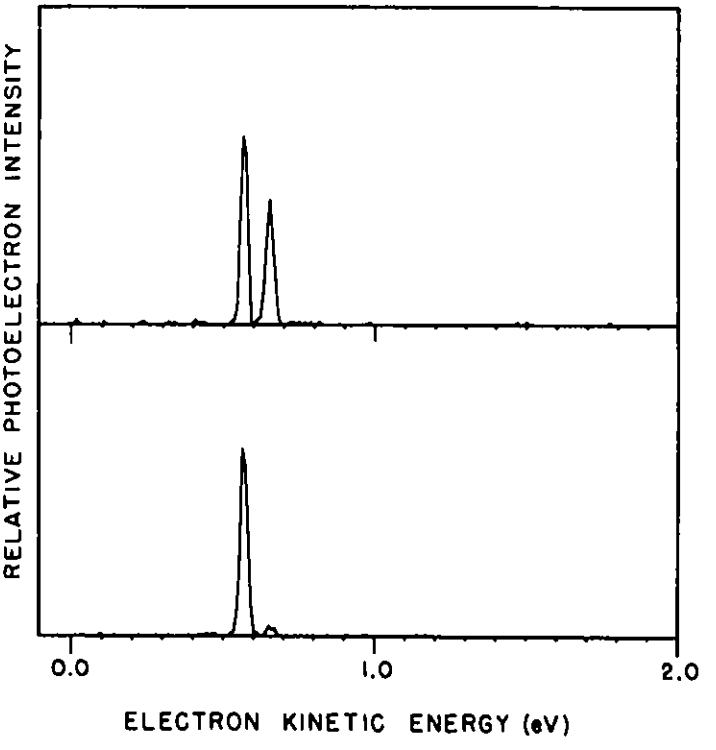

Fig. 1. Photoelectron spectra obtained at a laser wavelength of 2910 Å using a 35-μm jet. Upper spectrum: 0.14 Atm. stagnation pressure, 1.9 mJ; lower spectrum: 0.64 Atm. stagnation pressure, 0.25 mJ.

These results suggest an intriguing general method for distinguishing between dissociative states with different dissociation limits. For example, in the wavelength region near that of the present study, one can access dissociative states with the Xe $6s[3/2]_2^o$ + Xe $^1S_0$ dissociation limit. In the event that these states are overlapped with those of the present study, the photoelectron spectrum could be used to distinguish between the states with different dissociation limits. In this case, electrons obtained from photoionization of the $6s[3/2]_2^o$ level would be 0.121 eV slower than those from the $6s[3/2]_1^o$ level.[2]

References

1. W. Gornik, E. Matthias, and D. Schmidt, J. Phys. B 15, 3413 (1982).
2. C. E. Moore, Nat. Bur. Stand. Circ. 467, Vol. III (1949).

9. PHOTOELECTRON ANGULAR DISTRIBUTIONS FROM RESONANT MULTIPHOTON IONIZATION OF ATOMIC CARBON

S. T. Pratt, P. M. Dehmer, and J. L. Dehmer

In this paper, we report results obtained using resonantly enhanced multiphoton ionization (REMPI) to detect both ^3P and ^1D carbon atoms formed by UV multiphoton dissociation of CCl_4. In addition, we present photoelectron angular distributions for two-photon resonant, three-photon ionization via the $3p\ ^1S_0$ and $3p\ ^3D_2$ levels using both linear and circular polarized light. A schematic diagram of the energy levels of interest is shown in Figure 1.

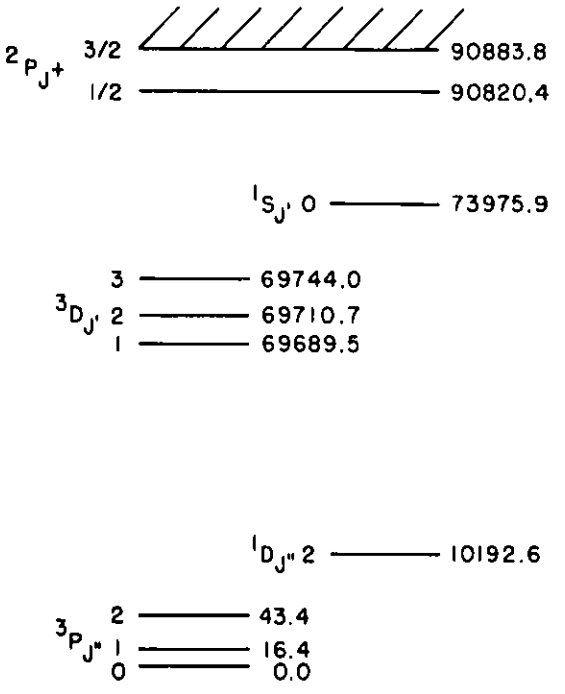

Fig. 1. Schematic energy level diagram for atomic carbon. Note that the energy axis is not to scale. Energies are taken from Reference 3.

The apparatus used in these studies has been described in detail previously.[1] It consists of a Nd:YAG pumped dye laser, a hemispherical electron energy analyzer, and a time-of-flight mass spectrometer. Typically, 0.2 mJ (for triplet studies) or 0.6 mJ (for singlet studies) of the frequency-doubled dye-laser output was separated from the fundamental and focussed by a 150-mm lens onto a molecular beam of CCl_4. As in the experiments described by Das et al.,[2] the same laser was used to photodissociate the CCl_4 and to resonantly ionize the carbon atoms produced. The REMPI spectra were recorded by scanning the dye laser wavelength and monitoring the C^+ ion signal. The laser was then tuned to the wavelength of the two-photon transition of

interest, and the photoelectron spectrum was recorded under the same conditions.

The photoelectron spectra from 0.0 to 4.5 eV recorded at the wavelengths corresponding to the $^3D_2 \leftarrow {}^3P_0$ and $^1S_0 \leftarrow {}^1D_2$ transitions display a single intense peak at 1.70 eV and 1.86 eV, respectively, corresponding to the production of $C^+ {}^2P$. The spin-orbit splitting of the $C^+ {}^2P_{3/2}$ levels is too small (8 meV) (see, for example, Manson and Starace[3]) to be resolved at the present limit of resolution (~40 meV). The photoelectron spectra also show a number of other features that are almost certainly correlated with the photoionization of the fragments CCl, CCl_2, and CCl_3, all of which are observed in the REMPI mass spectra.

Photoelectron angular distributions were determined in different manners for linear and circular polarized light. In the former case, the linear polarization from the dye laser was rotated with a Fresnel-Rhomb or a Babinet-Soleil compensator, and the photoelectron signal was measured as a function of the angle between the polarization axis of the light and the detector. For circular polarized light, the linear polarization of the dye laser was converted to circular polarization using the compensator, and the photoelectron signal was measured as a function of angle between the propagation direction of the light and the detector.

The REMPI spectrum obtained from photodissociation of CCl_4 followed by two-photon resonant, three-photon ionization of atomic carbon via the $3p\ {}^3D_{J'} \leftarrow {}^3P_{J''}$ transitions is shown in Figure 2. As is seen from the spectrum, the fine structure of the lower and upper states produces seven allowed transitions. The relative intensities of the peaks are consistent with those of Das et al.[2] obtained using two-photon laser-induced fluorescence following photodissociation of C_3O_2.

The photoelectron angular distribution obtained following two-photon resonant, three-photon ionization of atomic carbon via the $^1S_0 \leftarrow {}^1D_2$ transition using linear polarized light shown in Figure 3. Because the $^1S_0$ level must have M = 0, photoelectron angular distributions from this three-photon process can be treated as arising from single-photon ionization from the $^1S_0$ level. It is well known that photoelectron angular distributions following single-photon ionization of a randomly oriented sample using linear

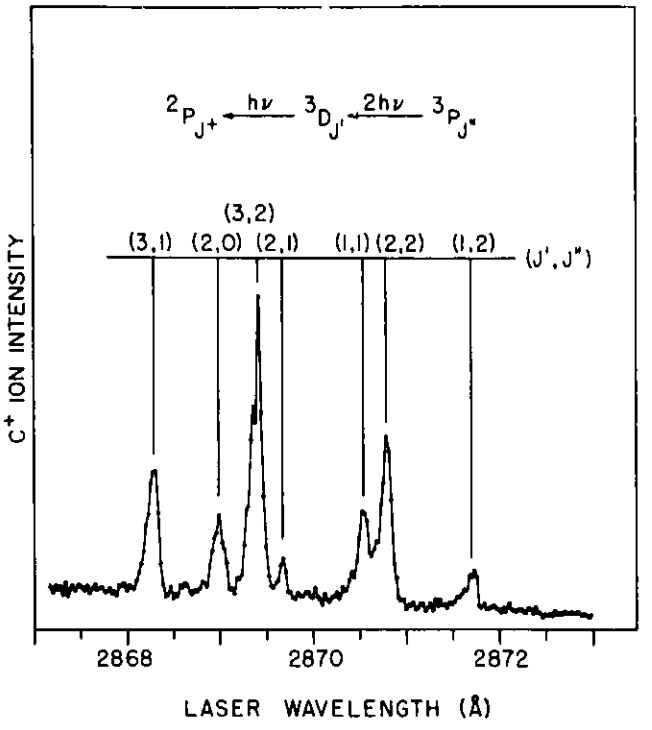

Fig. 2. Two photon resonant, three photon ionization spectrum of atomic carbon via the $^3D_{J'} \leftarrow {}^3P_{J''}$ transition. Atomic carbon was produced by UV multiphoton dissociation of CCl_4.

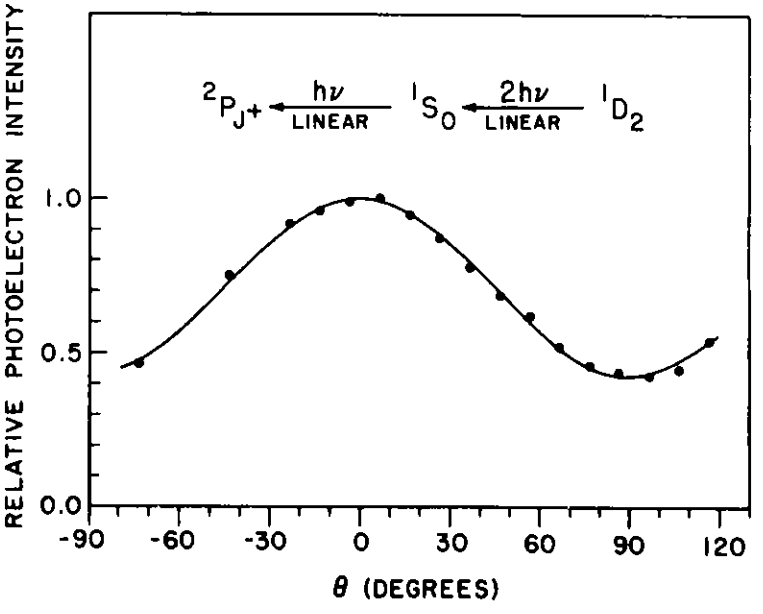

Fig. 3. Photoelectron angular distribution of two photon resonant, three photon ionization of atomic carbon via the $^1S_0 \leftarrow {}^1D_2$ transition using linear polarized light. Data points (+). The solid curve is a best fit to the form $1 + A_2 \cos^2\theta$, where $A_2 = 1.35 \pm 0.2$.

polarized light must have the functional form[3]

$$I(\theta) \propto 1 + A_2 \cos^2\theta. \qquad (1)$$

Here I is the photoelectron intensity, θ is the angle between the polarization axis of the light and the detector, and A_2 is an asymmetry parameter. The value of A_2 obtained by a least-squares fit to the data shown in Figure 3 is $A_2 = 1.35 \pm 0.2$. This corresponds[3] to $\beta = 0.62 \pm 1$. The fit is extremely good.

The photoelectron angular distributions obtained following two-photon resonant, three-photon ionization of carbon via the $^3D_2 \leftarrow {}^3P_0$ transition using linear and circularly polarized light are shown in Figures 4 and 5, respectively. It is clear from the data that the angular distributions obtained using linear and circular polarized light are quite different. While the $^3P_0$ ground state has J" = M" = 0 and is therefore unaligned, the two-photon transition to the $^3D_2$ level can induce alignment. In this case, the form of the photoelectron angular distribution is[4]

$$I(\theta) = 1 + A_2 \cos^2\theta + A_4 \cos^4\theta + A_6 \cos^6\theta \qquad (2)$$

for linear polarized light, and

$$I(\theta_2) = 1 + A_2' \cos^2\theta_Z + A_4' \cos^4\theta_Z + A_6' \cos^6\theta_Z \qquad (3)$$

for circular polarized light. Here the A_n and A_n' are higher-order asymmetry parameters, and in Equation (3) θ_Z is the angle between the propagation direction of the circular polarized light and the detector. Although the relation of A_2 and A_2' is known for single-photon ionization,[3] where the higher-order terms are zero, in general the derivation of the relation among the higher order A_n and A_n' is non-trivial. (See Reference 4. Note, however, that the form of the angular distribution for circular polarized light [Ref. 4, Equation (63)] is valid only for the single-electron model.)

The solid curves in Figures 4 and 5 were obtained by a least squares fit of the first two terms in Equations (2) and (3), respectively, that is, ignoring the $\cos^4\theta$ and $\cos^6\theta$ terms. The values of the asymmetry parameters so

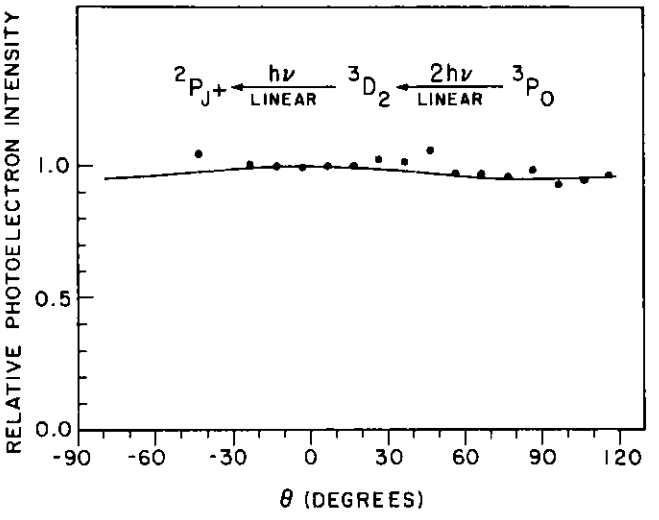

Fig. 4. Photoelectron angular distribution of two photon resonant, three photon ionization of atomic carbon via the $^3D_2 \leftarrow {}^3P_0$ transition using linear polarized light. Data points (+). The solid curve is a best fit to the form $1 + A_2 \cos^2\theta$, where $A_2 = 0.05 \pm 0.1$.

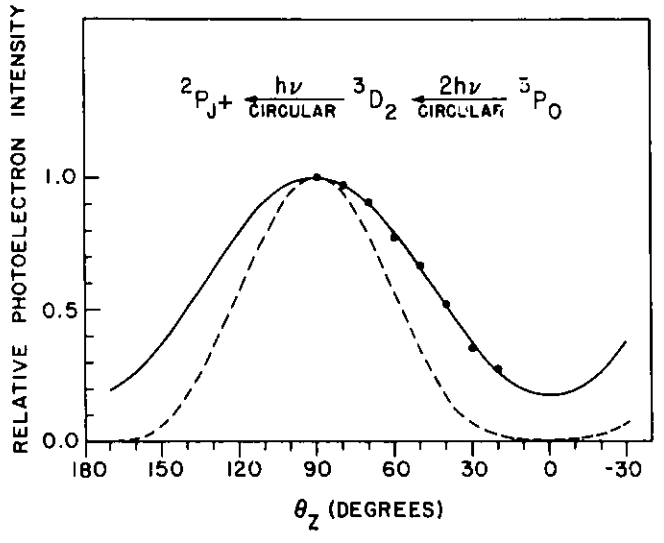

Fig. 5. Photoelectron angular distribution of two photon resonant, three photon ionization of atomic carbon via the $^3D_2 \leftarrow {}^3P_0$ transition using circular polarized light. Data points (+). The solid curve is a best fit to the form $1 - A_2' \cos^2\theta_Z$, where $A_2' = -0.83 \pm 0.1$, and the dashed line follows the functional form $\sin^4\theta_Z$.

obtained are $A_2 = 0.05 \pm 0.1$ for Figure 4 and $A_2' = -0.83 \pm 0.1$ for Figure 5. These values correspond to $\beta = 0.03 \pm 0.1$ and $\beta = 1.525 \pm 0.1$, respectively. Clearly the data indicate that A_4, A_4', A_6, and A_6' are small. The reason for the absence of higher-order terms is not certain at this time. However, it is clear that the present results cannot be interpreted within a single-electron framework.

While our understanding of these results is somewhat limited, we feel that they provide an interesting and tractable problem for future theoretical work. The results via the $^3D_2$ level will require an analysis in terms of the resonant multiphoton process. However, because the $^1S_0$ level cannot be

aligned, the angular distribution from that level should be interpretable in terms of single-photon ionization from an excited initial state.

References

1. S. T. Pratt, E. D. Poliakoff, P. M. Dehmer, and J. L. Dehmer, J. Chem. Phys. 78, 65 (1983).
2. P. Das, G. Ondrey, N. van Veen, and R. Bersohn, J. Chem. Phys. 79, 724 (1983).
3. S. T. Manson and A. F. Starace, Rev. Mod. Phys. 54, 389 (1982).
4. P. Lambropoulos, Adv. At. Mol. Phys. 12, 87 (1976).

10. ANGLE-RESOLVED PHOTOELECTRON STUDY OF THE VALENCE LEVELS OF BF_3 IN THE RANGE 17 ≤ hν ≤ 28 eV*

J. L. Dehmer, A. C. Parr,† S. H. Southworth, and D. M. P. Holland‡

Photoelectron branching ratios and angular distributions have been measured for the six outermost levels of BF_3 in the range 17 ≤ hν ≤ 28 eV with the use of synchrotron radiation. Comparisons are made with a recent multiple-scattering model calculation which indicates that a shape resonance in the e' electronic continuum should appear in five of the six channels studied. Good agreement between experiment and theory is found in a majority of the comparisons; however, experimental evidence for the expected e' shape resonance is clear in some cases but absent in others. The results are discussed in the context of other cases in which shape resonances, well known from inner-shell spectra, are obscured in valence-shell properties. Experiments that would help clarify the role of the e' shape resonance in the photoionization dynamics of BF_3 are suggested.

---

*Abstract of an article published in Phys. Rev. A 30, 1783 (1984).
†National Bureau of Standards, Gaithersburg, MD 20899.
‡Daresbury Laboratory, Daresbury, Warrington WA4 4AD, England.

11. PHOTOELECTRON BRANCHING RATIOS AND ASYMMETRY PARAMETERS FOR THE TWO OUTERMOST MOLECULAR ORBITALS OF HYDROGEN CYANIDE*

D. M. P. Holland,† A. C. Parr,‡ and J. L. Dehmer

Triply differential photoelectron spectroscopy has been performed on hydrogen cyanide in the photon energy range 14.5 to 24 eV, using synchrotron radiation. Photoelectron branching ratios and asymmetry parameters are presented for the two outermost molecular orbitals. The vibrationally resolved branching ratio $X\ ^2\Pi\ (v_3 = 1)/(v_3 = 0)$ exhibits strong non-Franck-Condon behavior from threshold to approximately 19 eV. The results are discussed in relation to similar studies on the isoelectronic molecules, N_2, CO, and C_2H_2. The evidence suggests that the prominent non-Franck-Condon feature observed in the $HCN^+\ X\ ^2\Pi$ channel may arise, at least in part, from a shape resonantly enhanced autoionizing state converging to a higher ionization potential.

---

*Abstract of an article published in J. Phys. B 17, 1343 (1984).
†Daresbury Laboratory, Daresbury, Warrington WA4 4AD, England
‡National Bureau of Standards, Gaithersburg, MD 20899.

12. PHOTOELECTRON BRANCHING RATIOS AND ASYMMETRY PARAMETERS OF THE TWO OUTERMOST MOLECULAR ORBITALS OF METHYL CYANIDE*

D. M. P. Holland,† A. C. Parr,‡ and J. L. Dehmer

Vibrationally resolved photoelectron branching ratios and asymmetry parameters have been determined for the two outermost molecular orbitals of methyl cyanide. The results are discussed briefly within the context of similar studies on cyanogen and hydrogen cyanide, and in relation to structures exhibited in the photoionization efficiency curve.

---

*Abstract of an article published in J. Electron Spectrosc. 34, 87 (1984).
†Daresbury Laboratory, Daresbury, Warrington WA4 4AD, England.
‡National Bureau of Standards, Gaithersburg, MD 20899.

13. FLUORESCENCE EXCITATION STUDIES OF MOLECULAR PHOTOIONIZATION IN EXTERNAL ELECTRIC FIELDS*

E. D. Poliakoff,† J. L. Dehmer, A. C. Parr,‡ and G. E. Leroi¶

Using molecular nitrogen as an example, we show that fluorescence excitation spectroscopy can be used to measure partial photoionization cross sections of free molecules in external electric fields. The production of the $N_2^+(B^2\Sigma_u^+)$ state was studied and the threshold for this process was found to shift linearly with the square root of the applied field. This behavior is compared with the hydrogenic case and with previously studied systems.

---

*Abstract of an article published in Chem. Phys. Lett. 111, 128 (1984).
†Department of Chemistry, Boston University, Boston, MA 02215.
‡National Bureau of Standards, Gaithersburg, MD 20899.
¶Department of Chemistry, Michigan State University, East Lansing, MI 48824.

14. SHAPE RESONANCES IN MOLECULAR FIELDS*

J. L. Dehmer

A shape resonance is a quasibound state in which a particle is temporarily trapped by a potential barrier (i.e., the "shape" of the potential), through which it may eventually tunnel and escape. This simple mechanism plays a prominent role in a variety of excitation processes in molecules, ranging from vibrational excitation by slow electrons to ionization of deep core levels by x-rays. Moreover, their localized nature makes shape resonances a unifying link between otherwise dissimilar circumstances. One example is the close connection between shape resonances in electron-molecule scattering and in molecular photoionization. Another is the frequent persistence of free-molecule shape resonant behavior upon adsorption on a surface or condensation into a molecular solid. The main focus of the full article* is a discussion of the basic properties of shape resonances in molecular fields, illustrated by the more transparent examples studied over the last ten years. Other aspects discussed are vibrational effects of shape resonances, connections between shape resonances in different physical settings, and examples of shape resonant behavior in more complex cases, which form current challenges in this field.

---

*Abstract of an article published in Resonances in Electron-Molecule Scattering, van der Waals Complexes, and Reactive Chemical Dynamics, ACS Symposium Series, No. 263, D. G. Truhlar, Editor (American Chemical Society, Washington, D.C., 1984), Chapter 8, pp. 139-163.

15. COMPLETE DIPOLE OSCILLATOR STRENGTH DISTRIBUTION AND ITS MOMENTS FOR N_2*

W. M. Kosman† and Scott Wallace‡

The complete dipole oscillator strength distribution for N_2 has been calculated using the multiple scattering model. From this, the moments of the distribution, $S(\mu)$ and $L(\mu)$, have been computed for $-6 \leq \mu \leq 2$. The results are analyzed by decomposing the total moments according to the contributions from various subshells and also according to the contributions from various spectral ranges, e.g., discrete versus ionizing excitations. Since many physical properties depend on these moments, this analysis can pinpoint the spectral ranges with the greatest influence. Special attention is devoted to the distinctly molecular effects on the dipole oscillator strength distribution and its momerts, particularly for those channels affected by shape resonances. The Rydberg series, for example, are significantly affected. This analysis offers an explanation for the weakness of certain dipole-allowed Rydberg series and suggests a tentative new assignment for Worley's third series.

---

*Abstract of a paper to be published in J. Chem. Phys.

†Faculty Research Participant, Division of Educational Programs, Argonne National Laboratory. Permanent address: Department of Chemistry, Valparaiso University, Valparaiso, IN 46383.

‡Department of Chemistry, Boston University, Boston, MA 02215. Present address: Goddard Space Flight Center, Building 23, Room W425, Greenbelt, MD 20771.

16. EIGENCHANNEL QUANTUM DEFECT THEORY OF OPEN-SHELL ATOMS: AUTOIONIZATION RESONANCES AND EIGENPHASE SHIFTS OF CHLORINE*

Z.-W. Wang† and K. T. Lu‡

Multichannel quantum defect theory is applied to the analysis of Rydberg levels and autoionization resonances of the chlorine atom. The analysis shows that recently observed photoionization cross sections above the $3p^4(^3P)$ threshold of the chlorine ion may be interpreted in terms of unresolved groups of resonances with three different total angular momenta J and approximately the same energy. Experimental data of Rydberg levels were used to determine the eigenphase shift (eigen-quantum defect) of electron-ion scattering wave functions. The LS coupling scheme is assumed for the electron + ion compound state. The channel interaction strengths and dipole matrix elements of even parity states relevant to electron-ion collisional and recombination processes are obtained.

*Abstract of a paper to be published in Phys. Rev. A.

†Visiting Foreign Scholar. Permanent address: Institute of Atomic and Molecular Physics, Jilin University, Changchun, People's Republic of China.

‡Graduate School, Academia Sinica, Beijing, People's Republic of China.

17. EIGENCHANNEL QUANTUM DEFECT THEORY OF OPEN-SHELL ATOMS: CALCULATION OF $3p^4(^3P)ns$ RYDBERG SPECTRA OF THE CHLORINE ATOM*

Z.-W. Wang† and K. T. Lu‡

Rydberg spectra of the chlorine atom, $3s^2 3p^4(^3P)ns$, J = 1/2, 3/2, and 5/2, are calculated by use of an eigenchannel quantum defect method. The results indicate that the channel interactions due to electrostatic and spin-orbit potentials are weak. The effect due to channel interaction of the $3s3p^6$ configuration is completely negligible. Agreement with emission data is excellent ($\lesssim$ 0.2% accuracy except for the lowest n = 4 levels). Autoionization resonances are predicted.

---

*Abstract of a paper to be published in Phys. Rev. A.

†Visiting Foreign Scholar. Permanent address: Institute of Atomic and Molecular Physics, Jilin University, Changchun, People's Republic of China.

‡Graduate School, Academia Sinica, Beijing, People's Republic of China.

18. ELECTRON IMPACT SPECTROSCOPY OF METHANE, SILANE, AND GERMANE*

M. A. Dillon, R.-G. Wang†, and David Spence

Electronic spectra of the group IV_a hydrides, i.e., methane (CH_4), silane (SiH_4), and germane (GeH_4) have been investigated by means of electron energy loss spectroscopy in an energy range that includes all single-electron excitation from the valence shell. Electron impact spectra of the three gases recorded using electrons of 200-eV incidence are displayed in Figures 1-3. For comparison with CH_4, the spectrum of CD_4 is presented in Figure 4. The conditions employed have been chosen to favor the excitation of states by direct scattering and to exclude those transitions requiring an exchange mechanism. Hence, all featues in Figures 1-3 are related to vertical transitions to symmetry allowed and forbidden singlet states. At small scattering angles, the intensity distribution, I, is given by the Born approximation as

$$I \propto K^{2(M-2)}, \tag{1}$$

where in atomic units

$$K = 2\left[E_0 - 1/2W - E_0^{1/2}(E_0-W)^{1/2}\cos\theta\right]^{1/2} \tag{2}$$

is the momentum transferred when a projectile electron with an incident energy E_0 is scattered through an angle θ and suffers an energy loss W. The integer M is called the transfer number; in case of closed-shell molecules exhibiting geometric symmetry, its value depends only on the irreducible representation of the excited state.

---

*Summary of the results from the following two articles: Electron Impact Spectroscopy of Methane and Methane-d_4, by Michael A. Dillon, R.-G. Wang, and David Spence, J. Chem. Phys. 80, 5581 (1984); and Electron Impact Spectroscopy of Silane and Germane, by Michael A. Dillon, R.-G. Wang, Z.-W. Wang, and David Spence, submitted for publication.

†Visiting Foreign Scholar. Permanent address: Department of Physics, Chengdu University of Science and Technology, Chengdu, Sichuan, People's Republic of China.

Fig. 1. Electron energy-loss spectra of methane obtained for an incident energy of 200 eV. The numbers to the right of K refer to values of K at excitation energies of 10 eV and 20 eV, respectively.

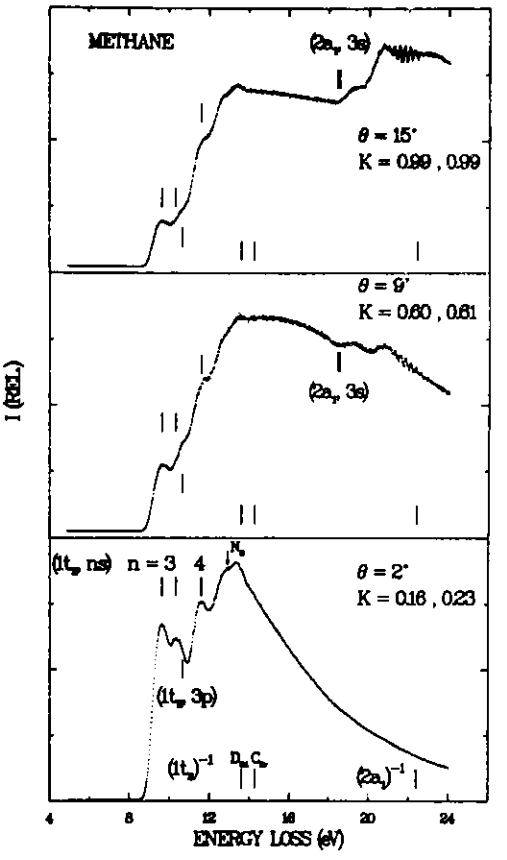

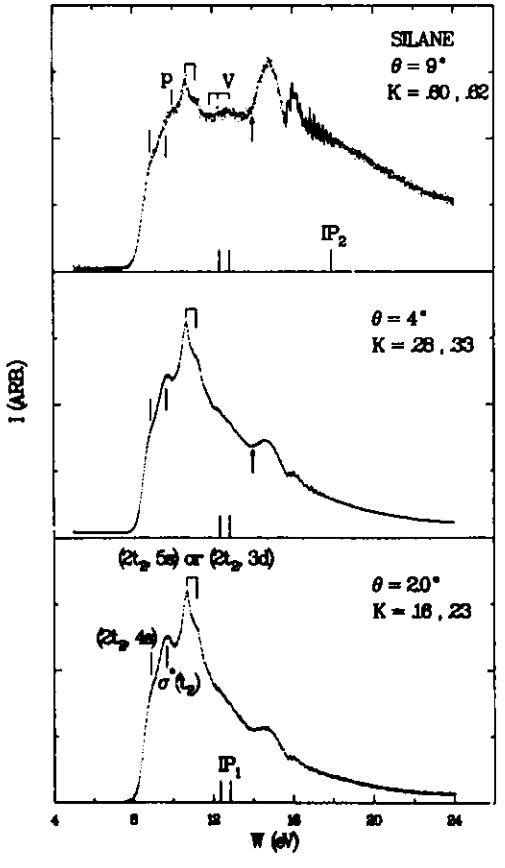

Fig. 2. Electron impact spectra of silane recorded with 200-eV incident electron energies. The scattered electron intensity at W = 20 eV varies by a factor of 12 over the angular range shown in the figure. Values of K refer to W = 10 eV and 20 eV, respectively. The arrow is positioned 3.8 eV relative to the zero energy of the $^2A_1$ positive ion.

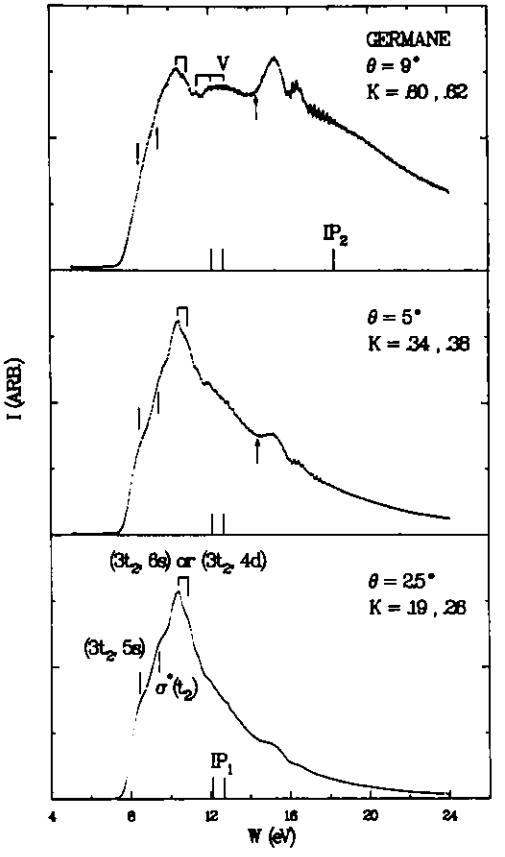

Fig. 3. Electron impact spectra of germane recorded with 200-eV incident electron energies. The scattered electron intensity at W = 20 eV varies by a factor of 10 over the angular range depicted in the figure. Values of K refer to W = 10 eV and 20 eV, respectively. The arrow is positioned 3.95 eV relative to the zero energy of the $^2A_1$ positive ion.

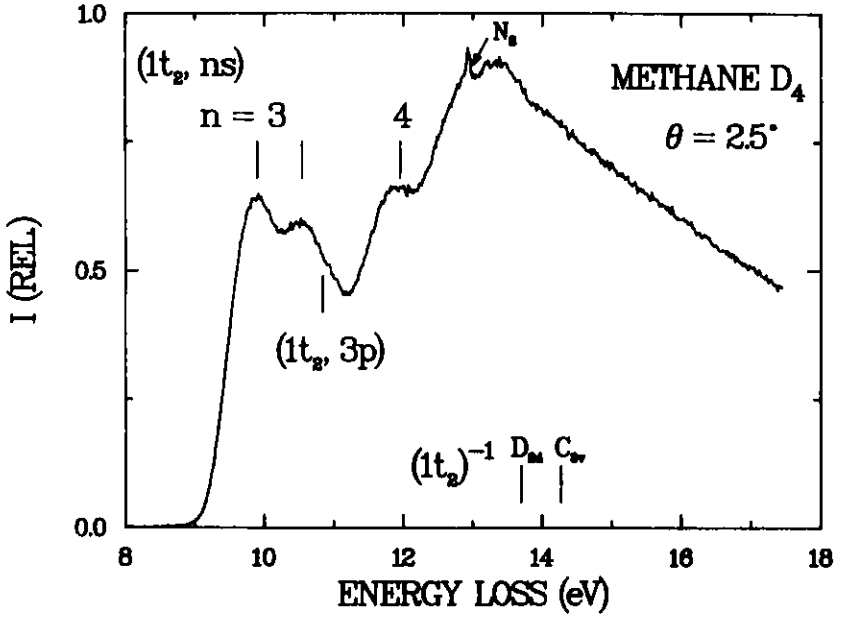

Fig. 4. Electron energy-loss spectrum of methane-d_4 obtained for an incident energy of 200 eV.

The ground-state configuration and ordering of all three molecules is $(1a_1)^2 \cdots (ma_1)^2(nt_2)^6\ {}^1A_1$ in Td symmetry. The lowest manifold of excited states arise from orbital transitions of the type s, p, d $\leftarrow t_2$. The promotion of a bonding t_2 valence electron to non-bonding Rydberg orbitals expands the molecular framework of these molecules, rendering their electronic spectra dissociative below the first ionization limit. Moreover, removal of the triply degenerate t_2 electron splits the $^2T_2$ ion core into three Jahn-Teller components, only two of which are easily seen in any of the photoelectron spectra. Thus, the spectra below the first IP in Figures 1-4, which we designate region 1, consist almost entirely of diffuse structures. The location of salient features in this energy range are listed in Tables 1 and 2. Term values were computed from the centroids of the respective positive-ion spectra. The term value for the first structure in each spectrum is ~ 4 eV, which is consistent with a s $\leftarrow t_2$ Rydberg transition. A structure of some interest at 11-12 eV in Figure 1 is amplified in Figure 5, which depicts a diffuse vibrational progression with a spacing identical to that observed in the photoelectron spectrum of methane. This may be the second member of the s $\leftarrow t_2$ Rydberg series converging to the $^2T_2$ positive ion.

The ~ 4 eV energy interval preceding the second IP, designated region 2, is the range of optically allowed autoionizing Rydberg series p, d, $\leftarrow a_1$ converging to the $^2A_1$ ground state ion in all three molecules. At larger scattering angles, members of the forbidden autoionizing series s, d $\leftarrow a_1$ are expected to substantially overlap those of the allowed series. The first band encountered in Figures 1-3 is easily identified as the first member of the s $\leftarrow a_1$ series by its term value of ~ 4 eV relative to the second IP. The 15° spectrum in Figure 1 and the 9° spectra in Figures 2 and 3 reveal the presence of much discrete structure converging to the respective $^2A_1$ ion states. The regions of the spectra containing the structure have been recorded independently and are displayed in Figures 6-8. All three spectra appear to consist of at least two progressions and an underlying continuum. The peaks are broadened considerably by both autoionization and instrumental resolution (~ 40 meV), and the spacings are consistent with a X-H symmetric stretching mode.

Peak positions and term values of suspected band origins (v' = 0) in Figure 6 are listed in Table 3. The band origins were obtained from an

Table 1. Energies and Term Values of Peaks in Region 1.

Feature	Methane			Methane		Methane-d_4		Methane-d_4	
	Energy (eV)[a,b]			Term Value (eV)		Energy (eV)[a,b]			Term Value (eV)
3s D_{2d}		9.65	0.66-			(9.90)	9.92	0.60--	
C_{3v}	(10.35)	10.31	0.70				10.52	0.62	
minimum		10.08			3.92		10.25		3.75
3p(3s)D_{2d}	10.65	(9.87)	0.78		2.92 (3.7)				
(3s)C_{3v}		(10.65)							
4s D_{2d}		11.61			1.96		11.95		1.7
v_1'		11.065							
v_2'		11.206							
v_3'		11.355							
v_4'		11.495							
maximum		13.35					13.44		

[a]Numbers in parentheses at the left refer to peak centroids rather than peak maxima.
[b]The two numbers to the right of the parentheses indicate the range of Jahn-Teller splittings due to the use of peak positions or centroids.

Table 2. Assignments of features in Region 1 of Figures 2 and 3. W is the energy location, T is the term value, and n^* is the effective principle quantum number.

	Silane			Germane		
assignment[a]	W(eV)	T(eV)	n^*	W(eV)	T(eV)	n^*
4s, 5s	8.9	3.8	1.89	8.45	3.95	1.86
$\sigma^*(t_2)$, $\sigma^*(t_2)$	9.7	3.0	2.16	9.45	2.95	2.15
4p, 5p	10.0	2.7	2.29	--	--	--
3d, 4d or 5s, 6s	11.0	1.7	2.92	10.7	1.7	2.83
v	12.8	--		12.8	--	--

[a]pairs of orbital symbols refer to assignments for silane and germane, respectively.

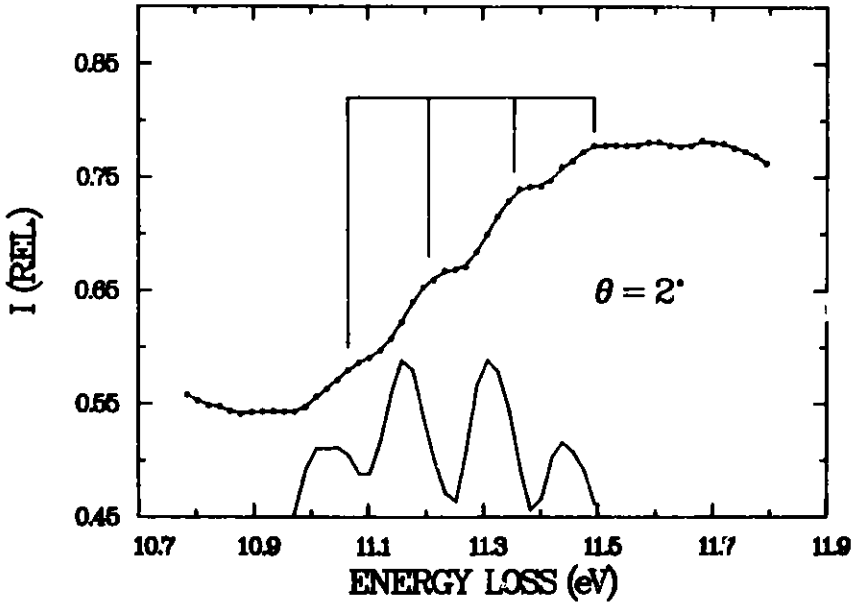

Fig. 5. Amplification of the 11-12 eV region in the 2° spectrum of Figure 1. •••• Experimental points, ——— Smoothed experimental points. The lower curve is the differentiated intensity distribution normalized and shifted to fit on the figure.

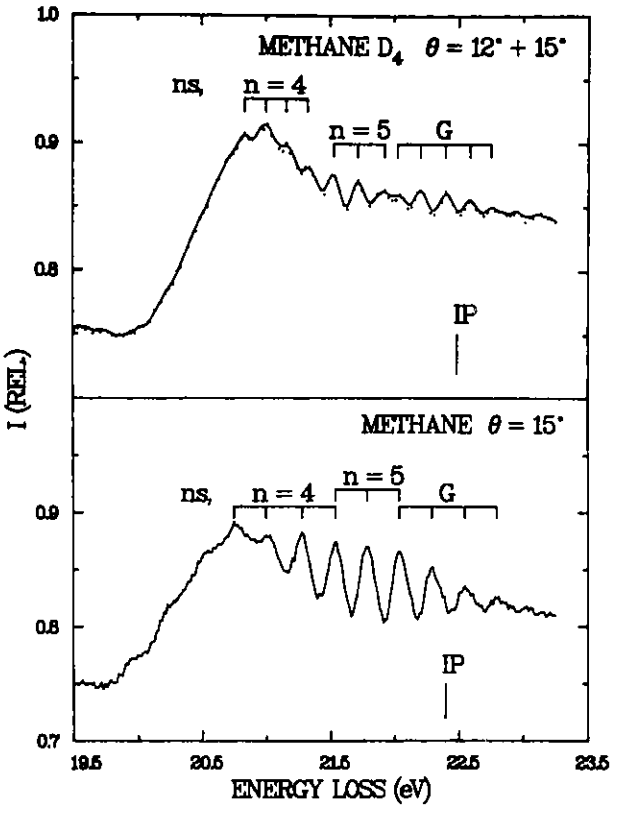

Fig. 6. Electron energy-loss spectra of methane and methane-d_4 in the neighborhood of the second ionization threshold (IP). Each spectrum consists of 256 data points with 250 k counts at the maximum of the methane spectrum. In the methane-d_4 spectrum: •••• Every third data point, —— Smoothed data points.

analysis of peak shift as a function of isotopic substitution. In Figures 7 and 8, peak positions are numerically labelled according to the sequence given in Table 4. The bracketed energies in the table are indicated by vertical arrows in the figures. In the case of SiH_4, this energy corresponds to the position of a small peak that has been obscured by an overlapping band from an adjacent progression. In addition, the GeH_4 spectrum exhibits a gap at ~ 16.75 eV, which appears to accommodate remnants of two vibrational bands. We have estimated their locations and the position of the assumed SiH_4 peak by employing the average level spacings given in Table 3. Term values of selected peaks measured relative to $^2A_1(v' = 0)$ at 17.95 eV and 18.21 eV for SiH_4 and GeH_4 are included in both the table and figures, together with the appropriate terminating orbitals. Lack of isotopic substitution experiments for silane and germane makes identification of band origins considerably less certain than the case of methane and methane-d_4.

Further progress in elucidating the electronic levels of the group IV_a hydrides awaits an accurate CI treatment that includes a calculation of optically forbidden levels.

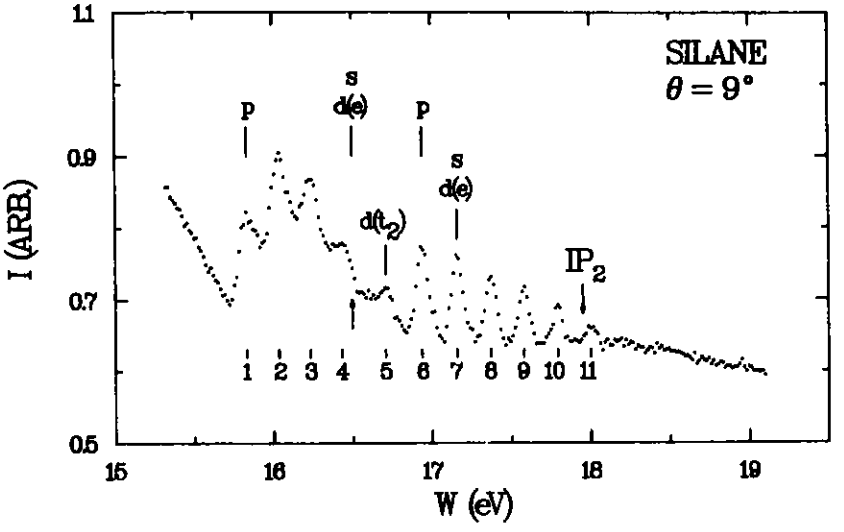

Fig. 7. Electron impact spectrum of silane recorded with 200-eV incident electrons in an energy loss range overlapping the positive-ion spectrum.

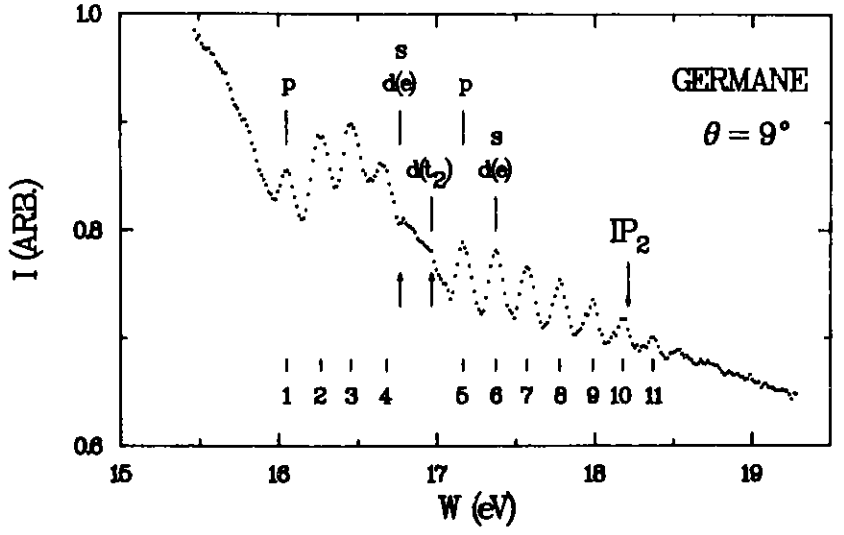

Fig. 8. Electron impact spectrum of germane recorded with 200-eV incident electrons in an energy loss range overlapping the positive-ion spectrum.

Table 3. Energies of the vibrational peaks in Figure 5. Included are the term values and effective quantum numbers (n^*) of suspected band origins.

Methane					Methane-d_4				
v'	Energy (eV)	Δv'	Term Value	(n^*)	v'	Energy (eV)	Δv'	Term Value	(n^*)
	19.902								
		0.279							
	20.181								
		0.280							
	20.461								
0	20.716		1.664	(2.86)	0	20.805		1.675	(2.85)
		0.261					0.189		
1	20.987				1	20.994			
		0.269					0.186		
2	21.256				2	21.180			
		0.258					0.162		
3,0	21.514		0.876	(3.94)	3	21.342			
		0.248							
1	21.762				0	21.526		0.954	(3.78)
		0.251					0.189		
2,0	22.013				1	21.715			
		0.252					0.178		
1	22.265				2	21.901			
		0.256							
2	22.521				0	22.049			
		0.251					0.166		
3	22.772				1	22.199			
							0.198		
					2	22.398			
							0.182		
					3	22.58			

Table 4. Energies (W) of bands in region 2 of Figures 2 and 3. Numbers (No.) refer to Figures 7 and 8. Term values, T and effective quantum numbers (n^*) are given for selected peaks.

	Silane					Germane				
No.	W(eV)	Δ(eV)	T	(n^*)	Type	W(eV)	Δ(eV)	T	(n^*)	Type
1	15.798		2.15	(2.51)	p	16.055		2.16	(2.51)	p
		0.199					0.201			
2	15.997					16.256				
		0.196					0.200			
3	16.193					16.456				
		0.195					0.196			
4	16.388	0.197 Avg.				16.652	0.199 Avg.			
						(16.766)		1.44	(3.07)	s, d(e)
	(16.453)		1.50	(3.01)	s, d(e)	(16.966)		1.24	(3.31)	$d(t_2)$
5	16.653		1.28	(3.26)	$d(t_2)$	17.166		1.04	(3.61)	p
		0.210					0.205			
6	16.892		1.06	(3.59)	p	17.371		0.84	(4.02)	s, d(e)
		0.216					0.198			
7	17.108		0.84	(4.02)	s, d(e)	17.569				
		0.212					0.206			
8	17.320					17.775				
		0.204					0.210			
9	17.524					17.985				
		0.213					0.192			
10	17.737					18.177				
		0.206					0.191			
11	17.943	0.210 Avg.				18.368	0.200 Avg.			
Broad Band	14.05 (onset)		3.8		σ^*-s and $\sigma^*(t_2)$	14.15 (onset)		3.95		σ^*-s and $\sigma^*(t_2)$
	14.8 (peak)					15.3 (peak)				

19. ELECTRON ENERGY LOSS SPECTROSCOPY OF MOLECULAR FLUORINE*

R.-G. Wang,† Z.-W. Wang,‡ M. A. Dillon, and David Spence

Introduction

The electronic structure of fluorine, which has been studied with traditional optical techniques for a period of about 60 years,[1-7] has only recently been understood in a fairly comprehensive way following the high-resolution absorption and emission studies of Colbourn et al.[7] Even then, optical techniques have been successful in identifying only two of the expected Rydberg series in the VUV.[8]

Recent renewed interest in the molecular halogens has arisen from their use in rare-gas halide lasers[9] and as laser systems in their own right.[10,11] This interest has provided motivation for two studies of the electronic structure of fluorine through electron energy-loss spectroscopy (EELS) by Nishimura et al.[12] and by Hitchcock et al.[13]

Despite this recent flurry of activity, several questions have remained concerning the electronic spectrum of F_2, principally, the vibrational labelling of electronic states, the effects of impurities on the spectrum, and the identification of laser levels. We have re-examined the spectrum of F_2 using EELS and have been able to resolve most of these questions.

The Orange Emission Band System

The earliest known spectrum of F_2 is an emission band system in the visible region of the spectrum[1] whose upper state was identified by Porter[4] to be a $^1\Sigma$ system for which only two vibrational levels were observed, the lower levels being presumed to be $^1\Pi$ states. The energies of the upper and lower states relative to the ground state were, however, not known.

---

*Summary of a paper published in J. Chem. Phys. 80, 3574 (1984).

†Visiting Foreign Scholar. Permanent address: Department of Physics, Chengdu University of Science and Technology, Chengdu, Sichuan, People's Republic of China.

‡Visiting Foreign Scholar. Permanent address: Institute of Atomic and Molecular Physics, Jilin University, Changchun, People's Republic of China.

From absorption spectra, Colbourn et al.[7] were able to identify the upper $^1\Sigma$ levels responsible for the orange emission bands as the two dominant structures marked I $^1\Sigma_u^+$ in Figure 1. As the upper level of the F_2 emission system is a $^1\Sigma_u^+$ state, the likely lower states are Π_g, (parity-forbidden from the ground state) and thus are not strong in optical or pseudo-optical spectra. In the present, large-angle spectrum shown in Figure 1, an additional band does appear at the expected location of the Π_g state and is labeled F $^1\Pi_g$ in this figure.

For the incident energy of 200 eV used in the present experiment, it is certain we are observing only the $^1\Pi_g$ and not the $^3\Pi_g$ state, as 200 eV is probably too high an incident energy to observe spin-forbidden states at this relatively small scattering angle. Figure 1 represents the first observation of the vibrationally resolved levels of the F $^1\Pi_g$ state in any experiment as a transition from the ground state.

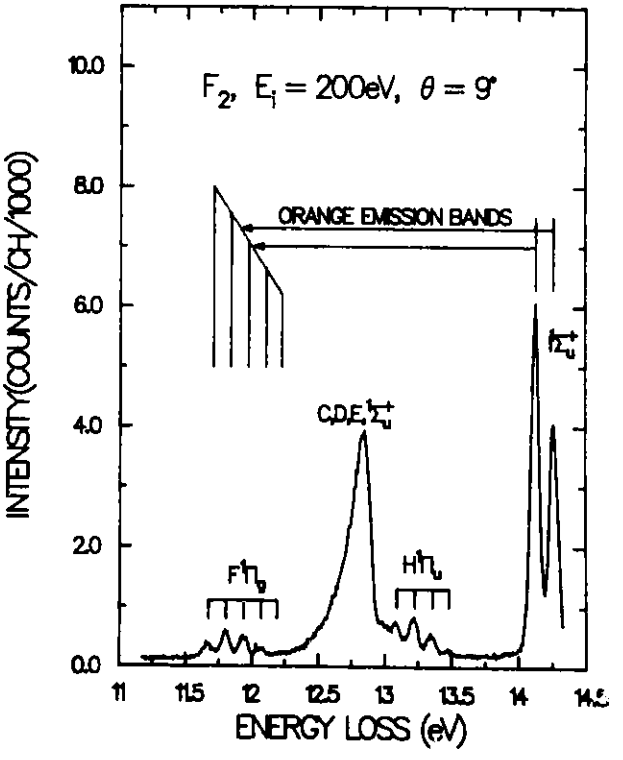

Fig. 1. Detail of energy loss spectrum in F_2 at a scattering angle of 9° and energy loss between 11 eV and 14.5 eV. Note the appearance at this angle of the F $^1\Pi_g$ parity forbidden state, which is the lower level of the orange emission bands shown above. This spectrum is the first to vibrationally resolve both upper and lower levels of this system as an absolute scale in transitions from the ground state.

Labelling of Vibrational Sequences

In order to settle published uncertainties concerning the vibrational labeling of the F $^1\Pi_g$ state,[4,7] we show a greatly magnified view of this state in Figure 2. The figure shows no trace of any vibrational level below that which we have marked as v = 0. In previous studies,[4,7] this level has tentatively been labeled v = 1. It would be difficult to imagine a Franck-Condon overlap that would result in an additional vibrational level below the v = 0 level indicated in Figure 2 which would yield a structure whose intensity is below our statistical noise level. Furthermore, as Rydberg orbitals are essentially non-bonding, the vibrational envelopes of the F_2^+, [X $^2\Pi$] positive-ion state, the F_2^- [X $^2\Pi$](3sσ)^2 $^2\Pi$ negative-ion state, and the F_2^* [X $^2\Pi$]3sσ $^1\Pi_g$ Rydberg state should all be the same. A comparison of the vibrational envelopes of these states, not shown here, does indicate the uniqueness of the vibrational labelling scheme of Figure 2. Documentation of electronic states obtained from the above spectra is given in Table 1 with a comparison to previous studies.

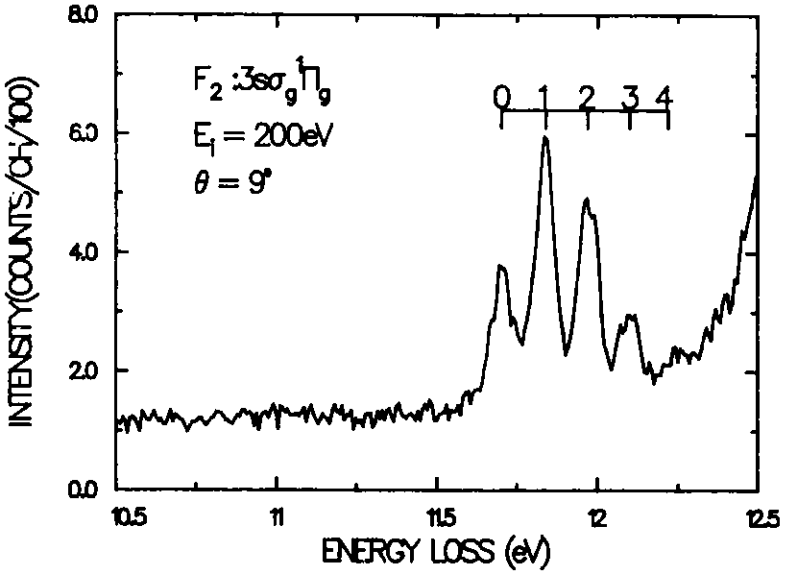

Fig. 2. Details of the vibrationally resolved F $^1\Pi_g$ state showing unambiguously for the first time the vibrational numbering sequence of this state.

Table 1. Comparison of energies (in eV) of electronic states of F_2 above 11.6 eV observed in the present experiments with those of previous experiments. Note the change in vibrational numbering of the F $^1\Pi_g$ state from previous work.

Present Data	Colbourn et al. Photoabsorption[a]	Hitchcock et al. Elec. Scatt.[b]	Nishimura et al. Elec. Scatt.[c]		Term Symbol[a,b]
11.702	11.695				v = 0
11.835	11.830		Not		v = 1
11.969	11.964		Resolved	F $^1\Pi_g$	v = 2
12.102	10.096				v = 3
12.221	12.225				v = 4
12.846	Many levels	12.87	12.85	CDE $^1\Sigma_u^+$	
13.090	13.094	13.09			v = 0
13.225	13.226	13.23	Not	H $^1\Pi_u$	v = 1
13.358	13.356	13.35	Resolved		v = 2
13.480	13.484	13.48			v = 3
14.126	14.127	14.13	14.13	I $^1\Sigma_u^+$	v = 0
14.260	14.264	14.26	14.27		v = 1
14.610	14.568	14.60		J $^1\Pi_u$	v = 0
14.704	14.715	14.70			v = 1
14.890	14.874	14.88	14.9	K $^1\Sigma_u^+$	
15.290	15.283	15.28	15.25	N $^1\Pi_u$	
15.524	15.531	15.50		Q $^1\Sigma_u^+$	
17.0		17.01		$^1\Sigma_u^+$	

[a]Reference 7.
[b]Reference 13.
[c]Reference 12.

The Effects of Impurities on F_2 Spectra

Because several features in previous spectra of F_2 remain unexplained, it is instructive to examine the manufacturing process for fluorine and the possible contaminants this process may introduce.[14] Fluorine is manufactured by the electrolysis of anhydrous potassium bifluoride, KHF_2, or KF.HF containing various concentrations of free HF. All commercial electrolysis cells now use carbon anodes, and possible contaminants introduced into the F_2 are listed[14] as HF, O_2, N_2, CF_4, SF_6, CO_2, and H_2O, all at the level of parts per thousand, and well within our detection capabilities. We note that the largest structures of Figure 3 correspond to only a couple of hundred counts, compared to 15,000 counts for the large structures seen in Figure 1.

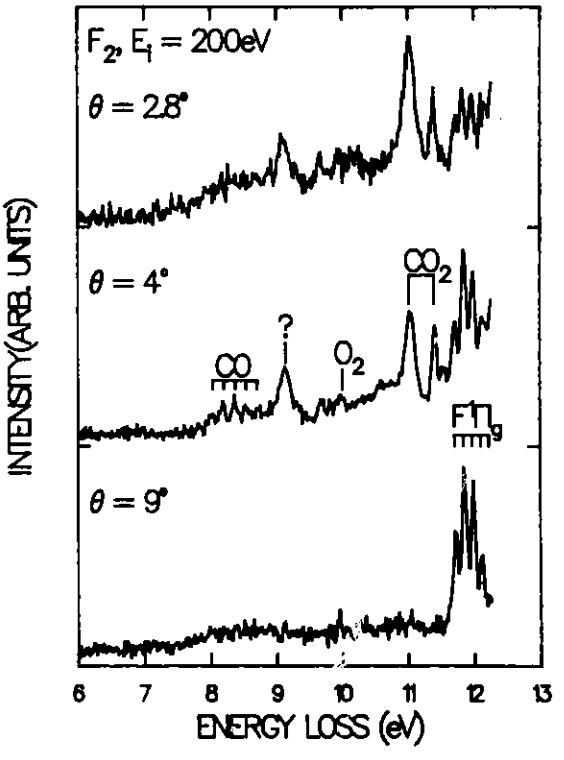

Fig. 3. Electron energy loss spectra obtained in F_2 at scattering angles of 2.8°, 4°, and 9° for an incident electron energy of 200 eV and energy loss between 5 eV and 12.5 eV. All of the features in these spectra, (except the F $^1\Pi_g$ state) and in earlier electron scattering studies (Refs. 12 and 13) can be attributed to generally known impurities, as discussed in the text. The energies of these impurity lines and bands are listed, together with identifications, in Table 2. Note that the largest features of these spectra correspond to only a couple of hundred counts, compared to about 15,000 counts for the large structures of Figure 1, which is an extension of the same θ = 2.8° spectrum shown here.

Armed with the list of impurities above, it is now trivial to identify the 11.10 and 11.43 features in all three studies[12,13] as arising from CO_2.[15] This identification is made not just on energy locations, but on peak widths also. Note the 11.43-eV peak reflects our instrumental resolution, whereas the 11.10-eV peak is much broader, characteristic of several overlapping states of CO_2. Note also that the relative peak strengths in the CO_2 spectrum obtained under similar conditions[15] to those of Figure 3 are such that only these two dominant CO_2 structures would be expected to be observed in our spectra shown in Figure 3.

The vibrational system beginning at about 8 eV in Figure 3, also seen as a broad feature in the E_i = 90 eV, θ = 5° spectrum of Nishimura et al.,[12] is readily identified as the A $^1\Pi$ state of CO, from both its energy and characteristic vibrational spacing.[15] It is definitely not N_2.[16] We have been unable to identify the structure at 9.13 eV with any particular impurity, although one should note that this appears as a small shoulder also in the E_i = 90 eV, θ = 5° spectrum of Nishimura et al.[12] The two small features at about 9.8 and 10 eV on Figure 3 may arise from H_2O.

From the above, we must conclude that all of the energy loss features observed between 5 eV and 11.5 eV by Nishimura et al.,[12] by Hitchcock et al.,[13] and by ourselves arise from generally identifiable impurities. A summation of these impurities is given in Table 2.

Discussion of F_2 Laser Transitions

In the initial description of lasing action in F_2, Rice et al.,[10] by analogy with I_2 and Br_2, proposed that lasing action occurred as a $^3\Pi_g \rightarrow {}^3\Pi_u$ transition; later Woodworth and Rice[11] expanded their model in a more complete description of the kinetics of F_2 lasing action.

The calculations of Cartwright and Hay[17] found the lower laser level, $^3\Pi_u$, to be bound, lending support for the model of Woodworth and Rice.[11] Given the energy of the $^3\Pi_u$ state to be about 3 eV,[12,17] combined with a laser photon energy of 7.95 eV, would place the upper $^3\Pi_g$ laser state at about 11.0 eV.

Our large-angle spectra, which would tend to show forbidden transitions, show no feature at 11 eV (Fig. 3), nor does the E_i = 30 eV, θ = 90° spectrum

Table 2. Energies of electronic states observed in F_2 in the energy range 5 to 11.5 eV in the present and previous electron scattering experiments, together with their identification. Energies are in eV.

Present Data $\theta = 4°$	Nishimura et al.[a] $\theta = 5°$	Hitchcock et al.[b] $\theta = 0°$		Identification
8.031				v = 0
8.199				v = 1
8.367			CO, A $^1\Pi$	v = 2
8.535				v = 3
8.704				v = 1
May be small underlying continuum	Broad band 8.5 eV	Broad band 8.5 eV	O_2	Schumann-Runge
10 eV	10 eV			1st long band
9.133				??
9.698				
11.020	11.0	11.10	CO_2	
11.39	11.4	11.43		

[a]Reference 12.
[b]Reference 13.

of Nishimura et al.[12] In fact, as we have pointed out, no experiment has been able to observe any F_2 state between 6 and 11.5 eV.

It is possible, of course, that the upper $^3\Pi_g$ state is that associated with the strong $^1\Pi_g$ state we observe beginning at 11.70 eV. If the singlet-triplet splitting (by analogy with chlorine)[18] was of the order of the vibrational spacing of the $^1\Pi_g$ state, the energy of the upper $^3\Pi_g$ would be about 11.6 eV, and the energy of the lower laser level, $^3\Pi_u$, would be about 3.6 eV, not necessarily outside the range of experimental[12] or theoretical[17]

limits. However, such discussion must remain speculative until a technique can be developed that is more sensitive to the detection of triplet states than has been used here (or previously).

References

1. H. G. Gale and G. S. Monk, Astrophys. J. 59, 125 (1924); 69, 77 (1929).
2. R. K. Steunenberg and R. C. Bogel, J. Am. Chem. Soc. 78, 901 (1956).
3. R. P. Ickowski and J. L. Margrave, J. Chem. Phys. 30, 403 (1959).
4. T. L. Porter, J. Chem. Phys. 48, 2071 (1968).
5. W. Sticker and L. Krauss, Z. Naturforsch. A23, 486 (1968).
6. J. L. Cole and J. L. Margrave, J. Mol. Spectrosc. 43, 65 (1972).
7. E. A. Colbourn, M. Degenais, A. E. Douglas, and J. W. Raymonda, Can. J. Phys. 54, 1343 (1976).
8. K. P. Huber and G. Herzberg, Molecular Spectra and Molecular Structure IV. Constants of Diatomic Molecules. (Van Nostrand, Princeton, 1979) p. 214.
9. B. E. Cherrington, Gaseous Electronics and Gas Lasers. (Pergamon Press, Oxford, 1979).
10. J. K. Rice, A. K. Hays, and J. R. Woodworth, Appl. Phys. Lett. 31, 31 (1977).
11. J. R. Woodworth and J. K. Rice, J. Chem. Phys. 69, 2500 (1978).
12. H. Nishimura, D. C. Cartwright, and S. Trajmar, J. Chem. Phys. 71, 5039 (1979).
13. A. P. Hitchcock, C. E. Brion, G. R. J. Williams, and P. W. Langhoff, Chem. Phys. 66, 435 (1982).
14. A. J. Woytek, in Kirk Othmer Encyclopedia of Chemical Technology, Third ed., Vol. 10, eds. H. F. Mark, D. F. Othmer, C. G. Overberger, and G. T. Seaborg (Wiley, New York, 1980) pp. 630-654.
15. E. N. Lassettre, A. Skerbele, M. A. Dillon, and K. J. Ross, J. Chem. Phys. 48, 5066 (1968).
16. E. N. Lassettre and A. Skerbele, J. Chem. Phys. 54, 1597 (1971).
17. D. C. Cartwright and P. J. Hay, J. Chem. Phys. 70, 3191 (1979).
18. J. Jureta, S. Cvejanovic, M. Kurepa, and D. Cvejanovic, Z. Phys. A, Atoms and Nuclei 304, 143 (1982).

20. ELECTRONIC STRUCTURE OF Cl_2 FROM 5 TO 15 eV BY ELECTRON ENERGY LOSS SPECTROSCOPY*

David Spence, R. H. Huebner, H. Tanaka,† M. A. Dillon, and R.-G. Wang‡

Although the optical absorption and emission spectra of molecular chlorine have been studied for 50 years or so, until recently most studies have been fragmentary, covering only limited energy regimes.[1-5] In fact, all except two of the bound excited states listed by Huber and Herzberg[5] are described as uncertain in both energy and excited-state configuration.

There recently has been renewed interest in the electronic spectra of the halogens, because of their use in rare gas-halide lasers[6] and because the halogens themselves may be important laser systems.[7,8] Recent studies of the chlorine molecule include the photoabsorption measurements of Moeller et al.[9] and of Douglas,[4] detailed ab-initio calculations by Peyerimhoff and Buenker,[10] and threshold electron studies by Jureta et al.[11] Of all these studies, only those by Jureta et al.[11] covered an extended energy range (2.5 eV to 11.5 eV) and were able to locate some optically forbidden states in addition to several known optically allowed states.[5,9] These latter studies included the first observation of the $4s\sigma_g\ ^{1,3}\Pi_g$ parity-forbidden states (at 7.83 eV for the triplet, and 7.87 eV for the singlet), whose energies had previously been predicted by Spence[12] (from considerations of negative-ion Feshbach resonances) to be 8.05 eV.

Despite the generally good agreement (within experimental errors) in spectroscopic energies obtained by absorption[9] and threshold electron spectra,[11] there are differences in some state assignments and subtle differences in the relative intensities of the observed states.

While in absorption spectroscopy only optically allowed states are observed, in the technique of threshold electron-impact spectroscopy,[11] both

---

*Summary of a paper published in J. Chem. Phys. 80, 2989 (1984).

†Visiting Foreign Scholar. Permanent address: Department of Physics, Sophia University, Tokyo, Japan.

‡Visiting Foreign Scholar. Permanent address: Department of Physics, Chengdu University of Science and Technology, Chengdu, People's Republic of China.

singlet and triplet states are excited with about equal probability, and there is no adjustable experimental parameter with which these may be separated. On the other hand, by exciting a gaseous target with relatively high (>100 eV) energy electrons and by measuring the spectra of inelastically scattered electrons as a function of the scattering angle, one may readily separate those structures in the spectra that arise from optically allowed states (low-angle spectra)[13,14] from those that arise from optically forbidden transitions (and are relatively more intense in large-angle scattering spectra).[15-17]

Consequently, we have reexamined the electronic spectrum of molecular chlorine using 200-eV incident electrons for energy-losses between 5 and 15 eV and scattering angles between 3° and 9°. Our measurements, which are complementary to those of Jureta et al.,[11] although confirming many structures reported by Jureta et al. and revealing several new ones, do indicate that several features in the spectra of Jureta and co-workers arise from hot-bands. The observation of hot bands in electron scattering spectra is unusual, but the ground-state vibrational spacings of Cl_2, 0.069 eV,[5] coupled with particularly favorable Franck-Condon overlaps,[10,11] make such structures relatively strong for some electronic transitions. This results in our renumbering the vibrational sequence of the $4s\sigma\ ^{1,3}\Pi_g$ states.

Where comparison can be made between our forward scattered (pseudo-optical) spectrum and the photoabsorption spectrum of Moeller et al.,[9] the agreement in energy locations is very good. Moreover, our angular measurements, which lend support to the assignments of Moeller et al.,[9] explain the difference in relative intensities observed by absorption[9] and threshold electron[11] experiments as arising from a consequence of the two techniques predominantly exciting different (although almost energetically coincident) electronic states. Thus, the present work represents a reconciliation of data derived from photoabsorption, threshold-electron, and high-incident-energy electron energy loss spectroscopy. A summary of our measurements is given in Tables 1 and 2. Details of portions of our spectra are shown in Figure 1, which shows the effect of "hot bands" on the spectrum corresponding to excitation of the $4s\sigma_g\ ^1\Pi_g$ parity forbidden state, and in Figure 2, which also shows the results of "hot bands" together with the emergence of a newly observed electronic band at larger scattering angles.

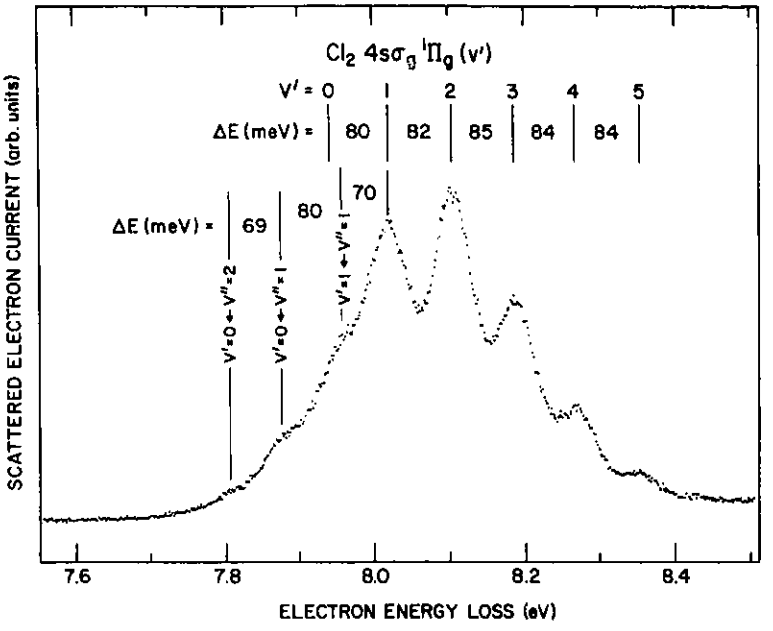

Fig. 1. Details of the electron energy loss spectrum of Cl_2 between 7.5 and 8.5 eV showing the $4s\sigma_g\,{}^1\Pi_g$ parity-forbidden state together with the presence of "hot bands" on the low-energy side.

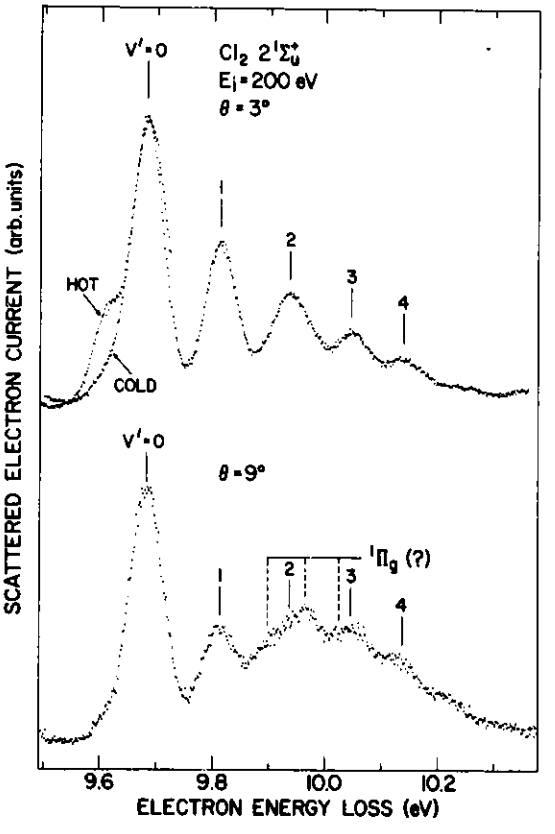

Fig. 2. Details of the electron energy loss spectrum of Cl_2 between 9.5 and 10.5 eV at scattering angles of 3° and 9°. The low-energy part of the 3° spectrum shows two superimposed spectra obtained at room temperature and at 150°C, indicating the presence of "hot" bands. The change in vibrational envelope as a function of angle is only consistent with the presence of three separate electronic states in this energy region. The vibrational energies of the $2\,{}^1\Sigma_u^+$ state are from Reference 9.

Table 1. Comparison of the energies of the $4s\sigma\ ^1\Pi_g$ states observed in the present experiments with those of previous work. Note we have changed the numbering system of the $^{1,3}\Pi$ vibrational levels observed by Jureta et al.[11] by one vibrational quantum as explained in the text. Energies are in electron volts.

Present Data	Jureta et al.[a]	Electron Config./Term Symbol	
	(7.83) (hot band)[b]		
	7.91		v=0
	7.99	$4s\sigma_g\ ^3\Pi_g$	v=1
	8.07		v=2
	8.15		v=3
	(7.87) (hot band)[b]		
7.939	7.95		v=0
8.019	8.03		v=1
8.101	8.11	$4s\sigma_g\ ^1\Pi_g$	v=2
8.186	8.19		v=3
8.270	8.27		v=4
8.354	(8.35)[b]		v=5

[a]Reference 11.
[b]Numbers in parentheses represent unresolved components.

Table 2. Comparison of the energies of the $2^3\Pi_u(1u)$, $2^1\Pi_u$ and $2^1\Sigma_u^+$ states observed in the present experiments with those of previous work. Only those optical levels which can be compared with electron impact data are included. Energies are in electron volts.

Present Data	Jureta et al.[a]	Moeller et al.[b]	Term Symbol[b]	
	9.13	9.116	$2^3\Pi(1u)$	v=0
	9.19	9.193		v=1
9.225	9.250	9.230	$2^1\Pi_u$	v=0
9.305	9.320	9.307		v=1
9.381	9.395	9.384		v=2
9.455	9.465	9.460		v=3
	9.530	9.534		v=4
	9.620 (hot band)			
9.682	9.695	9.688	$2^1\Sigma_u^+$	v=0
9.815	9.815 [c]	9.808		v=1
9.938	9.930	9.929		v=2
10.046		10.028		v=3
10.141				v=4
9.900				
9.966			$^1\Pi_g$ (?)	
10.025				

[a]Reference 11.
[b]Reference 9.
[c]May be due to presence of a nearby triplet state, as explained in the text.

References

1. J. Lee and A. D. Walsh, Trans. Faraday Soc. 55, 1281 (1959).
2. P. Venkateswarlu, Proc. Indian Acad. Sci. A26, 22 (1947).
3. A. E. Douglas and A. R. Loy, Can. J. Phys. 53, 1965 (1975).
4. A. E. Douglas, Can. J. Phys. 59, 835 (1981).
5. K. P. Huber and G. Herzberg, Molecular Spectra and Molecular Structure, Vol. 4, Constants of Diatomic Molecules (Van Nostrand, Princeton, 1979).
6. B. E. Cherrington, Gaseous Electronics and Gas Lasers (Pergamon Press, Oxford, 1979).
7. C. H. Chen and M. G. Payne, Appl. Phys. Letters 28, 219 (1976).
8. J. K. Rice, A. K. Hays, and J. R. Woodworth, Appl. Phys. Letters 31, 31 (1977).
9. T. Moeller, B. Jordan, P. Gurtler, G. Zimmerer, D. Hooks, J. Le Calve, and M. C. Castex, Chem. Phys. 76, 295 (1983).
10. S. D. Peyerimhoff and R. J. Buenker, Chem. Phys. 57, 279 (1981).
11. J. Jureta, S. Cvejanovic, M. Kurepa, and D. Cvejanovic, Z. Phys. A, Atoms and Nuclei 304, 143 (1982).
12. D. Spence, Phys. Rev. A 10, 1045 (1974).
13. E. N. Lassettre, A. Skerbele, and M. A. Dillon, J. Chem. Phys. 50, 1829 (1969).
14. M. A. Dillon and D. Spence, J. Chem. Phys. 74, 6070 (1981).
15. S. Trajmar, J. K. Rice, and A. Kuppermann, Advances in Chemical Physics (Wiley, New York, 1970).
16. M. A. Dillon, Creation and Detection of the Excited State, Vol. I, part 2, (Dekker, New York, 1971).
17. W. A. Goddard III, D. C. Huestis, D. Cartwright, and S. Trajmar, Chem. Phys. Letters 11, 329 (1971).

21. EXCITATION OF RYDBERG STATES OF $HgCl_2$ AND $HgBr_2$ BY ELECTRON IMPACT*

David Spence, R.-G. Wang,† and M. A. Dillon

We have examined the electronic structure of $HgCl_2$ and $HgBr_2$ from 5 eV to 14 eV by high-resolution electron energy-loss spectroscopy. Our measurements include the near-UV region, which has not been examined by any previous technique and which is found to be rich in Rydberg states. In particular, in each molecule we identify members of two optically allowed Rydberg series and one forbidden series with electronic structures $\sigma_g^2\,\sigma_u^2\,\pi_u^4\,\pi_g^3$ [$np\pi_u$, $np\sigma_u$ and $nd\pi_g$, or $(n+1)s\sigma_g$] that converge to the $^2\Pi_g$ ground ionic state. In addition, other structures that form the dominant energy-loss mechanisms in our spectra are identified as arising from optically allowed Rydberg states associated with the excited ionic states $^2\Pi_u$, $^2\Sigma_u$, and $^2\Sigma_g$. Measurements at energy losses below 9 eV confirm previous valence states observed in photoabsorption and suggest the existence of two new valence states in each molecule. Angular measurements facilitate identification of many of the newly observed structures in our electron energy-loss spectra.

A synopsis of our spectra shown in Figures 1 and 2 is given in Tables 1 through 3.

---

*Summary of a paper to be published in J. Chem. Phys.

†Visiting Foreign Scholar. Permanent address: Physics Department, Chengdu University of Science & Technology, Chengdu, Sichuan, The People's Republic of China.

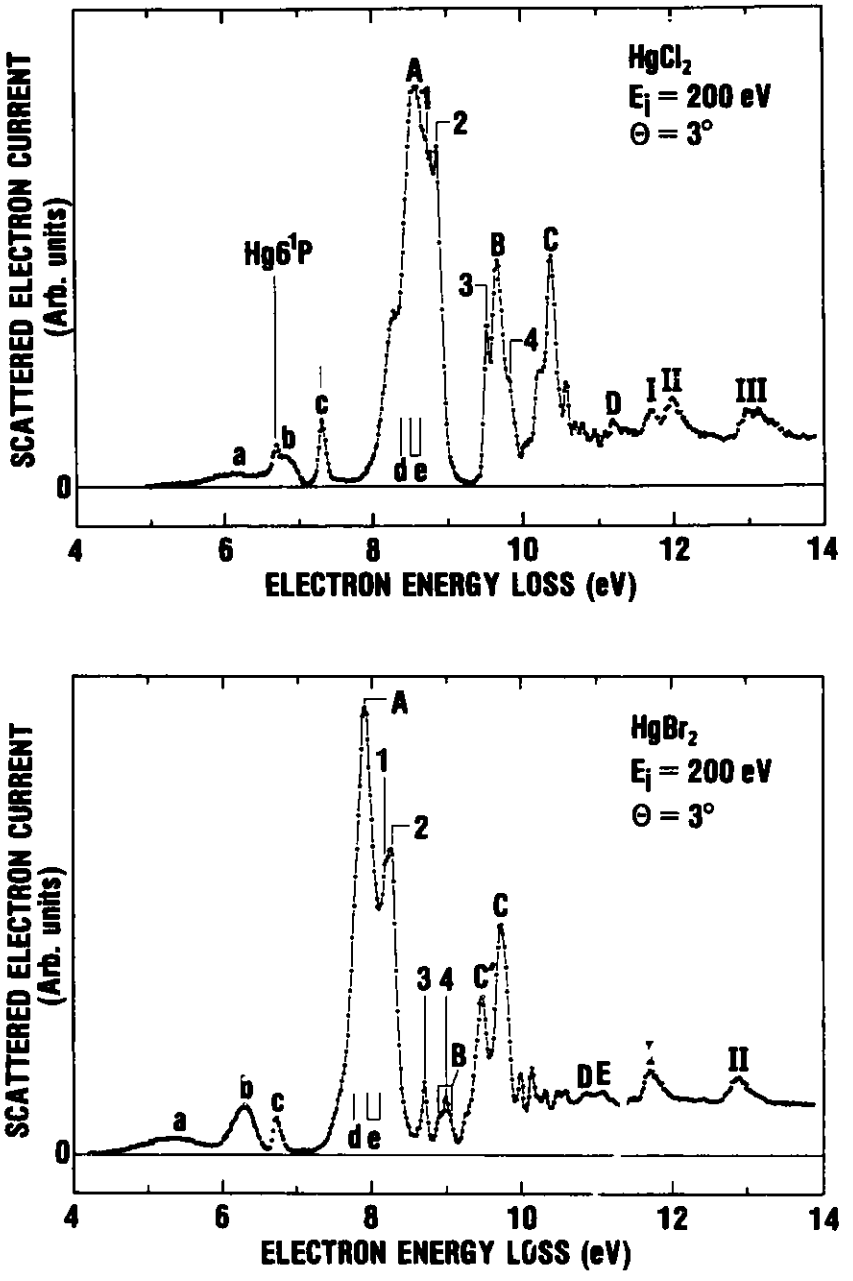

Fig. 1. Electron energy-loss spectrum of (top) $HgCl_2$ and (bottom) $HgBr_2$ between 4 eV and 14 eV obtained for an incident electron energy of 200 eV and a scattering angle of 3°. Under these conditions, most of the features in spectra arise from excitation of optically allowed states, and the four systems of annotation are, lower case letters - valence states, upper case letters - Rydberg states with excited ionic cores $^2\Pi_u$, $^2\Sigma_u$, and $^2\Sigma_g$, Arabic numerals - Rydberg states associated with ground state $^2\Pi_g$ ionic cores, and finally, Roman numerals - unresolved vibrational progressions in the ionization continuum. The instrumental resolution is 45 to 50 meV, corresponding to about 3 data points.

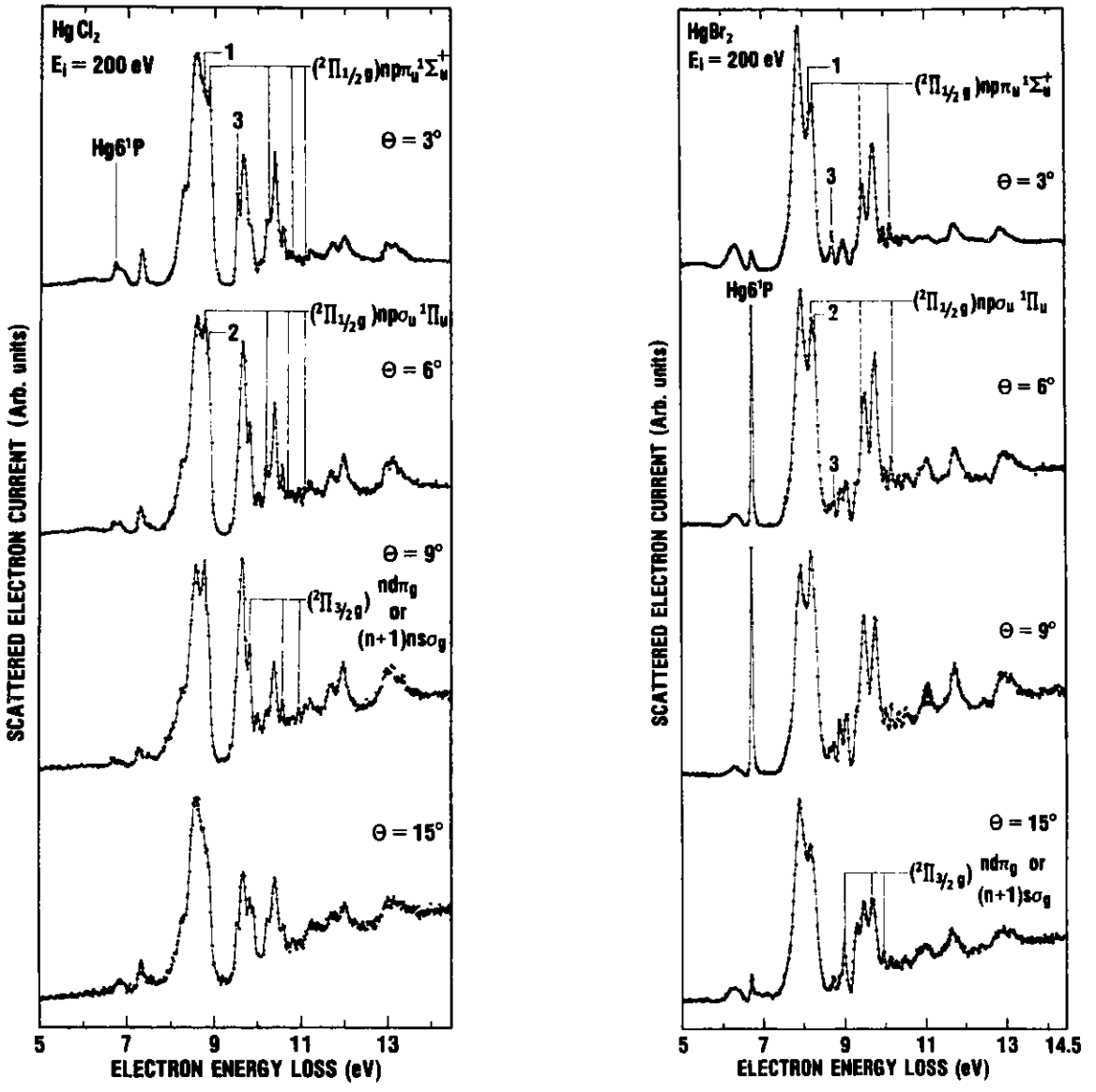

Fig. 2. Comparison of energy-loss spectra obtained in (left) $HgCl_2$ and (right) $HgBr_2$ for incident energies of 200 eV at scattering angles of 3°, 6°, 9°, and 15°. Note specifically, the very rapid decrease in magnitude of structures 2 and 3 with increasing θ, the slower decrease in structure 1, and the relative increase in structure 4, labelled here $(^2\Pi_{3/2g})nd\pi_g$ or $(n+1)s\sigma_g$, indicating this to be a forbidden transition from the ground state. Also note for $HgBr_2$ the sharp Hg $6\,^1P$ line for θ = 6° and 9°, showing clearly the instrumental resolution of about 3 data points in these two spectra, θ = 6° and 9°. The only other Hg contribution is the shaded area on the broad structure that is marked E in the bottom frame of Figure 1.

Table 1. Rydberg states of $HgCl_2$ and $HgBr_2$ resulting from excitation of π_u, σ_u, and σ_g electrons and associated with $^2\Pi_u$, $^2\Sigma_u$, and $^2\Sigma_g$ ionic cores.

Structure		Initial orbital	$HgCl_2$ energy (eV)	$HgBr_2$ energy (eV)	Quantum Defect			Excited Configuration
					$HgCl_2$	$HgBr_2$	CO_2	
A	π_u	8.57	7.91		1.05	1.06	1.06	$(^2\Pi_{1/2u})ns\sigma_g\ ^1\Pi_u$
B	σ_u	9.65	9.00		0.90	0.90	0.93	$(^2\Sigma_u)ns\sigma_g\ ^1\Sigma_u^+$
C'	π_u		9.46			0.21	0.31	$(^2\Pi_{3/2u})nd\sigma_g\ ^1\Pi_u$
C	π_u	10.40	9.75		0.20	0.24	0.31	$(^2\Pi_{1/2u})nd\sigma_g\ ^1\Pi_u$
D	σ_g	11.19	10.85		0.69	0.69	0.71	$(^2\Sigma_g)np\sigma_u\ ^1\Sigma_u^+$
E	σ_g		11.11			0.56	0.56	$(^2\Sigma_g)np\pi_u\ ^1\Pi_u$

	$HgCl_2$				$HgBr_2$				
Series	Energy (eV)	Effective Q.no.	Av. Q.D.	Probable configuration	Energy (eV)	Effective Q. no.	Av. Q.D.	Probable configuration	Ionic core term
1	8.78	2.24	0.78	$np\sigma_u\,^1\Pi_u$	8.16(5)	2.24	0.74	$np\sigma_u\,^1\Pi_u$	$^2\Pi_{1/2g}$
	(10.23)[a]	3.27			(10.15)	4.29			
	10.71	4.14							
	(11.05)	5.21							
2	8.88	2.26	0.72	$np\pi_u\,^1\Sigma_u^+$	8.26(5)	2.28	0.71	$np\pi_u\,^1\Sigma_u^+$	$^2\Pi_{1/2g}$
	(10.23)	3.27			(10.15)	4.29			
	10.80	4.39							
	(11.05)	5.21							
3	9.52	2.70	0.30		8.71	2.71	0.29		$^2\Pi_{3/2g}$
4	9.84	2.97	-0.02	$nd\pi_g$ or $(n+1)s\sigma_g$	9.02	2.97	0.06	$nd\pi_g$ or $(n+1)s\sigma_g$	$^2\Pi_{3/2g}$
	10.55	4.02			9.67	3.92			
	10.85	5.06			10.00	4.92			

[a]Numbers in parentheses used twice in a column represent unresolved components of two series.

Table 3. Energies (in eV) of valence states observed in $HgCl_2$ and $HgBr_2$ in the present experiments and in photoabsorption.

	Structure	Present data	Photoabsorption[a]			
			1	2	3	4
$HgCl_2$	a) $1\ ^1\Pi_u$	6.20				6.05
	b) $1\ ^1\Sigma_u$	6.85	6.85			6.79
	c) $2\ ^1\Sigma_u$	7.31		7.32		
	d)	8.35				
	e)	8.5 ± 0.2				
$HgBr_2$	a) $1\ ^1\Sigma_u$	5.39				5.395.51
	b) $1\ ^1\Sigma_u$	6.30				6.366.26
	c) $2\ ^1\Sigma_u$	6.80				
	d)	7.65 ± 0.1				
	e)	8.0 ± 0.2				

[a]Sources:

1. K. Sieland, Z. Phys. 76, 801 (1932); 77, 157 (1932)
2. M. Wehrli, Helv. Phys. Acta. 11, 339 (1938)
3. J. Maya, J. Chem. Phys. 67, 4976 (1976)
4. C. Roxlo and A. Mandl., J. Appl. Phys. 51, 2909 (1980)

22. OBSERVATION OF A RAPID CHANGE IN THE SHAPE OF THE $6\sigma \rightarrow np\pi$ WINDOW RESONANCES IN N_2O

David DeMille,* David Spence, and M. A. Dillon

In the past few decades, electronic structure in the ionization continuum of N_2O has been investigated by a variety of techniques. Excitation spectra have been reported employing both optical absorbtion[1,2] and electron energy-loss methods.[3-5] In addition, results of photoelectron spectroscopy[6,7] and photoion-mass spectroscopy[8] have provided information about ionic structure and ion disintegration channels. A paper by Fridh et al.[9] details most of what is known about the first 20 eV in the spectrum of N_2O and should be consulted for earlier references.

The ground state configuration of N_2O is[10-12]

$$1\sigma^2 \cdots 6\sigma^2 1\pi^4 7\sigma^2 2\pi^4 \; \tilde{X} \; {}^1\Sigma^+ \qquad (1)$$

in the $C_{\infty v}$ symmetry. The first four ionization potentials are 12.89 eV, 16.38 eV, 17.65 eV, and 20.10 eV,[6] which correspond to electron ejection from the 2π, 7σ, 1π, and 6σ orbitals. The range of ~ 4 eV below the fourth ionization threshold is the region of the expected optically allowed autoionizng series $nd\pi$, $nd\sigma$, $np\pi$, $np\sigma$, $ns\sigma + 6\sigma$ converging to the $\tilde{C}\ {}^2\Sigma^+$ ion state. In the course of re-examining this region by electron-impact spectroscopy, we have detected a rapid change with scattering angle in the shape of a series of window resonances.

Electron energy-loss (EELS) spectra of N_2O employing incident electrons of 200 eV recorded at scattering angles of 3° and 9° are displayed in Figure 1. The 3° electron-impact spectrum closely resembles a spectrum reported in connection with earlier optical work.[2] The observed structure consists mainly of four Rydberg series assigned on the basis of quantum defect arguments.[9,13-15] The 9° spectrum exhibits a striking alteration in the neighborhood of the $6\sigma \rightarrow np\pi$

*Participant in the Student Research Participation Program, Division of Educational Programs, Argonne National Laboratory. Present address: Department of Physics, University of Chicago, Chicago, IL 60637.

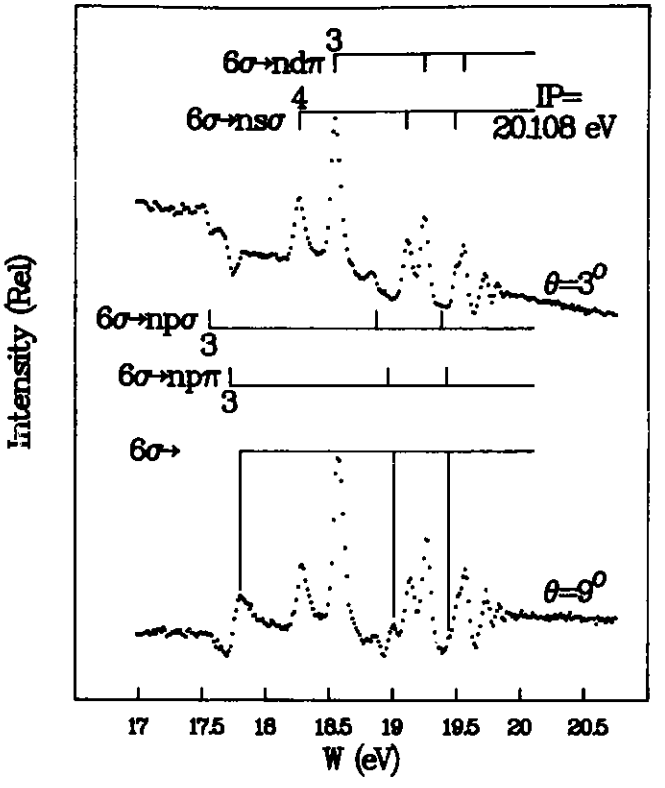

Fig. 1. Electron-impact spectra of N_2O recorded at an incident electron energy of 200 eV. The ratio of scattered electron intensities at 3° and 9° is 10:1.

window resonance series. While spectra obtained at larger scattering angles often manifest substantial contributions from symmetry-forbidden transitions, the quantum defect of new features is $\mu \sim 0.5$, which is characteristic of the adjacent npπ series. A simple resonance profile analysis confirms this connection. The scattered electron intensity, I, in the neighborhood of an isolated autoionizing transition will have the form[15]

$$I = I_o + I_r \frac{(\varepsilon + q)^2}{1 + \varepsilon^2}, \qquad (2)$$

where I_o and I_r are the background and resonance intensities, q is the Fano profile index, $\varepsilon = (W - W_r)/\frac{1}{2}\Gamma$, and W_r, Γ are the resonance location and width. The data presented in Figure 2 illustrate an attempt to fit Eq. (2) using $W_r = 17.7$ eV and $\Gamma \sim 0.1$ eV to the intensity distribution near the 3pπ resonance. The solid curves demonstrate a qualitative correspondence of Eq. (1) to the changing peak shape. A more accurate representation of the data would necessitate a multichannel approach in order to include the substantial effects of adjacent Rydberg states.

Fig. 2. Resonance profile [Eq. (2) solid curves] superimposed on experimental data points. The curves were drawn using W_r = 17.7 eV, $\Gamma \sim 0.1$ eV, and variable I_o.

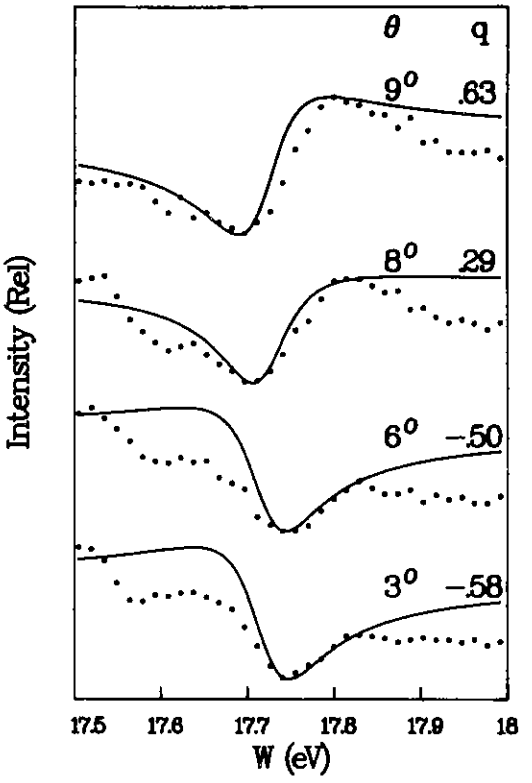

References

1. Y. Tanaka, A. S. Jursa, and F. J. LeBlanc, J. Chem. Phys. 32, 1205 (1960).
2. G. R. Cook, P. H. Metzger, M. Ogawa, J. Opt. Soc. Amer. 58, 129 (1968).
3. E. N. Lassettre, A. Skerbele, M. Dillon, and K. L. Ross, J. Chem. Phys. 48, 5066 (1968).
4. M. J. Weiss, S. R. Mielczarek, and C. E. Kuyatt, J. Chem. Phys. 54, 1412 (1971).
5. V. Y. Foo, C. E. Brion, and J. B. Hasted, Proc. Roy. Soc. Lond. A 322, 535 (1971).
6. D. W. Turner, C. Baker, A. D. Baker, and C. R. Brundle, Molecular Photoionization Spectroscopy (Wiley, New York, 1970).
7. P. M. Dehmer and J. L. Dehmer, J. Chem. Phys. 73, 126 (1980).
8. J. Berkowitz and J. H. D. Eland, J. Chem. Phys. 67, 2740 (1977).
9. C. Fridh, L. Åsbrink, and E. Lindholm, Chem. Phys. 27, 169 (1978).
10. V. Gelius, J. Electron. Spectry. 5, 985 (1974).
11. W. Domcke, L. S. Cederbaum, J. Schirmer, W. Von Niessen, C. E. Brion, and K. H. Tan, Chem. Phys. 40, 171 (1979).
12. R. Fantoni, A. Giardini-Guidoni, R. Tiribelli, R. Camilloni, and G. Stefani, Chem. Phys. Lett. 71, 335 (1980).
13. E. Lindholm, Ark. Fys. 40, 97 (1969).
14. E. Lindholm, Ark. Fys. 40, 129 (1969).
15. U. Fano and J. W. Cooper, Phys. Rev. 137, A1364 (1965).

23. REPORT OF THE WORKSHOP ON ELECTRONIC AND IONIC COLLISION CROSS SECTIONS NEEDED IN THE MODELING OF RADIATION INTERACTIONS WITH MATTER

Mitio Inokuti

The Workshop was held on 6-8 December 1983 at Argonne National Laboratory. It was attended by more than 40 scientists from outside the Laboratory and by about 10 members of the Laboratory staff. A full record of the Workshop is available as a topical report entitled "Proceedings of the Workshop on Electronic and Ionic Collision Cross Sections Needed in the Modeling of Radiation Interactions with Matter," ANL-84-28, issued in May 1984. The following excerpt from the Foreword of the Proceedings conveys the spirit of the Workshop.

"Detailed understanding of the changes that radiation actions produce in molecular substances is crucial to such important applications as dosimetry, estimation of the health effects of radiation, medical diagnostics and therapy, and radiation processing of materials in industry. At the earliest stage, radiation actions are caused by collisions of electrons and other energetic particles with molecules and by the resulting excitation, ionization, and dissociation of molecules. In particular, electron collisions are the most basic, because any ionizing radiations lead to the production of many energetic electrons in matter. As a consequence, there emerge many new molecular species. Because most of these new species are highly reactive, chemical changes result.

Although it is true that complete understanding of radiation actions requires knowledge in a vast range of fields, such as condensed-phase physics and chemical kinetics, knowledge of elementary collision processes is the most fundamental. Any sound discussion about molecular mechanisms of radiation actions must include some elements of the physics and cross-section data of those collision processes.

For applications to analysis of radiation actions, the cross-section data must fulfill what I call the "trinity of requirements": the data must be (1) correct, (2) absolute, and (3) comprehensive. By the term "comprehensive," I mean that the data must pertain to a wide range of variables involved, e.g., the incident energy and the scattering angle. Much too often, the data we see

in the literature are discordant (thus causing suspicion as to the correctness), relative (as opposed to absolute), and fragmentary (rather than comprehensive). The failure of the trinity of requirements is understandable because much of the collision study is motivated by interest in basic physics; to prove or disprove a point in physics, it is often sufficient and is indeed efficient to take data that are relative and limited to a small range of variables. I believe that the trinity of requirements also applies to the modeling done in other areas, e.g., discharge phenomena, plasmas, and astrophysics.

The main thrust of my work and that of some of my colleagues over the past two decades has been to find methods to test the data correctness, to provide comprehensive data for cases of importance to applications, and to develop systematics of data over different molecular species.

The term "modeling" in the Workshop title refers to the mathematical analysis of the consequences of many collision processes for characterizing the physical stage of radiation actions. It requires as input some knowledge of collision cross sections. Traditionally, work on cross sections and work on the modeling are conducted by separate groups of scientists.

It was the purpose of the Workshop to bring these two groups together in a forum that would promote effective communication. Cross-section workers described the status of their work and told what data were available or trustworthy. Modeling workers told what kind of data were needed or were most important. ••••••

Finally, I acknowledge on behalf of all the participants the most generous support provided by the University of Chicago through the Argonne Board of Governors, as well as assistance by the Division of Educational Programs and by the Office of Conference Services (Office of Public Affairs) of Argonne National Laboratory."

24. WHAT FORMULAS ARE GOOD FOR REPRESENTING DIPOLE AND GENERALIZED OSCILLATOR-STRENGTH SPECTRA?*

Mitio Inokuti and M. A. Dillon

Introduction

The dipole oscillator-strength distribution $df/d\varepsilon$ for a single continuum excitation of an atom or molecule is a function of the kinetic energy ε of an outgoing electron. The distribution describes many optical phenomena such as absorption, refraction, and reflection; in particular, $df/d\varepsilon$ is equal to the cross section for ionization by a photon with energy $\varepsilon + I$, apart from a universal constant, where I is the ionization threshold for the relevant shell.[1] Furthermore, $df/d\varepsilon$ governs the ionization by glancing collisions of fast charged particles.[2] Recent years have seen considerable accumulation of experimental data on $df/d\varepsilon$.[3,4] Those data are indeed valuable for many applications in radiation physics, plasma physics, atmospheric physics, and astrophysics. In most of these applications, one needs a comprehensive set of data, i.e., numerical values of $df/d\varepsilon$ over a wide range of ε, say, from several eV to many keV. Most often, one needs data at all ε at which $df/d\varepsilon$ is appreciable; however, it is unrealistic to expect measurements to cover all the ε values. Consequently, one must find a method for systematizing the data so that one can extrapolate or interpolate them dependably.

It is from the above consideration that we started a series of studies[5-8] aimed at answering the question in the title. The present lecture is in effect a summary of those studies.

Part 1 treats analytic properties of $df/d\varepsilon$ considered as a function of ε. To begin, one distinguishes two factors that together constitute $df/d\varepsilon$.[9] The first factor is defined in terms of the dipole matrix element with respect to the final-state wavefunction whose amplitude near the origin is independent of ε. This factor is analytic at all finite ε, except for a universal singularity[5] at $\varepsilon = -I$, where I is the relevant threshold ionization energy.

---

*Summary of a lecture presented at XIIth Yugoslav Summer School and International Symposium on Physics of Ionized Gases (SPIG), Sibenik, Yugoslavia, 3-7 September 1984.

The other factor stems from the normalization of the final-state wavefunction on the energy scale. This factor plays important roles in at least three respects.[6] First, when the phase shift rapidly varies with real ε (a situation that we shall loosely call a resonance), the normalization factor exhibits a maximum, and its local behavior may be approximated by a Lorentzian form. Second, the same factor is crucial for consideration of the high-ε asymptotic behavior. Finally, the analytic continuation of the same factor to negative ε naturally leads to properties of bound states including the discrete oscillator-strength spectrum. Through several examples, we shall illustrate the use of all the analytic properties in the practical fitting of the $df/d\varepsilon$ data.

Part 2 deals with the generalized oscillator strength, which is the only non-trivial factor in the differential cross section for the inelastic scattering of a charged particle by an atom or molecule, evaluated within the first Born approximation.[2] The distribution $df(K,\varepsilon)/d\varepsilon$ of the generalized oscillator strength for ionization is a function of both ε and momentum transfer K. The K-dependence of this function at a fixed ε is best elucidated through an analysis from the point of view of the theory of functions of a complex variable (which may be either K or K^2). This point of view was first advanced by Lassettre,[10] who specifically treated the generalized oscillator strength for the excitation to a bound excited state. Our recent work[8] is an extension of the work of Lassettre. Results of our analysis lead to practical methods for fitting the data specifically for ionization.

1. DIPOLE OSCILLATOR-STRENGTH DISTRIBUTION

1.1 The Reduced Matrix Element and the Normalization Factor

The essential ingredient of $df/d\varepsilon$ is the single-electron radial dipole matrix element. For a transition from an initial bound orbital $r^{-1}P_{n_0\ell_0}(r)$ to a final continuum orbital $r^{-1}P_{\varepsilon\ell}(r)$ of an atom, the radial matrix element $R_\ell(\varepsilon)$ is defined by

$$R_\ell(\varepsilon) = \int_0^\infty P_{\varepsilon\ell}(r)\, r\, P_{n_0\ell_0}(r)\,dr, \tag{1}$$

where $\ell = \ell_0 \pm 1$. It is convenient to distinguish two causes for the ε-dependence of $P_{\varepsilon\ell}(r)$, and hence of $R_\ell(\varepsilon)$. First, $P_{\varepsilon\ell}(r)$ obeys the Schrödinger

equation

$$[d^2/dr^2 - 2V(r) - \ell(\ell + 1)r^{-2} + 2\varepsilon]P_{\varepsilon\ell}(r) = 0, \tag{2}$$

where (and in what follows) we use the atomic-unit system (in which $e = \hbar = m = 1$). Suppose that $\bar{P}_{\varepsilon\ell}(r)$ is the solution of Eq. (2) whose amplitude near the origin is independent of ε, i.e.,

$$\bar{P}_{\varepsilon\ell}(r) = r^{\ell + 1} \qquad \text{near } r = 0. \tag{3}$$

However, $P_{\varepsilon\ell}(r)$ appropriate for Eq. (1) must satisfy the normalization condition

$$\int_0^\infty P_{\varepsilon\ell}(r)\, P_{\varepsilon'\ell}(r)dr = \delta(\varepsilon - \varepsilon'), \tag{4}$$

and it differs from $\bar{P}_{\varepsilon\ell}(r)$ by a factor $C_\ell(\varepsilon)$. That is to say,

$$P_{\varepsilon\ell}(r) = C_\ell(\varepsilon)\, \bar{P}_{\varepsilon\ell}(r). \tag{5}$$

Thus we may write

$$R_\ell(\varepsilon) = C_\ell(\varepsilon)\, \bar{R}_\ell(\varepsilon), \tag{6}$$

where $\bar{R}_\ell(\varepsilon)$ is the matrix element with respect to $\bar{P}_{\varepsilon\ell}(r)$, and it may be called the reduced matrix element. For real ε (i.e., for physical values of ε), the functions $P_{\varepsilon\ell}(r)$ and $\bar{P}_{\varepsilon\ell}(r)$ may be taken as real, without loss of generality. Therefore, $C_\ell(\varepsilon)$, $\bar{R}_\ell(\varepsilon)$, and $R_\ell(\varepsilon)$ are all real-valued for real ε.

Analytic properties of $\bar{R}_\ell(\varepsilon)$, now considered as a function of complex variable ε, are simple.[5] It is analytic for all finite ε except at a universal singularity at $\varepsilon = -I$. The cause for this singularity is elementary. First, consider contributions to $\bar{R}_\ell(\varepsilon)$ from finite r. From the general theory of differential equations, one knows that $\bar{P}_{\varepsilon\ell}(r)$ at any r is analytic for all finite ε, because ε appears in Eq. (2) as a constant coefficient. Therefore, the contribution to $\bar{R}_\ell(\varepsilon)$ from finite r is a function analytic for all finite ε. Next, consider the contribution to $\bar{R}_\ell(\varepsilon)$ from

large r at which the asymptotic behavior of the wavefunctions prevails. There the dominant factor of $P_{n_0\ell_0}(r)$ is $\exp[-(2I)^{1/2}r]$, and the dominant factor of $\bar{P}_{\varepsilon\ell}(r)$ is $\exp(\pm ikr)$. The product of the two exponentials gives $\exp[\pm ik - (2I)^{1/2}]r$. Thus $\bar{R}_\ell(\varepsilon)$ diverges at $\pm ik = (2I)^{1/2}$, i.e., at $\varepsilon = -I$. (More generally for $\mathrm{Re}[\pm ik - (2I)^{1/2}] > 0$, the integral diverges, but its analytic continuation is definable there. Thus $\bar{R}_\ell(\varepsilon)$ is singular at the point $\pm ik = (2I)^{1/2}$ only.) Although the location of the singularity is physically inaccessible, it is nevertheless important to recognize its presence. In other words, it is appropriate to represent $\bar{R}_{\varepsilon\ell}(\varepsilon)$ in terms of a variable that incorporates the singularity.

An example of such a variable is

$$g = \varepsilon/(\varepsilon + I). \tag{7}$$

To see its significance, one may view Eq. (7) as a conformal mapping from the complex ε plane onto the complex g plane. The half plane on the right of the vertical line $\mathrm{Re}\ \varepsilon = -I/2$ (the shaded region in Fig. 1) is mapped onto the interior of the unit circle. The singularity $\varepsilon = -I$ is mapped to $g \to \infty$. Physical data for the oscillator-strength pertain to real positive ε (forming the continuum), and to discrete negative values ε_1, ε_2, ... of ε (forming the discrete spectrum); we may call the set of all those ε values "the physical domain." By Eq. (7), the physical domain (indicated by the heavy line and

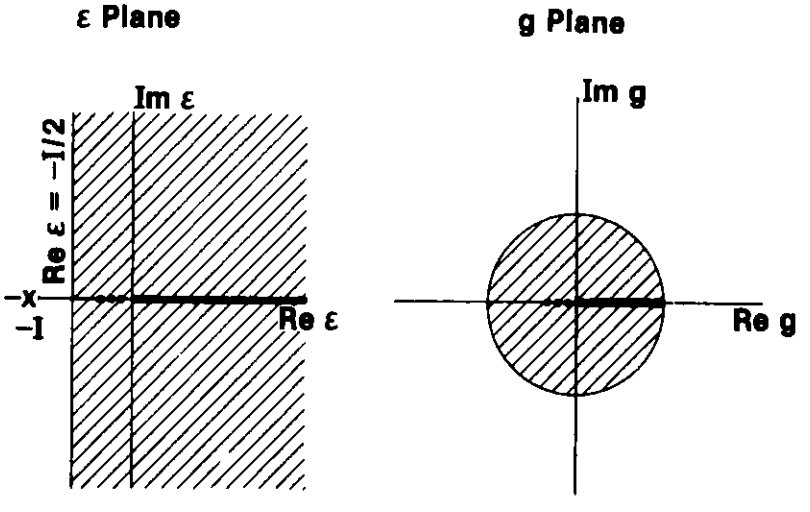

Fig. 1. Conformal mapping $g = \varepsilon/(\varepsilon + I)$.

dots in Fig. 1) is mapped onto a segment of the real axis on the g plane, and this segment is entirely within the interior of the unit circle. Because $\bar{R}_\ell(\varepsilon)$ has no singularity other than $\varepsilon = -I$, it is analytic in g certainly within the unit circle, and thus may be expressed by an absolutely convergent series in powers of g. In many examples,[5-7] the use of a polynomial in g of a modest degree is sufficient for effective representation of data on df/dε.

The quantity $C_\ell(\varepsilon)$ may be called the normalization factor or the enhancement factor,[9] and is closely related to what the solid-state theorist calls the density of states. General properties of $C_\ell(\varepsilon)$ have been studied both analytically and numerically.[6] When the phase shift $\delta_\ell(\varepsilon)$ changes rapidly with ε, $C_\ell(\varepsilon)$ shows a maximum. We may call this situation a resonance; in this case, the fitting of df/dε requires some parameterization of $C_\ell(\varepsilon)$, the use of a new variable, or both.[6] Further discussion of this topic is presented in Section 1.3.

1.2 Examples

1.2.1 Atomic hydrogen

It is instructive to look at the well-known expression for the df/dε of atomic hydrogen initially in the ground state,[5] i.e.,

$$df/d\varepsilon = (2^8/3)(1 + k^2)^{-4} \exp\left(-4k^{-1}\arctan k\right) [1 - \exp(-2\pi/k)]^{-1}, \qquad (8)$$

where k is wave number or the momentum of an outgoing electron measured in the atomic units, i.e., $k = (2\varepsilon)^{1/2}$. The ionization threshold energy I is 1/2 in atomic units.

Several observations regarding Eq. (8) are noteworthy. First, there is the factor $(1 + k^2)^{-4}$, which is singular at $\varepsilon = k^2/2 = -1/2$. In addition, $\exp[-4k^{-1} \arctan k]$ is also singular at the same value of ε. Indeed, the product of the two factors can be expressed by a power series in $g = k^2/(1 + k^2)$, i.e.,

$$(1 + k^2)^{-4} \exp\left(-4k^{-1}\arctan k\right) = \exp(-4) \sum_{n=0}^{\infty} c_n g^n. \qquad (9)$$

In Eq. (9), the coefficients c_n rapidly approach zero with increasing n ($c_0 = 1$, $c_1 = -2.67$, $c_2 = 2.09$, $c_3 = -0.278$, and $c_4 = -0.086$);[5] indeed, the

series is rapidly convergent for all finite ε.

The last factor

$$\tau(\varepsilon) = [1 - \exp(-2\pi/k)]^{-1} \tag{10}$$

arises from the normalization of the final state. It is indeed a factor in $C_1^2(\varepsilon)$ for the Coulomb field, which takes the form $C_1^2(\varepsilon) = (2/3)^2\ (1 + k^2)\ \tau(\varepsilon)$. It is mildly varying with real values of $\varepsilon = k^2/2$ between zero and infinity. Near the ionization threshold ($1 \gg k > 0$), $\tau(\varepsilon)$ is close to unity and varies little with ε. For large real positive values of ε, $\tau(\varepsilon)$ behaves smoothly (i.e., as $k/2\pi$).

Consider the same function $\tau(\varepsilon)$ as a function of a complex variable k. At $k = i/n$, where n is a non-zero integer, $\tau(\varepsilon)$ is singular. It has a pole there with residue $2\pi n^2$. Thus, the integral taken over a contour that encircles the eigenenergy $\varepsilon = -1/(2n^2)$ is

$$\oint (df/d\varepsilon)d\varepsilon = (2^8/3)n^5(n - 1)^{2n-4}(n + 1)^{-2n-4}, \tag{11}$$

which is nothing but the discrete oscillator strength for the excitation to the np state. This is precisely how the discrete spectrum arises. In general, $C_\ell(\varepsilon)$ provides a mathematical mechanism for the appearance of the discrete spectrum.[6]

1.2.2 Atomic sodium

For the valence-shell ionization (3s → εp transition), $df/d\varepsilon$ has a zero minimum, which stems from a change of sign of the matrix element $\bar{R}_1(\varepsilon)$. It is thus a particularly appropriate example for testing our fitting procedure. As Figure 2 shows, a polynomial in g of the fourth degree is adequate for representing a set of theoretical data based on the Hartree-Slater model. The normalization factor $C_1(\varepsilon)$ is a mild function of ε, and its variation calls for no particular parameterization, except at $\varepsilon \to \infty$.

1.2.3 Methane

This example[7] demonstrates the effectiveness of the polynomial in g in fitting experimental data for a molecule.[4] For the justification of our

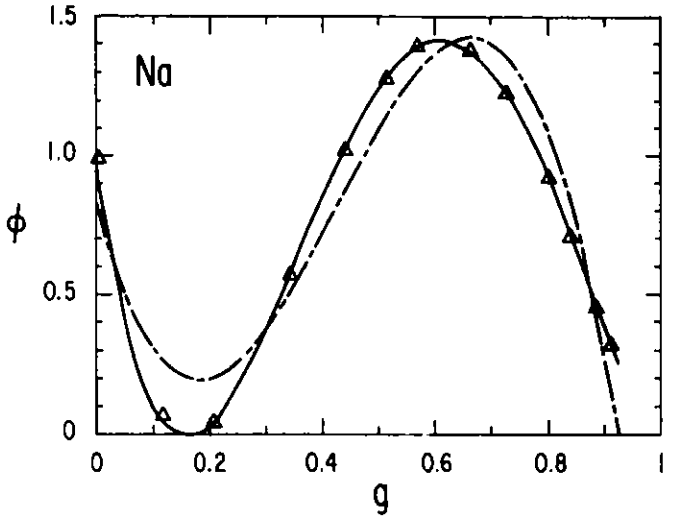

Fig. 2. Dipole oscillator-strength distribution for the 3s → εp transition of atomic sodium.[5] The vertical axis represents $\phi = (df/d\varepsilon)/(df/d\varepsilon)_{\varepsilon=0}$, i.e., the distribution normalized to unity at the threshold. The triangles represent the original data. The chained curve shows a least-squares fit with a third-degree polynomial in g, and the solid curve a similar fit with a fourth-degree polynomial.

procedure, we should note a few points. First, an electron in any molecule or in its vicinity is subject to an anisotropic field of force, and therefore its wavefunction is necessarily a superposition of partial waves having different angular momenta ℓ. Consequently, $df/d\varepsilon$ consists of contributions from terms specified by different ℓ. Nevertheless, the singularity position $\varepsilon = -I$ is independent of ℓ; thus, we can use the same variable g for molecules.

Figure 3 shows the (partial) oscillator-strength distribution for the ionization from the outermost orbital $2t_2$. The circles represent original experimental data,[4] and the curve represents results of the fitting with the use of a third-degree polynomial in g.

1.3 The Role of the Normalization Factor

In the preceding examples there was no need for explicit characterization of $C_\ell(\varepsilon)$. A counter-example arises when the phase shift $\delta_\ell(\varepsilon)$ rapidly varies with ε. As Manson and Cooper[9] fully documented, $\delta_\ell(\varepsilon)$ for the d waves, and more conspicuously for the f waves in the field of heavier atoms, often show rapid changes in the vicinity of certain energies. This occurs when the

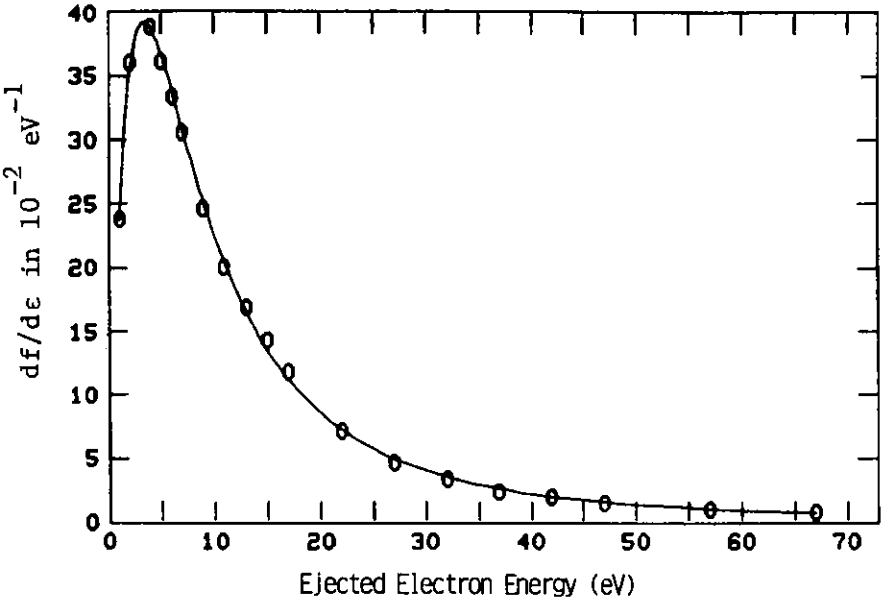

Fig. 3. Dipole oscillator-strength distribution for the ionization from the $1t_2$ orbital of methane.[7]

effective potential $V(r) + \ell(\ell + 1)/2r^2$ has a barrier at some r strong enough to trap temporarily an outgoing electron. We may loosely call this phenomenon a (shape) resonance. In the neighborhood of a resonance, $C_\ell^2(\varepsilon)$ in general has a maximum and often dominates the ε-dependence of $df/d\varepsilon$, as noted by Manson and Cooper.[9]

When there is a resonance, $C_\ell(\varepsilon)$ has a pair of simple poles at $\varepsilon = \varepsilon_R \pm i\Gamma/2$, where ε_R may be called the resonance energy and Γ the width. The behavior of $C_\ell^2(\varepsilon)$ in the neighborhood of real $\varepsilon = \varepsilon_R$ is Lorentzian, i.e.,

$$C_\ell^2(\varepsilon) = A + B/(\eta^2 + 1), \tag{12}$$

where $\eta = 2(\varepsilon - \varepsilon_R)/\Gamma$, A is a background term that varies smoothly with energy, and B is a parameter that describes the peak intensity. Certainly Eq. (12) may be easily incorporated into the data fitting.

Alternatively, we may introduce a new variable[6] that acounts for a resonance. As Figure 4 shows, we note the singularity $\varepsilon = -I$ of the reduced matrix element, and the poles at $\varepsilon = \varepsilon_R \pm i\Gamma/2$. Thus, we may use a conformal mapping, say from ε to h, that transforms a domain containing all three of the singularities to the exterior of the unit circle $|h| = 1$, and, at the same time, transforms the physical domain into the interior of the unit circle. An

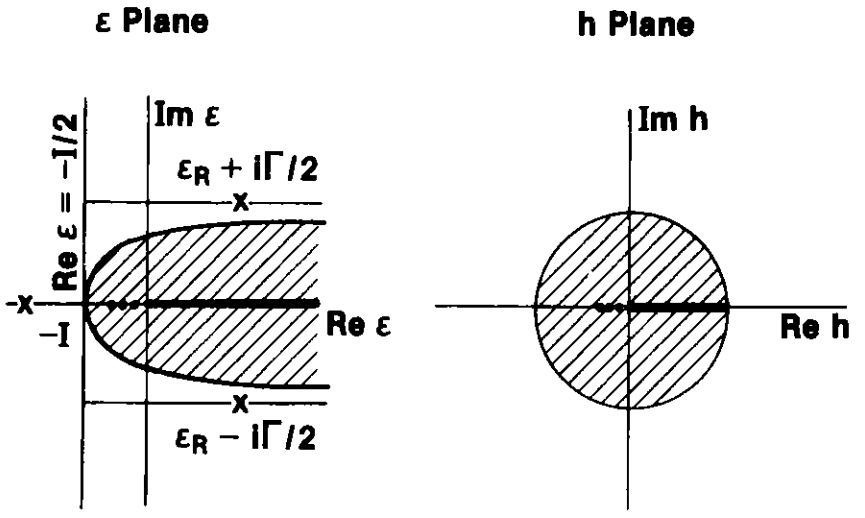

Fig. 4. Conformal mapping $h = [\exp(\pi\varepsilon/\Gamma) - 1]/[\exp(\pi\varepsilon/\Gamma) - b]$. The shaded area on the ε-plane is mapped onto the interior of the unit circle on the h-plane.[6]

example is

$$h = [\exp(\pi\varepsilon/\Gamma) - 1]/[\exp(\pi\varepsilon/\Gamma) - b], \tag{13}$$

where

$$b = 2\exp(-\pi I/2\Gamma) - 1. \tag{14}$$

In the limit $\Gamma \to \infty$, the effect of the resonance should disappear; indeed, h then approaches g defined by Eq. (7).

Now df/dε is analytic in h within the unit circle, and hence is expressible by an absolutely convergent series in powers of h for any ε in the physical domain.

Figure 5 illustrates the use of a polynomial in h. The original data (represented by the circles) are results of the Hartree-Slater calculation on the valence-shell ionization of Ar. The oscillator-strength distribution includes contributions from the 3p → d channel (which has a resonance) and from the 3p → s channel (which has no resonance); inclusion of the latter necessitates no new consideration about the variable h.

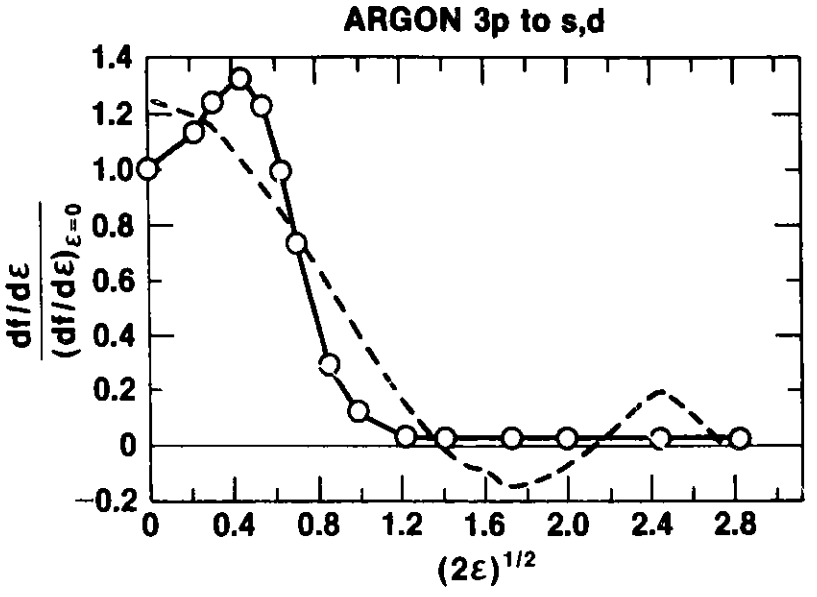

Fig. 5. Dipole oscillator-strength distribution for the 3p → εs, εd transition of argon.[6] The vertical axis represents the distribution normalized to unity at the threshold, and the horizontal axis the momentum $k = (2\varepsilon)^{1/2}$ of the ejected electron, measured in atomic units. The solid curve shows a least-squares fit with a third-degre polynomial in h. The broken curve shows a similar fit with a third-degree polynomial in ε, which is clearly unsuccessful.

2. GENERALIZED OSCILLATOR STRENGTH

2.1 Discrete Excitation

The generalized oscillator strength $f_n(K)$ for the excitation from the ground state (denoted by 0) to a discrete state n at momentum transfer K is defined by

$$f_n(K) = 2E_n K^{-2} \left| \langle n | \Sigma_j \exp(iKx_j) | 0 \rangle \right|^2, \tag{15}$$

where x_j is a Cartesian coordinate component of the jth electron, and E_n is the excitation energy. Properties of $f_n(K)$ are a central object of study in the Bethe theory of inelastic collisions of charged particles.[2] For definiteness, let us consider a discrete excitation in which an electron in the initial orbital $r^{-1}P_{n_0\ell_0}(r)$ in an atom makes a transition to the final orbital $r^{-1}P_{n\ell}(r)$. Then, $f_n(K)$ may be expressed as a weighted sum[11] of the squares of the matrix element

$$R(K) = \int_0^\infty P_{n\ell}(r)\, j_\lambda(Kr)\, P_{n_0\ell_0}(r)dr, \tag{16}$$

where $j_\lambda(Kr)$ is the spherical Bessel function of the first kind, and its order λ ranges from $|\ell - \ell_0|$ to $\ell + \ell_0$ in steps of two. Obviously R(K) depends on the indices n, ℓ, n_0, ℓ_0, and λ. However, for the simplicity of notation, we suppress these indices, inasmuch as we deal with R(K) with the same set of indices.

Let us consider analytic properties of R(K) as a function of complex variable K. Recall that $j_\lambda(Kr)$ is an entire function of K, i.e., is analytic at all finite K (at fixed values of λ and r). Likewise, $P_{n\ell}(r)$ and $P_{n_0\ell_0}(r)$ are entire functions of r. Therefore, the integral in Eq. (16) would be an entire function of K if the integration were to be taken over a finite interval of r. Actually R(K) is given by the integral extending to infinity, and this has an important consequence in the analyticity of R(K), as first recognized by Lassettre.[10]

Although a thorough analysis requires much preliminary discussion and attention to details, it is elementary to see how Lassettre's main point comes about. Consider contributions to the integral in Eq. (16) from those large distances r at which the asymptotic behavior of the integrand may be used. First of all, $P_{n_0\ell_0}(r)$ contributes the factor $\exp[-(2I)^{1/2}r]$, apart from a power in r (whose significance will be touched upon in the next paragraph). Likewise, $P_{n\ell}(r)$ contributes the factor $\exp[-(2I - 2E_n)^{1/2}r]$. Finally, recall that $j_\lambda(Kr) \to (Kr)^{-1} \cos[Kr - (\lambda + 1)\pi/2]$. Combining the three factors, the integrand has the factor exp(-Mr), where

$$M = (2I)^{1/2} + (2I - 2E)^{1/2} \pm iK. \tag{17}$$

When M vanishes, the integral diverges. In other words, R(K) has two singularities on the K-plane, given by

$$K = \pm i\alpha \equiv \pm i[(2I)^{1/2} + (2I - 2E)^{1/2}]. \tag{18}$$

The asymptotic behavior of the integrand contains factors other than the exponential. They amount to a power of r, and this determines the nature of the singularities (e.g., their orders if they are poles).

In general, $f_n(K)$ is a function of K^2, provided one either assumes rotational invariance or considers an average over the orientations of an atom

or molecule. Considered as a function of K^2, $f_n(K)$ is analytic except at the singularity at $K^2 = -\alpha^2$. Lassettre thus concluded that a suitable expression for data fitting is

$$f_n(K) = (1 - y)^p \sum_{n=0}^{N} c_n y^n, \tag{19}$$

where $y = x/(1 + x)$ and $x = K^2/\alpha^2$. The choice of the key variable y follows considerations of a conformal mapping, similar to those we saw in the choice of g in Part 1. The power p of the front factor is chosen so that the expression has the known asymptotic behavior[12] at large K^2, which depends on the symmetry and angular momenta of the states involved.

Although theory only tells that the series of Eq. (19) extended to $N \to \infty$ is absolutely convergent for $|y| < 1$, which includes all physical values of K^2, in practice a truncated series with a modest number of terms often represents data excellently. The power of the Lassettre expression, Eq. (19), has been fully demonstrated in many examples.[13-21] There are many merits of analytic representation. It summarizes data in a few parameters and facilitates extrapolation and interpolation, in the same way the quantum-defect theory does. Analytic representation leads to many applications that include calculations by the use of $f_n(K)$ data. Examples of such calculations concern a spectroscopic quantity such as the energy difference between singlet and triplet states,[16,17] a kinetic quantity such as the rate of intermolecular energy transfer,[19,20] and cross sections for electron inelastic collisions in distorted-wave and similar approximations.[21]

2.2 Ionization

2.2.1 Basics

The density $df(K, \varepsilon)/d\varepsilon$ of the generalized oscillator strength per unit range of the kinetic energy ε of an ejected electron is defined by an expression similar to Eq. (15); the only difference is that one puts as a final state a continuum wavefunction normalized on the energy scale. Thus, $df(K, \varepsilon)/d\varepsilon$ for single ionization may be expressed[11] in terms of the matrix element

$$R(K, \varepsilon) = \int_0^\infty P_{\varepsilon\ell}(r)\, j_\lambda(Kr)\, P_{n_0\ell_0}(r)\, dr, \tag{20}$$

which is a continuum version of Eq. (16). We shall concentrate on the dependence on K and ε.

To begin with, we use Eq. (5) and write

$$R(K, \varepsilon) = C_{\ell}(\varepsilon)\, \bar{R}(K, \varepsilon), \tag{21}$$

where $\bar{R}(K, \varepsilon)$ is the matrix element with respect to the (unnormalized) final-state wavefunction $\bar{P}_{\varepsilon\ell}(r)$. All the information about $C_{\ell}(\varepsilon)$ that we discussed in connection with the dipole oscillator-strength distribution applies.

The integrand in $\bar{R}(K, \varepsilon)$ is an entire function of both K and ε. Again, because the integral extends to infinity, it has singularities. Their locations can be readily found by examination of the asymptotic behavior of the integrand. To this, $P_{n_0\ell_0}(r)$ contributes the factor $\exp[-(2I)^{1/2}r]$, and $j_{\lambda}(Kr)$ contributes $\exp(\pm iKr)$, as before. The final-state wavefunction $P_{\varepsilon\ell}(r)$ contributes $\exp(\pm ikr)$, where $k = (2\varepsilon)^{1/2}$. Altogether these lead to the factor $\exp(-Mr)$, where

$$M = (2I)^{1/2} \pm iK \pm ik. \tag{22}$$

Thus, $\bar{R}(K, \varepsilon)$ are singular whenever $M = 0$. One may say that $\bar{R}(K, \varepsilon)$ has singularities either on the K plane (for fixed ε) or on the ε plane (for fixed K).

The analytic representation of data for ionization is in general more complicated and challenging than that for discrete excitation; indeed, it has been carried out only in a few instances.[8,22] There are two main reasons for this. First, there are two variables K^2 and ε to be used for the representation of the generalized oscillator strength, i.e., for the full characterization of the Bethe surface.[2] Second, there are two distinct elements of physics to be considered, viz, glancing collisions (accompanied by small K^2 and chiefly associated with lower ε), and hard collisions (characterized by large ε and comparable values of $K^2/2$, both greatly exceeding I). In what follows, we shall outline two approaches resulting from a recent study.[8]

2.2.2 Representation by a rational fraction

One way to incorporate the singularities given by Eq. (22) is the use of a rational fraction, i.e., a ratio of two polynomials in K^2, or of its generalizations. From the foregoing analysis one can determine the denominator form. For this purpose, we observe that the vanishing of M is equivalent to $2I = -(K \pm k)^2$, and thence to the vanishing of

$$D = [(K + k)^2 + 2I]\ [(K - k)^2 + 2I]. \tag{23}$$

Notice that $D > 0$ for all real K and k, that D is an even function of both K and k, and that D is invariant under the interchange of K and k. There are many expressions for D, e.g.,

$$D = (k^2 - K^2 + 2I)^2 + 8IK^2, \tag{24a}$$

$$D = (K^2 - k^2 + 2I)^2 + 8Ik^2, \tag{24b}$$

$$D = (K^2 - k^2)^2 + 4I(K^2 + k^2) + 4I^2. \tag{24c}$$

Equation (24a) shows that for fixed K^2, D as a function of k^2 attains a minimum at $k^2 = K^2 - 2I$ (provided $K^2 > 2I$). Equation (24b) shows that, for fixed k^2, D as a function of K^2 attains a minimum at $K^2 = k^2 - 2I$ (provided $k^2 > 2I$). The quantity D is monotonic in K^2 for fixed k^2 if $k^2 < 2I$.

For sufficiently large momentum transfer, an atomic electron should behave nearly as if it were free, the binding effect being of secondary importance. (This situation may be called an impulse collision, a quasi-free scattering, or a binary encounter, and justifies a class of approximations.) If the struck electron were free, then it would receive the kinetic energy $K^2/2$, which we call the recoil energy. Thus, the generalized oscillator strength must have a maximum in the neighborhood of $K^2 = k^2$, which is known as the Bethe ridge.[2] When $k^2 \gg 2I$, the denominator D is decisive for the description of this ridge. (As seen in Fig. 6, the maximum of $df(K, \epsilon)/d\epsilon$ begins to develop at quite low ϵ values, at which the role of D is not yet decisive.) It may be noted that D appears in the denominator of the known expressions for $df(K, \epsilon)/d\epsilon$ for atomic hydrogen, as given, for instance, by Inokuti[2] [in Eq. (3.10)] and by Holt.[23]

The foregoing considerations lead to an expression

$$df(K, \varepsilon)/d\varepsilon = D^{-3-m/2} \sum_{n=0}^{\mu} A_n (K^2)^n, \qquad (25)$$

where m is a modest integer, and A_n are coefficients to be determined, say, by the least-squares method. The upper limit index μ is chosen so that the correct high-K asymptotic behavior[12] of $df(K, \varepsilon)/d\varepsilon$ is incorporated; for instance $\mu = m + 1$ for an initial s state and $\mu = m$ for an initial p state. Figure 6 shows an example of a highly successful fitting of the generalized oscillator-strength density, specifically for the 2s-subshell ionization of the Al atom.

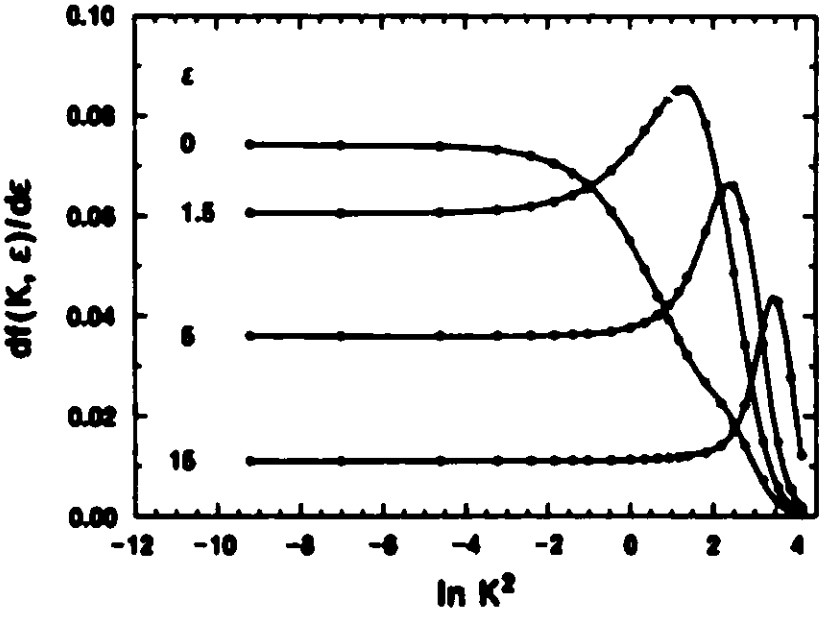

Fig. 6. The generalized oscillator-strength density for the ionization of the 2s-subshell of the aluminum atom.[8] The vertical axis represents $df(K, \varepsilon)/d\varepsilon$, and the horizontal axis ln K^2, both measured in atomic units. The dots represent the original data based on the Hartree-Slater model as described by Inokuti and Manson.[24] Each of the solid curves shows a least-squares fit to Eq. (25) with m = 4 (i.e., by use of a fifth-degree polynomial, in the numerator). The data sets refer to the ejected-electron energy ε = 0, 1.5, 5, and 15 atomic units.

2.2.3 Use of a conformal mapping

Another line of approach begins with the examination of the singularity position on the K^2 plane. Note that N = 0 of Eq. (22) leads to $K^2 = k^2 - 2I \pm$

singularities are located at the positions given by

$$Q_x \equiv \mathrm{Re}\, K^2 = k^2 - 2I, \qquad Q_y \equiv \mathrm{Im}\, K^2 = 2(2I)^{1/2}k. \tag{26}$$

If we eliminate k from the above equations, we obtain the equation

$$Q_x = Q_y^2/8I - 2I \tag{27}$$

for the locus of the singularities as k^2 varies. This locus is a parabola, as seen in Figure 7.

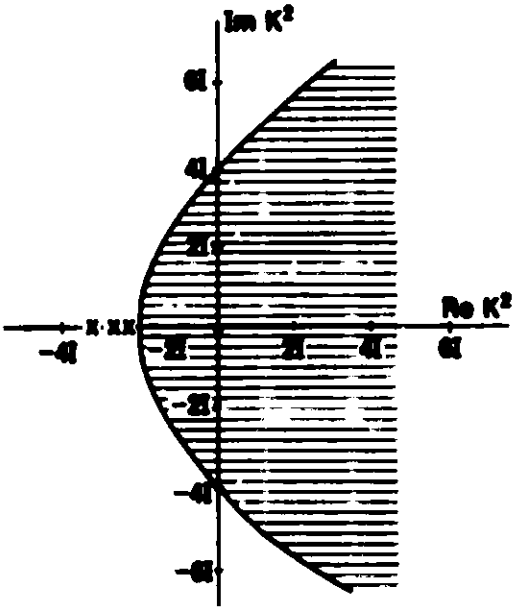

Fig. 7. The locus of the singularities of the generalized oscillator-strength density $df(K, \epsilon)/d\epsilon$ on the K^2 plane. The parabola is given by Eqs. (26) and (27). For each value of $k^2 > 0$, there are two singularities whose locations are symmetric with respect to the real axis. With increasing k^2, the locations move from left to right on the parabola. Under the conformal mapping given by Eq. (28), the shaded domain on the K^2 plane is mapped onto the interior of the unit circle on the w-plane. The shaded domain includes all the physical values, i.e., real and positive values, of K^2. The singularities of $f_n(K)$ for bound states (indicated by X's) are located on the real axis to the left of the parabola.

Consider a conformal mapping given by

$$w = \tanh^2[\pi K/4(2I)^{1/2}]. \tag{28}$$

The domain inside the parabola on the K^2 plane, which includes all physical values $K^2 > 0$, is mapped onto the interior of the unit circle $|w| = 1$. By definition the singularities for all values of $k^2 > 0$ are on the parabola and are mapped to the boundary of the unit circle. Consequently, a power series in w will be suitable for representing the K^2-dependence of $df(K, \varepsilon)/d\varepsilon$ for any $\varepsilon > 0$; it will be absolutely convergent for any $|w| < 1$, and hence for all physical values of K^2 and ε. The singularities for the bound-state generalized oscillator strength $f_n(K)$, as given by Eq. (18), are on the real axis with Re $K^2 < -2I$, i.e., outside the parabola. Therefore, the power series in w is usable also for $f_n(K)$.

3. CONCLUDING REMARKS

It is hoped that the foregoing discussion has conveyed the sense of importance we attach to the study of analytic properties of various quantities related to atomic structure and scattering. Our treatment of the dipole matrix element can be readily adapted to other matrix elements; an example may be Slater integrals that arise in multichannel or many-electron treatments. Extension of our analysis may be possible to energy spectra of secondary electrons due to charged-particle collisions. Finally, we note that Lassettre[25-28] has extended his original idea in other directions, and thus has elucidated analytic properties of collision amplitudes and momentum eigenfunctions for atoms. As an expression of our respect, admiration, and affection, we dedicate the present paper to Professor Lassettre.

References

1. U. Fano and J. W. Cooper, Rev. Mod. Phys. 40, 441 (1968); 41, 724 (1969).
2. M. Inokuti, Rev. Mod. Phys. 43, 297 (1971).
3. J. Berkowitz, Photoabsorption, Photoionization, and Photoelectron Spectroscopy (Academic Press, New York, 1979).
4. C. E. Brion and A. Hamnett, in Advances in Chemical Physics. Vol. 45 The Excited State in Chemical Physics, Part 2, edited by J. W. McGowan (John-Wiley, New York, 1981) p. 1.
5. M. A. Dillon and M. Inokuti, J. Chem. Phys. 74, 6271 (1981).
6. M. A. Dillon and M. Inokuti, Analytic Representation of the Dipole Oscillator-Strength Distribution. II. The Normalization Factor for Electron Continuum States in Atomic Fields. (to appear in J. Chem. Phys.)
7. M. A. Dillon, in Proceedings of the Workshop on Electronic and Ionic Collision Cross Sections Needed in the Modeling of Radiation Interactions with Matter, Argonne National Laboratory, 6-8 December 1983, Report No. ANL-84-28, p. 96.

8. M. A. Dillon, M. Inokuti, and Z.-W. Wang, Analytic Representation of the Generalized Oscillator Strength for Ionization. (to appear in Radiat. Res.)
9. S. T. Manson and J. W. Cooper, Phys. Rev. 165, 126 (1968).
10. E. N. Lassettre, J. Chem. Phys. 43, 4479 (1965).
11. S. T. Manson, Phys. Rev. A 5, 668 (1972).
12. A. R. P. Rau and U. Fano, Phys. Rev. 162, 68 (1967).
13. E. N. Lassettre, A. Skerbele, and M. A. Dillon, J. Chem. Phys. 50, 1829 (1969).
14. A. Skerbele and E. N. Lassettre, J. Chem. Phys. 52, 2708 (1970).
15. A. Skerbele and E. N. Lassettre, J. Chem. Phys. 56, 845 (1972).
16. E. N. Lassettre and A. Skerbele, J. Chem. Phys. 60, 2464 (1974).
17. K. N. Klump and E. N. Lassettre, Can. J. Phys. 53, 1825 (1975).
18. K. N. Klump and E. N. Lassettre, Chem. Phys. Lett. 51, 99 (1977).
19. K. N. Klump and E. N. Lassettre, J. Chem. Phys. 68, 886 (1978).
20. K. N. Klump and E. N. Lassettre, J. Chem. Phys. 68, 3511 (1978).
21. M. A. Dillon and M. Inokuti, J. Chem. Phys. 76, 5887 (1982).
22. M. A. Dillon, J. Chem. Phys. 68, 2037 (1978).
23. A. R. Holt, J. Phys. B 2, 1209 (1969).
24. M. Inokuti and S. T. Manson, in Electron Beam Interactions with Solids for Microscopy, Microanalysis and Microlithography, edited by D. F. Keyser et al. (Scanning Electron Microscopy, Inc., AMF O'Hare, Illinois, 1984) p. 1.
25. E. N. Lassettre, J. Chem. Phys. 57, 4357 (1972).
26. E. N. Lassettre, J. Chem. Phys. 58, 1991 (1973).
27. W. M. Huo and E. N. Lassettre, J. Chem. Phys. 72, 2374 (1980).
28. E. N. Lassettre, Momentum eigenfunctions and first-order collision amplitudes as functions of a complex variable. Comments At. Mol. Phys. (submitted for publication).

25. TOTAL IONIZATION CROSS SECTIONS FOR ELECTRON IMPACT

F. J. de Heer* and Mitio Inokuti

We conducted an extensive review of experimental techniques for measuring the total ionization cross sections for electron impact, and undertook a critical survey of current data for neutral atoms and molecules. Results are presented in Chapter 7 (pp. 232-276) of a monograph entitled "Electron Impact Ionization," edited by T. D. Märk and G. H. Dunn, and to be published in 1985 by Springer-Verlag, Vienna. One of our main conclusions is that the current data are far from being complete and reliable and that the time is ripe for renewed efforts toward better measurements.

---

*FOM Institute for Atomic and Molecular Physics, Kruislaan 407, 1098 SJ Amsterdam, The Netherlands.

26. ELECTRON PRODUCTION IN PROTON COLLISIONS: TOTAL CROSS SECTIONS*

M. E. Rudd,† Y.-K. Kim,‡ D. H. Madison,¶ and J. W. Gallagher§

Existing data on ionization of neutral atoms and molecules by proton impact are reviewed, and electron production cross-section data are collected. The three major experimental methods are discussed and possible sources of error identified. Some theoretical cross sections are discussed and well-established methods of relating them to other measured cross sections are reviewed. A mathematical equation is fitted to the weighted experimental data for each target, and these fits are adjusted to be consistent with appropriate theoretical calculations and with electron impact and photoionization data. Recommended values of total cross sections for proton-impact ionization are given.

*Abstract of an article to be published in Rev. Mod. Phys.

†Department of Physics and Astronomy, University of Nebraska-Lincoln, Lincoln, NE 68588-0111.
‡National Bureau of Standards, Gaithersburg, MD 20899.
¶Department of Physics, Drake University, Des Moines, IA 50311.
§Joint Institute for Laboratory Astrophysics, University of Colorado and National Bureau of Standards, Boulder, CO 80309.

27. HOW DO WE DECIDE WHETHER THE FIRST BORN APPROXIMATION APPLIES TO INELASTIC COLLISIONS OF CHARGED PARTICLES WITH AN ATOM OR MOLECULE?*

Mitio Inokuti and S. T. Manson†

Because of the 1930 work by Bethe,[1] we know that if the first Born approximation (FBA) applies, then the scattering amplitude is a function of the single scalar variable, i.e., the magnitude of the momentum transfer $\hbar K$, apart from a kinematic factor. In other words, the angular distribution of inelastic scattering is completely governed by $\hbar K$ and does not depend explicitly upon the incident-particle energy. This is true so long as a target atom or molecule is either spherical or is randomly oriented so that one may assume the rotational symmetry of the target. The above statement is a straightforward consequence of the result that the FBA amplitude is essentially determined by the matrix element of the operator $\Sigma_j \exp(i\vec{K}\cdot\vec{r}_j)$ taken between the initial eigenstate and the final eigenstate of the target.[2] Lassettre and co-workers[3-5] used the statement skillfully and systematically in their analysis of electron-impact data.

A motivation of our study is to help resolve a general issue in atomic-collision physics. There are two major sources of uncertainties in the evaluation of cross sections. First, one uses an approximation for treating the collision process, e.g., the FBA, the distorted-wave approximation, or the close-coupling approximation. Second, explicit evaluation of cross sections within any of these approximations must use as input eigenfunctions for the target in the initial state and in the final state at least, and possibly in the intermediate states. It is important to distinguish these two sources of uncertainties as clearly as possible. For instance, once we are sure that the FBA holds, then uncertainties in the cross-section evaluation are fully attributable to the uncertainties in the target eigenfunctions.

---

*Abstract of a paper presented at the XIII International Conference on the Physics of Electronic and Atomic Collisions, Berlin, July 1983. See the Abstracts of Contributed Papers, edited by J. Eichler, W. Fritsch, I. V. Hertel, N. Stolterfoht, and U. Wille, (International Conference on the Physics of Electronic and Atomic Collisions, 1983) p. 151.

†Department of Physics & Astronomy, Georgia State University, Atlanta, Georgia 30303.

The well-known result stated in the first paragraph is a necessary condition for the applicability of the FBA, and has not been regarded as a sufficient condition.[2-5] In other words, if the FBA applies, then the magnitude $\hbar K$ of the momentum transfer determines all the dynamics of the inelastic collision.

We have studied for some time the logical converse of the well-known result. If the magnitude of the momentum transfer completely determines the scattering amplitude or the angular distribution of inelastic scattering, then are we sure that the FBA holds? To paraphrase the question further, we have seriously asked whether a sufficient condition for the applicability of the FBA is the dependence of the scattering amplitude solely on the magnitude of the momentum transfer. There are many other ways to pose virtually the same question. For instance, if an observed angular distribution of secondary electrons of fixed kinetic energy is axially symmetric around the vector momentum transfer $\hbar\vec{K}$, then can we say that the scattering amplitude should be fully described within the FBA? Another example concerns the polarization of excited states resulting from electron or other charged-particle impact.[6] If the FBA holds, then the target polarization must be completely determined by the momentum-transfer direction; in other words, the final state of the target must have the magnetic quantum number $M = 0$, with respect to the quantization axis along vector $\hbar\vec{K}$. Is the logical converse of this statement true?

We now have a tentative answer to the question in the affirmative. That is to say, if the angular distribution of inelastic scattering is fully determined by the magnitude of the momentum transfer $\hbar K$ (but is independent of its direction), then the same angular distribution will be given by the FBA. We have no completely rigorous proof for this, but have strong plausibility arguments.

References

1. H. Bethe, Ann. Phys. (Leipzig) 5, 325 (1930).
2. M. Inokuti, Rev. Mod. Phys. 43, 297 (1971).
3. E. N. Lassettre and S. A. Francis, J. Chem. Phys. 40, 1208 (1964).
4. E. N. Lassettre, Can. J. Chem. 47, 1733 (1969).
5. E. N. Lassettre, A. Skerkele, and M. A. Dillon, J. Chem. Phys. 50, 1829 (1969).
6. U. Fano and J. H. Macek, Rev. Mod. Phys. 45, 553 (1973).

28. STOPPING POWERS OF ELECTRONS AND POSITRONS

Mitio Inokuti

The International Commission on Radiation Units and Measurements (ICRU) several years ago appointed a Committee on Stopping Powers, whose charge is to conduct a survey of experimental and theoretical data for substances of radiological and dosimetric interest and to produce reports on the current status of the topic, including recommended values of stopping powers.

The first phase of the work, concerning electrons and positrons, was completed in 1983 by the Committee [consisting of M. J. Berger (Chairman), M. Inokuti (Vice-Chairman), H. H. Andersen, H. Bichsel, J. A. Dennis, D. Powers, S. M. Seltzer, and J. E. Turner]. An initial report entitled "Stopping Powers for Electrons and Positrons" was issued in October 1984 as ICRU Report 37.

That report starts with a review of the theory of the collision stopping power. It extensively treats the mean excitation energies for all elements and many compounds, critically analyzes values in the literature, and presents recommended values for many substances. The discussion also includes the density effect, shell corrections, and low-energy phenomena. Then, the radiative stopping power is also calculated by use of contemporary advanced theories.

From the total stopping power (i.e., the sum of the collision stopping power and the radiative stopping power) evaluations was made of the range (in the continuous-slowing-down approximation) and of the radiation yield were made.

Stopping-power values were tabulated for electrons at kinetic energies 10 keV - 1 GeV for 27 elemental substances and 49 compounds (including mixtures).

Plans are laid out for future work. The second phase concerns protons and the alpha particles, and the third phase heavier ions.

29. INNER-SHELL CORRECTIONS TO THE BETHE STOPPING-POWER FORMULA EVALUATED FROM A REALISTIC ATOMIC MODEL*

Mitio Inokuti and S. T. Manson†

Suppose that a particle of charge ze and speed $v = \beta c$ collides with an atom and transfers to it energy E and momentum $\hbar K$. In place of $\hbar K$ one may use the variable $Q = (\hbar K)^2/2m$, which means the kinetic energy that would be transferred to an atomic electron were it not bound to the atom. Let $d^2\sigma/dEdQ$ be the doubly differential cross section for the inelastic collision. Then, the mean energy loss of the particle per unit pathlength in matter containing N atoms per unit volume is given as

$$-dE/dx = N \int_{E_{min}}^{E_{max}} dE \int_{Q_{min}}^{Q_{max}} dQ \quad E d^2\sigma/dEdQ. \tag{1}$$

In the Bethe theory, one starts with the first Born approximation for $d^2\sigma/dEdQ$, uses several general properties of the integrands and of the integration limits, and eventually arrives at

$$-dE/dx = (4\pi z^2 e^4/mv^2)\, NZ\, [\ln(2mv^2/I) - \ln(1 - \beta^2)$$

$$-\beta^2 - C/Z - 1/2\delta] \quad , \tag{2}$$

where Z is the atomic number, I is the mean excitation energy, C/Z is the shell correction, and δ is the density correction. (See U. Fano[1] for the derivation.)

The shell correction is most important for inner shells and may be expressed in terms of the density $df(Q,E)/dE$ of the generalized oscillator

---

*Abstract of a paper presented at the VIIth International Congress of Radiation Research, Amsterdam, July 1983. See the Proceedings, edited by J. J. Broerse, G. W. Barendsen, H. B. Kal, A. J. van der Kogel (Martinus Nijhoff Publishers, 1983) Paper No. A1-19.

†Department of Physics & Astronomy, Georgia State University, Atlanta, Georgia 30303.

strength as

$$C/Z = 1/2 \int_{E_{min}}^{E_{max}} dE \left\{ \int_{0}^{E^2/2mv^2} [df/(Q,E)/dE - df(0,E)/dE]Q^{-1}dQ \right.$$

$$\left. - \int_{2mv^2}^{\infty} df(Q,E)/dE\ Q^{-1}dQ \right\}, \qquad (3)$$

according to Fano. This expression has been evaluated with the use of the hydrogenic model for the K- and L-shell,[2,3] as well as the M-shell.[4] The shell correction also has been calculated for the free-electron model.[5] The results from the hydrogenic model and the free-electron model are the standards now in use in analysis of experimental data.

We have been studying for some time the generalized oscillator strength for the ionization of the K- and L-shell.[6,7] Our calculation is based on a central potential derived from the Hartree-Slater model that should be far more realistic than the hydrogenic model. We have compared the generalized oscillator strengths evaluated from the two models for the K- and L-shell of all atoms up to Z = 30, and found sizable differences in practically every case in which an ejected electron carries low kinetic energies, i.e., energies of several Rydbergs or less.

The evaluation of the shell correction according to Eq. (3) is in progress. Results will be compared with other studies, such as the direct numerical evaluation[8] of Eq. (1).

References

1. U. Fano, Ann. Rev. Nucl. Sci. 13, 1 (1963).
2. M. C. Walske, Phys. Rev. 88, 1283 (1952).
3. M. C. Walske, Phys. Rev. 101, 940 (1956).
4. H. Bichsel, Phys. Rev. A 28, 1147 (1983).
5. E. Bonderup, Kgl. Danske Videnskab. Selskab. Mat.-Fys. Medd. 35, No. 17 (1967).
6. S. T. Manson and M. Inokuti, J. Phys. B 13, L323 (1980).
7. M. Inokuti and S. T. Manson, in Proceedings of the First Pfefferkorn Conference on Electron Beam Interactions with Solids for Microscopy, Microanalysis, and Microlithography, Asilomar, Pacific Grove, California, 18-23 April 1982, edited by D. F. Kyser, H. Niedrig, D. E. Newbury, and R. Shimizu (Scanning Electron Microscopy, Inc., 1984) p. 1.
8. E. J. McGuire, Phys, Rev. A 26, 1858 (1982).

30. A THEORETICAL STUDY OF EXCITED-STATE FORMATION DUE TO SUBEXCITATION ELECTRONS IN RARE GAS - NITROGEN MIXTURES.*

C. A. Naleway,† Mitio Inokuti, and M. C. Sauer, Jr.‡

The pulse radiolysis of low pressures of helium or neon containing trace amounts of nitrogen results in the formation of excited states of N_2. The formation and radiative decay of the $C^3\Pi_u$ state of N_2 has been experimentally measured and previously reported.[1]

A model has been developed to theoretically examine the evolution of excited states of N_2 within an inert-gas environment. The helium subexcitation spectrum of electrons as developed by Platzman[2] defines the initial source of excitation energy for the N_2. The further degradation of these low-energy electrons is followed in time down to the threshold for excitation of the $N_2(C^3\Pi_u)$ state. The continuous-slowing-down approximation is invoked, and all loss processes associated with momentum transfer to helium, as well as all accessible inelastic loss processes associated with N_2, are considered. The theoretical rate of formation of $C^3\Pi_u$ emission is in qualitative agreement with the experiment and supports the experimentally observed dependence of the rate upon N_2 pressure.

References

1. R. Cooper, L. Denison, and M. C. Sauer, Jr., J. Phys. Chem. 86, 5093 (1982).
2. R. L. Platzman, Radiat. Res. 2, 1 (1955).

---

*Abstract of a paper presented at the 32nd Annual Meeting, Radiation Research Society, Orlando, Florida, 25-29 March 1984. A full paper is being prepared for publication.
†Division of Chemistry, American Dental Association, 211 E. Chicago Avenue, Chicago, Illinois 60611.
‡Chemistry Division, Argonne National Laboratory.

31. MECHANISMS FOR THE SPUTTERING OF CONDENSED-GAS SOLIDS BY CHARGED PARTICLES*

R. E. Johnson† and Mitio Inokuti

It has been known for some time that fast ions and electrons erode surfaces of insulating materials quite efficiently.[1] In these materials, the process of erosion, which may be also called sputtering, is a consequence of the electronic excitation and ionization caused by the incident charged particles either directly or through secondary particles. In metals, by contrast, sputtering is a consequence of atomic cascades due to energy transfer to the atomic translational motion.

The sputtering of the insulating materials, especially of condensed-gas solids and organic solids, is a special example of radiation effects. This topic deserves examination from a basic-physics point of view, including the initial energy delivery and the track structure. Moreover, the sputtering is amenable to detailed experimental studies; for instance, one can measure the yields of ejected molecular species.

In molecular solids (thin samples of which may be produced by condensation of gaseous molecules at low temperature), the total yield of sputtering due to fast ions is independent of temperature so long as the temperature is extremely low. (At higher temperatures, the total yield becomes temperature-dependent.) The species ejected in the sputtering of the D_2O ice are predominantly D_2O at low temperatures, but include appreciable amounts of O_2 and D_2 at higher temperatures.[2]

The information about sputtering is in many ways complementary to the information about luminescence, i.e., about photons emitted from materials under irradiation. By relating sputtering data to luminescence data, we gain some understanding of the mechanisms involved and discuss some aspects of the

---

*Abstract of a paper presented at the VIIth International Congress of Radiation Research, Amsterdam, July 1983. See the Proceedings, edited by J. J. Broerse, G. W. Barendsen, H. B. Kal, A. J. van der Kogel, (Martinus Nijhoff Publishers, 1983) Paper No. A1-22.

†Department of Nuclear Engineering and Engineering Physics, University of Virginia, Charlottesville, Virginia 22901.

electronic relaxation processes. Of particular interest in this context are those non-radiative relaxation processes that lead to bond rupture and other permanent chemical and molecular-structural changes.

From the above point of view, we have considered in some detail the molecular mechanisms of the relaxation process leading to the dissociation or the production of an atomic or molecular species heaving appreciable kinetic energy. On the basis of the general knowledge of molecular energy levels (including luminescence data), we readily recognize that any single-electron excitation in a molecular solid (which consists of closed-shell structure) leads to entirely new interatomic forces. Therefore, an appreciable fraction of the electronic excitation energy will be converted to the translational energy of atoms, which in turn contributes to the sputtering. For argon and other rare-gas solids, i.e., for those examples for which the best basic data seemed to be at hand, we have put forth an analysis of the data on the sputtering at low temperatures, where the total yield is independent of temperature.[3] The same general idea that we used for rare-gas solids should be applicable to other molecular solids, although with some modifications.

There are other important issues to be discussed for the full understanding of the sputtering mechanism. For example, the observed total yield of sputtering at low temperatures certainly increases with the electronic stopping power, and is not proportional to it. Thus, it is important to analyze the modes of transport of the electronic-excitation energy to the surface region and the possible effects of closely packed excited (but un-ionized) molecules.[4] At higher temperatures, where the total sputtering yield depends on the temperature, the mobilities of radicals or other issues are likely to be important.[5]

References

1. W. L. Brown, L. J. Lanzerotti, and R. E. Johnson, Science 218, 525 (1982).
2. W. L. Brown, W. M. Augustyniak, E. Simmons, K. J. Marcantonio, L. J. Lanzerotti, R. E. Johnson, J. W. Boring, C. T. Reimann, G. Foti, and V. Pirronello, Nucl. Instrum. Methods 198, 1 (1982).
3. R. E. Johnson and M. Inokuti, Nucl. Instrum. Methods 206, 289 (1983).
4. R. E. Johnson and W. L. Brown, Nucl. Instrum. Methods 198, 103 (1982).
5. W. L. Brown, W. M. Augustyniak, L. J. Lanzerotti, R. E. Johnson, and R. Evatt, Phys. Rev. Lett. 45, 1632 (1981).

32. THE OPTICAL PROPERTIES AND COMPLEX DIELECTRIC FUNCTION OF METALLIC ALUMINUM FROM 0.04 TO 10^4 eV*

D. Y. Smith,† E. Shiles,‡ and M. Inokuti

Measurements of the optical properties of metallic aluminum are reviewed and available data are analyzed to obtain the bulk values of the optical constants and the complex dielectric function from 0.04 eV to 10 keV. The intra- and interband contributions to the dielectric function are discussed briefly, and recently proposed values for the Drude parameters describing the intraband absorption are critically considered. Factors influencing experimental measurements are discussed, with emphasis on sample properties such as surface oxide layers, bulk inclusion of gases, surface roughness, and degree of crystallinity. The results of recent optical measurements are tabulated, along with recommended values of the optical properties resulting from a self-consistent Kramers-Kronig analysis of reflectance, transmission, and electron-energy-loss studies. The tabular data include the complex dielectric function, the complex index of refraction, and the reflectance and phase shift for normal incidence on a smooth, oxide-free surface. Detailed tabulations are given for the infrared, visible, and ultraviolet regions of the spectrum.

---

*Abstract of a topical report, ANL-83-24, issued in March 1983. This article will be included in Handbook of Optical Constants of Solids, edited by E. Palik, to be published by Academic Press.

†Materials Science and Technology Division, Argonne National Laboratory.
‡Gulf Research and Development Company, Houston, Texas 77236.

FUNDAMENTAL MOLECULAR PHYSICS AND CHEMISTRY PROGRAM

PAPERS AND ABSTRACTS
1 January - 31 December 1983

Journal Articles

P. M. Dehmer, Rydberg States of van der Waals Molecules -- A Comparison With Rydberg States of Atoms and of Chemically-Bonded Species, Comments At. Mol. Phys. 13, 205-227 (1983)

P. M. Dehmer and W. A. Chupka, Photoabsorption and Photoionization of HD, J. Chem. Phys. 79, 1569-1580 (1983)

P. M. Dittman, Dan Dill, and J. L. Dehmer, Valence-Shell Photoabsorption by CO_2 and Its Connections with Electron-CO_2 Scattering, Chem. Phys. 78, 405-423 (1983)

D. L. Ederer, R. P. Madden, A. C. Parr, G. Rakowsky, E. B. Saloman, J. Cooper, R. Stockbauer, T. E. Madey, and J. L. Dehmer, An Overview of Research at NBS Using Synchrotron Radiation at SURF-II, IEEE Trans. Nucl. Sci. NS-30, 1020-1025 (1983)

D. M. P. Holland, A. C. Parr, and J. L. Dehmer, Photoelectron Asymmetry Parameters and Branching Ratios For Sulphur Dioxide in the Photon Energy Range 14 To 25 eV, J. Electron Spectrosc. 32, 237-243 (1983)

D. M. P. Holland, A. C. Parr, D. L. Ederer, J. B. West, and J. L. Dehmer, Triply Differential Photoelectron Studies of the Four Outermost Valence Orbitals of Cyanogen, Int. J. Mass Spect. Ion Phys. 52, 195-208 (1983)

D. M. P. Holland, J. B. West, A. C. Parr, D. L. Ederer, R. Stockbauer, R. D. Buff, and J. L. Dehmer, Constant Photoelectron Energy Spectroscopy of Acetylene, J. Chem. Phys. 78, 124-130 (1983)

K.-N. Huang, Theoretical Triply Differential Cross Section of Electron-Impact Ionization of Atoms, Phys. Rev. A 28, 1969-1872 (1983)

K.-N. Huang, Y.-K. Kim, K. T. Cheng, and J. P. Desclaux, Energy Level Scheme and Transition Probabilities of Cl-Like Ions, At. Data and Nucl. Data Tables 28, 355-377 (1983)

M. Inokuti, How Do Japanese Scientists Learn the Art of Writing Papers in English? I and II (in Japanese), Butsuri [Proc. Phys. Soc. Japan] 38, 537-542 (July 1983); 38, 622-627 (August 1983)

R. E. Johnson and Mitio Inokuti, Electronic Relaxation in Rare-Gas Solids: Ejection of Atoms by Fast Charged Particles, Nucl. Instrum. Methods 206, 289-297 (February 1983)

R. E. Johnson and M. Inokuti, The Local-Plasma Approximation to the Oscillator-Strength Spectrum: How Good Is It and Why?, Comments Atom. Molec. Phys. 14(2), 19-31 (1983)

W. R. Johnson, D. Kolb, and K.-N. Huang, Electron-Dipole, Quadrupole, and Magnetic-Dipole Susceptibilities and Shielding Factors for Closed-Shell Ions of the He, Ne, Ar, Ni(Cu+), Kr, Pb, and Xe Isoelectronic Sequences, At. Data and Nucl. Data Tables 28, 333-340 (1983)

Y.-K. Kim, Angular and Energy Distributions of Secondary-Electrons from Helium. I. Slow Electrons Ejected by Electron Impact, Phys. Rev. A 28, 656-666 (1983)

A. C. Parr, D. M. P. Holland, D. L. Ederer, and J. L. Dehmer, Effects of Resonances in Molecular Photoionization with Triply Differential Photoelectron Spectroscopy, Int. J. Mass Spect. Ion Phys. 46, 285-288 (1983)

A. C. Parr, S. H. Southworth, J. L. Dehmer, and D. M. P. Holland, Photoelectron Spectrometer for High Resolution Angular Resolved Studies, Nucl. Instr. Meth. 208, 767-770 (1983)

E. D. Poliakoff, J. L. Dehmer, P. M. Dehmer, and A. C. Parr, Vibrationally Resolved Photoelectron Angular Distributions for H_2, Chem. Phys. Lett. 96, 52-56 (1983)

S. T. Pratt and P. M. Dehmer, On the Dissociation Energy of $ArCO_2^+$, J. Chem. Phys. 78, 6336-6338 (1983)

S. T. Pratt, P. M. Dehmer, and J. L. Dehmer, Resonant Multiphoton Ionization of H_2 via the $B^1\Sigma_u^+$, v=7, J=2 and 4 Levels With Photoelectron Energy Analysis, J. Chem. Phys. 78, 4315-4320 (1983)

S. T. Pratt, P. M. Dehmer, and J. L. Dehmer, Two Photon Resonant, Four Photon Ionization of CO Via the $A\ ^1\Pi$ State With Photoelectron Energy Analysis, J. Chem. Phys. 79, 3234-3239 (1983)

S. T. Pratt, E. D. Poliakoff, P. M. Dehmer, and J. L. Dehmer, Photoelectron Studies of Resonant Multiphoton Ionization of CO via the $A^1\Pi$ State, J. Chem. Phys. 78, 65-72 (1983)

R.-G. Wang, M. A. Dillon, and David Spence, A Phenomenological Study of Heterogeneous Chemical Reactions of Mercuric Chloride on Heated Stainless Steel Surfaces, J. Chem. Phys. 79, 1100-1101 (1983)

Books, Reports, and Conference Papers

J. L. Dehmer, P. M. Dehmer, and S. T. Pratt, Multiphoton Ionization as a Probe of Molecular Photoionization Dynamics, in Electron-Molecule Collisions and Photoionization Processes, V. McKoy, H. Suzuki, K. Takayanagi, and S. Trajmar, Editors, (Verlag Chemie International Inc., 1983) pp. 21-25

P. M. Dehmer, Dissociation in Small Molecules, in Desorption Induced by Electronic Transitions, N. H. Tolk, M. M. Traum, J. C. Tully, and T. E. Madey, Editors, (Springer-Verlag, Berlin, 1983) pp. 164-168

M. A. Dillon, R. J. Hanrahan, R. Holroyd, Y.-K. Kim, M. C. Sauer, Jr., L. H. Toburen, Editors, Proceedings of the Workshop on the Interface Between Radiation Chemistry and Radiation Physics, Argonne, 9-11 September 1982, ANL-82-88 (March 1983)

M. Inokuti, Radiation Physics as a Basis of Radiation Chemistry and Biology, in Applications of Atomic Collision Physics. Vol. IV. Condensed Matter, H. S. W. Massey, B. Bederson, and E. W. McDaniel, Editors, (Academic Press, Inc., New York, December 1983) Chapter 3, pp. 179-236

Y.-K. Kim, Theory of Electron-Atom Collisions, in NATO Advanced Study Institute on the Physics of Electron-Ion and Ion-Ion Collisions, F. Brouillard and J. W. McGowan, Editors, (Plenum, 1983) pp. 101-165

D. Y. Smith, E. Shiles, and M. Inokuti, The Optical Properties and Complex Dielectric Function of Metallic Aluminum From 0.04 eV To 10^4 eV, Argonne National Laboratory Report No. ANL-83-24 (1983)

David Spence, Reng-guang Wang, and Michael A. Dillon, Excitation and Dissociation Mechanisms in Molecules With Application to Mercuric Halide Laser Systems, in Electron-Molecule Collisions and Photoionization Processes, V. McKoy, H. Suzuki, K. Takayanagi, and S. Trajmar, Editors, (Verlag Chemie International Inc., 1983) pp. 193-197

Abstracts

J. L. Dehmer, A. C. Parr, S. H. Southworth, and D. M. P. Holland, Triply Differential Photoelectron Studies of Autoionization and Shape-Resonance Effects in Molecular Photoionization, Fourteenth Annual Meeting of the Division of Electron and Atomic Physics, The American Physical Society, Boulder, CO, 23-25 May 1983, Bull. Am. Phys. Soc. 28, 809 (1983)

J. L. Dehmer, A. C. Parr, S. H. Southworth, and D. M. P. Holland, Triply Differential Photoelectron Studies of Resonant Molecular Photoionization, in Proceedings of the Thirteenth International Conference on the Physics of Electron and Atomic Collisions, Berlin, West Germany, 27 July - 2 August 1983, p. 42

P. M. Dehmer, Decay of Rydberg States via Autoionization and Predissociation, Fourteenth Meeting of the Division of Electron and Atomic Physics, Boulder, CO, May 23-25, 1983, Bull. Am. Phys. Soc. 28, 779 (1983)

P. M. Dehmer, S. T. Pratt, E. D. Poliakoff, and J. L. Dehmer, Photoelectron Studies of Resonant Multiphoton Ionization of CO via the $A\ ^1\Pi$ State, Fourteenth Meeting of the Division of Electron and Atomic Physics, Boulder, CO, May 23-25, 1983, Bull. Am. Phys. Soc. 28, 792 (1983)

I. B. Goldberg, K.-N. Huang, and R. H. Pratt, Photoionization Parameters of the Uranium $7s_{1/2}$ Shell, VIIth International Conference on Vacuum Ultraviolet Radiation Physics, (The Hebrew University of Jerusalem, Israel, August 1983)

K.-N. Huang, An Overview of Photon-Atom Interaction, in Proceedings of the Symposium on Atomic and Molecular Science, Academia Sinica of the Republic of China (Taipei, Taiwan, March 1983)

K.-N. Huang, Theoretical Triply Differential Cross Section of Electron-Impact Ionization of Atoms, Bull. Am. Phys. Soc. 28, 810 (1983)

K.-N. Huang, Forbidden Transitions in the Ground-State Multiplet of First- and Second-Row Atoms, in Abstracts of Fourth Topical Conference on Atomic Processes in High Temperature Plasmas (Princeton, NJ, April 1983)

Mitio Inokuti and S. T. Manson, Inner-Shell Corrections to the Bethe Stopping-Power Formula Evaluated From a Realistic Atomic Model, in Proceedings of the Seventh International Congress of Radiation Research, Amsterdam, 3-8 July 1983. Sessions A. Physics and Chemistry. J. J. Broerse, G. W. Barendsen, H. B. Kal, and A. J. van der Kogel, Editors, (Martinus Nijhoff Publishers, The Netherlands, 1983) A1-19

M. Inokuti and S. T. Manson, How Do We Decide Whether the First Born Approximation Applies to Inelastic Collisions of Charged Particles with an Atom or Molecule?, in Proceedings of the Thirteenth International Conference on the Physics of Electron and Atomic Collisions, Berlin, West Germany, 27 July - 2 August 1983, p. 151

R. E. Johnson and M. Inokuti, Mechanisms of the Sputtering of Condensed-Gas Solids by Charged Particles, in Proceedings of the Seventh International Congress of Radiation Research, Amsterdam, 3-8 July 1983. Sessions A. Physics and Chemistry. J. J. Broerse, G. W. Barendsen, H. B. Kal, and A. J. van der Kogel, Editors, (Martinus Nijhoff Publishers, The Netherlands, 1983) A1-22

Yong-Ki Kim, Relativistic Calculations of Atomic Structure, Fourth Topical Conference on Atomic Processes in High Temperature Plasmas, American Physical Society, (Princeton, NJ, 13-15 April 1983)

Y.-K. Kim, Slow Electrons Ejected From He by Electron Impact, Fourteenth Meeting of the Division of Electron and Atomic Physics, Boulder, CO, May 23-25, 1983, Bull. Am. Phys. Soc. 28, 796 (1983)

Yong-Ki Kim, Slow Electrons Ejected From He by Electron Impact, in Proceedings of the Seventh International Congress of Radiation Research, Amsterdam, 3-8 July 1983. Sessions A. Physics and Chemistry. J. J. Broerse, G. W. Barendsen, H. B. Kal, and A. J. van der Kogel, Editors, (Martinus Nijhoff Publishers, The Netherlands, 1983) A1-27

G. E. Leroi, J. L. Dehmer, A. C. Parr, and E. D. Poliakoff, Polarization of Fluorescence: A Probe of Molecular Autoionization Dynamics, VII International Conference on Vacuum Ultraviolet Radiation Physics, Jerusalem, Israel, 8-12 August 1983, Book of Abstracts; also in Ann. Israel Phys. Soc., in press

A. C. Parr, S. H. Southworth, J. L. Dehmer, and D. M. P. Holland, Angle Resolved Photoelectron Spectrometers, 3rd National Conference on Synchrotron Radiation Instrumentation, Brookhaven National Laboratory, Upton, Long Island, NY, 12-14 September 1983, Book of Abstracts

E. D. Poliakoff, J. L. Dehmer, A. C. Parr, and G. E. Leroi, Fluorescence Polarization as a Probe of Molecular Autoionization, Fourteenth Annual Meeting of the Division of Electron and Atomic Physics, The American Physical Society, Boulder, CO, 23-25 May 1983, Bull. Am. Phys. Soc. 28, 809 (1983)

E. D. Poliakoff, J. L. Dehmer, A. C. Parr, and G. E. Leroi, Fluorescence Polarization as a Probe of Molecular Autoionization, in Proceedings of the Thirteenth International Conference on the Physics of Electron and Atomic Collisions, Berlin, West Germany, 27 July - 2 August 1983, p. 43

E. D. Poliakoff, J. L. Dehmer, A. C. Parr, and G. E. Leroi, Fluorescence Excitation Studies of Molecular Photoionization in the Presence of External Electric Fields, VII International Conference on Vacuum Ultraviolet Radiation Physics, Jerusalem, Israel, 8-12 August 1983, Book of Abstracts; also in Ann. Israel Phys. Soc., in press

S. T. Pratt, P. M. Dehmer, and J. L. Dehmer, Resonant Multiphoton Ionization of H_2 via the B $^1\Sigma_u^+$ State With Photoelectron Energy Analysis, Fourteenth Meeting of the Division of Electron and Atomic Physics, Boulder, CO, May 23-25, 1983, Bull. Am. Phys. Soc. 28, 808 (1983)

S. T. Pratt, P. M. Dehmer, and J. L. Dehmer, Resonant Multiphoton Ionization of H_2 via the B $^1\Sigma_u^+$ State With Photoelectron Energy Analysis, in Proceedings of the Thirteenth International Conference on the Physics of Electron and Atomic Collisions, Berlin, West Germany, 27 July - 2 August 1983, p. 70

S. T. Pratt, E. D. Poliakoff, P. M. Dehmer, and J. L. Dehmer, Photoelectron Studies of Resonant Multiphoton Ionization of CO via the A $^1\Pi$ State, in Proceedings of the Thirteenth International Conference on the Physics of Electron and Atomic Collisions, Berlin, West Germany, 27 July - 2 August 1983, p. 69

David Spence, Dorothy Stuit, M. A. Dillon, and R.-G. Wang, High Resolution Total Electron Impact Excitation of Individual He 2^3S and 2^1S States, in Proceedings of the Thirteenth International Conference on the Physics of Electron and Atomic Collisions, Berlin, West Germany, 27 July - 2 August 1983, p. 117

David Spence, R.-G. Wang, and M. A. Dillon, Electron Energy Loss Spectroscopy in Molecular Chlorine, in Proceedings of the Thirteenth International Conference on the Physics of Electron and Atomic Collisions, Berlin, West Germany, 27 July - 2 August 1983, p. 265

R.-G. Wang, M. A. Dillon, and David Spence, Optically Forbidden Transitions in Saturated Hydrocarbons, Fourteenth Meeting of the Division of Electron and Atomic Physics, Boulder, CO, May 23-25, 1983, Bull. Am. Phys. Soc. 28, 811 (1983)

R.-G. Wang, M. A. Dillon, and David Spence, Electron Energy Loss Spectra of HCl, Fourteenth Meeting of the Division of Electron and Atomic Physics, Boulder, CO, May 23-25, 1983, Bull. Am. Phys. Soc. 28, 811 (1983)

R.-G. Wang, M. A. Dillon, D. Spence, and Z.-W. Wang, Studies of Forbidden Transitions in Saturated Hydrocarbons by Electron Impact Spectroscopy, Symposium on Atomic Spectroscopy (1983), Book of Abstracts, LBL-16509, p. 45

Z.-W. Wang, R.-G. Wang, and K. T. Lu, Graphic Analysis of Open-Shell Chlorine. Symposium on Atomic Spectroscopy (1983), Book of Abstracts, LBL-16509, p. 80

Distribution for ANL-83-100 Part I

Internal:

N. Akiyoshi (5)
C. C. Baker
J. Berkowitz
H. G. Berry
J. L. Dehmer
P. M. Dehmer
J. D. DePue
M. A. Dillon
H. Drucker
T. H. Dunning
A. J. Dvorak
E. Egganter
P. Frenzen
B. R. T. Frost
D. S. Gemmell
S. Gordon
S. L. Gotlund
E. Huberman
R. H. Huebner
M. Inokuti
K. L. Kliewer
A. B. Krisciunas (15)
K. Liu
P. Messina
E. G. Pewitt
S. T. Pratt
J. Rundo
M. C. Sauer
J. P. Schiffer
R. A. Schlenker
D. Y. Smith
D. Spence
R. W. Springer
E. P. Steinberg
C. M. Stevens
ER Division (70)
ANL Patent Dept.
ANL Contract File
ANL Libraries
TIS Files (6)

External:

DOE-TIC, for distribution per UC-48 (132)
Manager, Chicago Operations Office, DOE
A. W. Trivelpiece, Office of Energy Research, DOE
Environmental Research Division Review Committee:
- J. W. Firor, National Center for Atmospheric Research, Boulder
- D. W. Moeller, Harvard School of Public Health
- R. A. Reck, General Motors Research Labs.
- P. G. Risser, Illinois Natural History Survey, Champaign
- D. W. Thomson, Pennsylvania State U.
- R. E. Wildung, Battelle Pacific Northwest Lab.

W. J. Argersinger, Jr., U. Kansas
Arkansas, U. of, Library for Medical Sciences, Little Rock
L. Armstrong, Jr., Johns Hopkins U.
J. C. Ashley, Oak Ridge National Lab.
P. Ausloos, National Bureau of Standards, Washington
J. A. Auxier, Oak Ridge National Lab.
P. S. Bagus, IBM Research Labs., San Jose
J. N. Bardsley, U. Pittsburgh
N. F. Barr, Office of Health and Environmental Research, USDOE
J. W. Baum, Brookhaven National Lab.
B. Bederson, New York U.
M. J. Berger, National Bureau of Standards, Washington
R. S. Berry, U. Chicago
C. C. Bhalla, Kansas State U.
H. Bichsel, Seattle
W. H. Blahd, Veterans Administration Center, Los Angeles
M. J. W. Boness, Avco Everett Research Corp., Everett, Mass.
R. A. Bonham, Indiana U.
J. W. Boring, U. Virginia
D. J. Brenner, Columbia U.
A. B. Brill, Brookhaven National Lab.
B. H. Bruckner, National Center for Radiological Health, USHEW, Rockville, Md.
S. R. Bull, U. Missouri

R. A. Burnstein, Illinois Inst. Technology
P. D. Burrow, U. Nebraska
L. K. Bustad, Washington State U.
T. A. Carlson, Oak Ridge National Lab.
R. S. Caswell, National Bureau of Standards, Washington
R. J. Celotta, National Bureau of Standards, Washington
H. Cember, Northwestern U.
E. S. Chang, U. Massachusetts
T-N. Chang, U. Southern California
C. Y. Chen, U. California, San Diego
K. T. Cheng, Lawrence Livermore National Lab.
J. E. Christian, Purdue U.
L. G. Christophorou, Oak Ridge National Lab.
W. A. Chupka, Yale U.
C. W. Clark, National Bureau of Standards, Washington
R. G. Cochran, Texas A&M U.
S. H. Cohn, Brookhaven National Lab.
Colorado, U. of, Joint Inst. for Laboratory Astrophysics
R. N. Compton, Oak Ridge National Lab.
J. W. Cooper, National Bureau of Standards, Washington
Cornell University, Library, Geneva, N. Y.
D. H. Crandall, Oak Ridge National Lab.
B. Crasemann, U. Oregon
J. A. Cummings, Wisconsin State U.
A. Dalgarno, Harvard College Observatory and Smithsonian Astrophysical Observatory
S. Datz, Oak Ridge National Lab.
R. D. Deslattes, Jr., National Bureau of Standards, Washington
D. Dill, Boston U.
D. A. Douthat, U. Alaska
G. H. Dunn, U. Colorado
M. P. Durso, Environmental Measurements Lab., USDOE, New York
D. L. Ederer, National Bureau of Standards, Washington
C. W. Edington, Office of Health and Environmental Research, USDOE
C. E. Edmund, Milwaukee, Wis.
R. D. Evans, Scottsdale, Ariz.
U. Fano, U. Chicago
M. R. Flannery, Georgia Inst. Technology
A. C. Gallagher, U. Colorado
W. R. Garrett, Oak Ridge National Lab.
R. Geballe, U. Washington
S. Geltman, U. Colorado
G. H. Gillespie, Physical Dynamics, Inc., La Jolla
W. A. Glass, Battelle Northwest Lab.
M. Goldman, U. California, Davis
A. E. S. Green, U. Florida
T. A. Green, Sandia National Labs., Albuquerque
C. H. Greene, Louisiana State U.
R. Grunewald, U. Wisconsin, Milwaukee
A. J. Haverfield, Battelle Northwest Lab.
R. J. W. Henry, Louisiana State U.
G. R. Holeman, Yale U.
Houston, U. of, Libraries
G. S. Hurst, Oak Ridge National Lab.

Illinois, U. of, Library, Chicago
R. A. Isaacson, National Science Foundation
K. H. Johnson, Massachusetts Inst. Technology
R. E. Johnson, U. Virginia
W. R. Johnson, U. Notre Dame
B. R. Junker, Office of Naval Research, Arlington, Va.
R. J. Kandel, Office of Basic Energy Sciences, USDOE
H. P. Kelly, U. Virginia
W. V. Kessler, Purdue U.
Y-K. Kim, National Bureau of Standards, Washington
E. W. Klappenbach, U.S. Environmental Protection Agency, Chicago
W. M. Kosman, Valparaiso U.
M. O. Krause, Oak Ridge National Lab.
A. Kuppermann, California Inst. Technology
C. E. Kuyatt, National Bureau of Standards, Washington
P. Lambropoulos, U. Southern California
N. F. Lane, U. Colorado
E. N. Lassettre, Carnegie-Mellon U.
Y. T. Lee, U. California, Berkeley
S. H. Levine, Pennsylvania State U.
J. C. Light, U. Chicago
W. C. Lineberger, U. Colorado
S. Lipsky, U. Minnesota
L. Lohr, Jr., U. Michigan
D. C. Lorents, SRI International, Menlo Park
K. T. Lu, National Bureau of Standards, Gaithersburg
J. H. Macek, U. Nebraska
R. P. Madden, National Bureau of Standards, Washington
J. L. Magee, Lawrence Berkeley National Lab.
C. J. Maletskos, Gloucester, Mass.
S. T. Manson, Georgia State U.
E. A. Martell, National Center for Atmospheric Research, Boulder
J. V. Martinez, Office of Basic Energy Sciences, USDOE
Mayo Clinic Library, Rochester
S. P. McGlynn, Louisiana State U.
D. H. McKelvie, U. Arizona
V. McKoy, California Inst. Technology
J. E. McLaughlin, Environmental Measurements Lab., USDOE, New York
R. Meer, Massachusetts General Hospital
G. G. Meisels, U. Nebraska
J. Mentall, NASA Goddard Space Flight Center
A. L. Mertz, Los Alamos National Lab.
E. Merzbacher, U. North Carolina at Chapel Hill
Michigan Technological U. Library, Houghton
D. W. Moeller, Kresge Center for Environmental Health, Boston
R. D. Moseley, Jr., U. New Mexico Medical School
G. Murphy, Iowa State U.
W. G. Myers, Ohio State U. Hospital
D. P. Naismith, U. North Dakota
R. K. Nesbet, IBM Research Labs., San Jose
W. R. Ney, National Council on Radiation Protection and Measurements, Bethesda
G. Nichols, Jr., Boston, Mass.
D. W. Norcross, U. Colorado
O. F. Nygaard, Case Western Reserve U.

M. J. Ohanian, U. Florida
A. L. Orvis, Mayo Clinic
W. R. Ott, National Bureau of Standards, Washington
J. Ovadia, Michael Reese Hospital, Chicago
L. R. Painter, U. Tennessee
A. Pagnamenta, U. Illinois, Chicago
J. Pan, Purdue U., Calumet Campus
A. C. Parr, National Bureau of Standards, Washington
J. M. Peek, Sandia National Labs., Albuquerque
A. V. Phelps, U. Colorado
E. D. Poliakoff, Boston U.
M. L. Pool, Western Illinois U.
M. Pope, New York U.
C. Powell, National Bureau of Standards, Washington
R. H. Pratt, U. Pittsburgh
A. R. P. Rau, Louisiana State U.
W. P. Reinhardt, U. Colorado
J. S. Risley, North Carolina State U. at Raleigh
R. H. Ritchie, Oak Ridge National Lab.
J. S. Robertson, Office of Energy Research, USDOE
W. C. Roesch, Battelle Northwest Lab.
C. C. J. Roothaan, U. Chicago
H. H. Rossi, Columbia U.
M. E. Rudd, U. Nebraska
J. H. Rust, U. Chicago
E. L. Saenger, Cincinnati General Hospital
E. Salmon, McLean, Va.
J. A. R. Samson, U. Nebraska
R. P. Saxon, SRI International, Inc., Menlo Park
R. H. Schuler, U. Notre Dame
D. A. Shirley, U. California, Berkeley
T. W. Shyn, U. Michigan
Siemens Gammasonics, Inc., Des Plaines, Ill.
R. M. Sinclair, National Science Foundation
W. K. Sinclair, National Council on Radiation Protection and Measurements, Bethesda
J. B. Smathers, Texas A&M U.
F. T. Smith, SRI International, Inc., Menlo Park
L. V. Spencer, Hopkinsville, Ky.
A. F. Starace, U. Nebraska
R. F. Stebbings, Rice U.
R. L. Stockbauer, National Bureau of Standards, Washington
P. M. Stone, Office of Fusion Energy, USDOE
S. Tani, Marquette U.
H. S. Taylor, U. Southern California
L. S. Taylor, Bethesda, Md.
A. Temkin, Goddard Space Flight Center
C. E. Theodosiou, U. Toledo
J. K. Thomas, U. Notre Dame
C. A. Tobias, U. California, Berkeley
L. H. Toburen, Battelle Northwest Lab.
S. Trajmer, Jet Propulsion Lab.
J. E. Turner, Oak Ridge National Lab.
A. C. Upton, New York U. Medical Center

M. N. Varma, Office of Energy Research, USDOE
D. Varney, Eastern Kentucky U.
S. D. Vesselinovitch, U. Chicago
S. Wallace, Massachusetts Inst. Technology
W. L. Wiese, National Bureau of Standards, Washington
R. H. Williams, U. Michigan
W. E. Wilson, Battelle Northwest Lab.
H. F. Winters, IBM Research Labs., San Jose
W. F. Witzig, Pennsylvania State U.
R. W. Wood, Office of Health and Environmental Research, USDOE
H. O. Wyckoff, International Commission on Radiation Units and Measurements, Bethesda
K. F. Wylie, U. Mississippi
M. A. Zaider, Columbia U.
R. N. Zare, Stanford U.
Comision Nacional de Energia Atomica, Library, Buenos Aires, Argentina
Cancer Institute Library, Melbourne, Australia
Ian E. McCarthy, Flinders U. of South Australia, Adelaide, Australia
J. F. Williams, U. of Western Australia, Perth, Australia
R. A. Dudley, IAEA, Vienna, Austria
J. M. Debois, St. Norbertus Hospital, Duffel, Belgium
A. Heyndrickx, U. Ghent, Belgium
N. Brearley, U. British Columbia, Vancouver, Canada
C. E. Brion, U. British Columbia, Vancouver, Canada
Canadian Forces Base, Halifax, Canada
J. D. Carette, Universite Laval, Quebec, Canada
D. Charlton, Concordia U., Montreal, Canada
G. Cowper, Atomic Energy of Canada Ltd., Chalk River
Defence Research Establishment Library, Ottawa, Canada
G. R. Freeman, U. Alberta, Edmonton, Canada
Health and Welfare Canada, Radiation Protection Bu., Ottawa
J. W. McConkey, U. Windsor, Canada
J. W. McGowan, U. Western Ontario, London, Canada
C. Pomroy, Dept. National Health and Welfare, Ottawa, Canada
L. Sanche, U. Sherbrooke, Sherbrooke, Canada
A. G. Szabo, National Research Council of Canada, Ottawa
Toronto, U. of, Library, Canada
C. Willis, National Research Council of Canada, Ottawa
De-Ji Fu, Chinese Academy of Sciences, Shanghai, People's Republic of China
Qing-Quan Gou, Chengdu U. of Science and Technology, People's Republic of China
Ji-Ming Li, Chinese Academy of Sciences, Beijing, People's Republic of China
R-G. Wang, Chengdu U. of Science and Technology, People's Republic of China
Zhi-wen Wang, Jilin U., Changchun, People's Republic of China
C-H. Cheng, Atomic Energy Council, Taipei, Republic of China
K.-N. Huang, Academia Sinica, Taipei, Republic of China
Czechoslovak Atomic Energy Commission, Zbraslav nad Vltavou
H. H. Andersen, H. C. Ørsted Inst., Copenhagen, Denmark
N. Andersen, H. C. Ørsted Inst., Copenhagen, Denmark
M. Faber, Finsen Inst. Copenhagen, Denmark
P. Hvelplund, Aarhus U., Denmark
J. Lindhard, Aarhus U., Denmark
P. Sigmund, Odense U., Denmark
G. E. Adams, MRC Radiobiology Unit, Harwell, England
J. W. Boag, Sutton, Surrey, England

P. R. J. Burch, U. Leeds, England
Y. Cocking, MRC Radiobiology Unit, Harwell, England
K. Codling, U. Reading, England
J. A. Dennis, National Radiological Protection Board, Harwell, England
K. T. Dolder, The University, Newcastle-upon-Tyne, England
J. A. Edgington, Queen Mary College, London, England
J. F. Fowler, Mt. Vernon Hospital, Northwood, England
D. T. Goodhead, MRC Radiobiology Unit, Harwell, England
S. J. Harris, U. Surrey, Guildford, England
M. T. Herbert, National Radiological Protection Board, Chilton, England
C. R. Hill, Inst. of Cancer Research, Belmont, England
G. V. Marr, U. Reading, England
W. V. Mayneord, Tadworth, Surrey, England
M. R. C. McDowell, Royal Holloway College, Surrey, England
D. H. Peirson, U. K. AERE, Harwell, England
E. E. Pochin, National Radiological Protection Board, Harwell, England
F. H. Read, U. Manchester, England
K. J. Ross, U. Southampton, England
M. J. Seaton, U. College London, England
A. J. Swallow, Christie Hospital & Holt Radium Inst., Manchester, England
J. B. West, Daresbury Lab., Daresbury, England
T. Åberg, Helsinki U. of Technology, Otaniemi, Finland
Institute of Radiation Protection, Library, Helsinki, Finland
P. Pyykkö, Åbo Akademi, Turku, Finland
A. Allisy, Bu. International des Poids et Mesures, Sèvres, France
M. Barat, U. Paris, Orsay, France
J-P. Briand, Lab. de Physique Atomique et Nucleaire, Paris, France
J. Coursaget, CEA, Saclay, France
J. P. Desclaux, CEN/G DRF-CPN, Grenoble, France
J. Durup, U. Paris, Orsay, France
L. F. Ferreira, U. Paris, Orsay, France
P. M. Guyon, U. Paris, Orsay, France
R. I. Hall, U. Paris, Paris, France
V. K. Lan, Observatoire de Paris, Meudon, France
M. Tronc, Lab. de Collisions Electroniques, Orsay, France
R. Voltz, Centre de Recherches Nucleaires, Strasbourg-Cronenbourg, France
S. Watanabe, Observatoire de Paris, Meudon, France
F. Wuilleumier, U. Paris, Orsay, France
P. Armbruster, Gesellschaft für Schwerionenforschung, Darmstadt, Germany
J. Booz, Institut für Medizin, Jülich, Germany
J. S. Briggs, U. Freiburg, Germany
R. J. Buenker, U. Bonn, Germany
G. Drexler, Institute für Strahlenschutz, Munich, Germany
H. Ehrhardt, U. Kaiserslautern, Germany
J. Eichler, Hahn-Meitner-Institut, Berlin, Germany
J. Geiger, U. Kaiserslautern, Germany
Gesellschaft für Strahlenforschung m.b.H., Frankfurt, Germany
B. Grosswendt, Physikalisch-Technische Bundesanstalt, Braunschweig, Germany
R. Haensel, U. Kaiserslautern, Germany
D. Harder, U. Göttingen, Germany
I. V. Hertel, Freie U., Berlin, Germany
H. Hotop, U. Kaiserslautern, Germany
A. Kaul, Inst. für Strahlenhygiene, Neuherberg, Germany
J. Kessler, Physikalisches Inst. der Universität Münster, Germany

F. Linder, U. Kaiserslautern, Germany
W. Mehlhorn, U. Freiburg, Germany
H. Muth, U. Saarlandes, Homburg, Germany
E. Oberhausen, U. Saarlandes, Homburg, Germany
H. G. Paretzke, Institut für Strahlenschutz, Neuherberg, Germany
S. D. Peyerimhoff, U. Bonn, Germany
G. zu Putlitz, Gesellschaft für Schwerionenforschung, Darmstadt, Germany
H. Schmoranzer, U. Kaiserslautern, Germany
B. Sonntag, Deutsches Elektronen Synchrotron, Hamburg, Germany
G. Stöcklin, Kernforschungsanlage Jülich, Germany
N. Stolterfoht, Hahn-Meitner-Institut, Berlin, Germany
K. J. Vogt, Kernforschungsanlage, Jülich, Germany
R. K. Hukkoo, Bhabha Atomic Research Centre, Bombay, India
A. N. Tripathi, U. Roorke, India
I. B. Berlman, Hebrew U., Jerusalem, Israel
Y. Feige, Israel AEC, Yavne, Israel
A. Benco, Commission of the European Communities, Ispra, Italy
E. Casnati, CNEN, Rome, Italy
A. Cigna, ENEA-CRE, Saluggia, Italy
G. F. Clemente, CNEN, Rome, Italy
F. A. Gianturco, U. di Roma, Italy
V. Prodi, CNEN, Bologna, Italy
O. Rimondi, Istituto di Fisica, Ferrara, Italy
S. Arai, Inst. Physical and Chemical Research, Saitama-ken, Japan
Y. Hatano, Tokyo Inst. Tech., Tokyo, Japan
T. Higashimura, Kyoto U., Japan
H. Inokuchi, Inst. for Molecular Science, Okazaki, Japan
Y. Itikawa, Inst. Space and Astronautical Science, Tokyo, Japan
S. Iwata, Keio U., Yokohama, Japan
S. Kaneko, U. Tokyo, Japan
Y. Kaneko, Tokyo Metropolitan U., Japan
K. Kimura, Inst. for Molecular Science, Okazaki, Japan
I. Koyano, Inst. for Molecular Science, Okazaki, Japan
M. Matsuzawa, U. of Electro-Communications, Tokyo, Japan
H. Nakamura, Institute for Molecular Science, Okazaki, Japan
M. Nakamura, Tsukuba U., Ibaraki-ken, Japan
H. Nishimura, Niigata U., Japan
N. Oda, Tokyo Inst. of Technology, Tokyo, Japan
T. Sasaki, National Lab. for High Energy Physics, Ibaraki, Japan
S. Sato, Tokyo Inst. Technology, Japan
H. Suzuki, Sophia U., Tokyo, Japan
T. Takahashi, Inst. of Physical and Chemical Research, Saitama-ken, Japan
K. Takayanagi, Inst. of Space and Astronautical Science, Tokyo, Japan
H. Tanaka, Sophia U., Tokyo, Japan
K. Tanaka, Inst. for Molecular Science, Okazaki, Japan
T. Watanabe, Inst. Physical and Chemical Research, Saitama-ken, Japan
Korea Advanced Energy Research Inst., Seoul, Korea
Sang-Soo Lee, The Korea Advanced Inst. of Science, Seoul, Korea
H. H. Brongersma, Philips Research Laboratories, Eindhoven, The Netherlands
F. J. de Heer, FOM Inst. for Atomic and Molecular Physics, Amsterdam, The Netherlands
M. Gavrilla, FOM Inst. for Atomic and Molecular Physics, Amsterdam, The Netherlands
J. Kistemaker, FOM Inst. for Atomic and Molecular Physics, Amsterdam, The Netherlands

J. Los, FOM Inst. for Atomic and Molecular Physics, Amsterdam, The Netherlands
A. Niehaus, Utrecht U., The Netherlands
M. van der Wiel, FOM Inst. for Atomic and Molecular Physics, Amsterdam, The Netherlands
J. M. Warman, Interuniversity Reactor Inst., Delft, The Netherlands
P. G. Burke, Queen's U., Belfast, Northern Ireland
M. U. Shaikh, Pakistan Atomic Energy Commission, Rawalpindi
J. R. Greening, The Royal Infirmary, Edinburgh, Scotland
R. D. Cherry, U. Cape Town, South Africa
A. Brahme, Karolinska Inst., Stockholm, Sweden
O. Goscinski, Uppsala U., Sweden
I. Jansson, National Inst. of Radiation Protection, Stockholm, Sweden
K. Liden, Dept. of Radiation Physics--Lasarettet, Lund, Sweden
A. E. Nahum, U. Umeå, Sweden
G. Wendin, Inst. of Theoretical Physics, Göteborg, Sweden
A. Donath, Service Cantonal de Controle des Irradiations, Geneva, Switzerland
A. Gunther, CERN, Geneva, Switzerland
G. D. Alkhazov, Academy of Sciences of the U.S.S.R., Leningrad
M. Ya. Amusia, Academy of Sciences of the U.S.S.R., Leningrad
E. Komarov, Central Res. Inst. of Roentgenology and Radiology, Leningrad, U.S.S.R.
V. Tal'roze, Academy of Sciences of the U.S.S.R., Moscow
D. Cvejanovic, Faculty of Natural and Mathematical Sciences, Belgrade, Yugoslavia
M. Kurepa, Inst. of Physics, Belgrade, Yugoslavia
D. Srdoc, Rudjer Boskovic Inst., Zagreb, Yugoslavia
L. Vuskovic, Inst. of Physics, Belgrade, Yugoslavia